Impact of Geometric Uncertainties on Dose Calculations for Intensity Modulated Radiation Therapy of Prostate Cancer

by

Runqing Jiang

A thesis
presented to the University of Waterloo
in fulfillment of the
thesis requirement for the degree of
Doctor of Philosophy
in
Physics

Waterloo, Ontario, Canada, 2007

AUTHOR'S DECLARATION

I hereby declare that I am the sole author of this thesis. This is a true copy of the thesis, including any required final revisions, as accepted by my examiners.

I understand that my thesis may be made electronically available to the public.

Abstract

Intensity-modulated radiation therapy (IMRT) uses non-uniform beam intensities within a radiation field to provide patient-specific dose shaping, resulting in a dose distribution that conforms tightly to the planning target volume (PTV). Unavoidable geometric uncertainty arising from patient repositioning and internal organ motion can lead to lower conformality index (CI) during treatment delivery, a decrease in tumor control probability (TCP) and an increase in normal tissue complication probability (NTCP). The CI of the IMRT plan depends heavily on steep dose gradients between the PTV and organ at risk (OAR). Geometric uncertainties reduce the planned dose gradients and result in a less steep or "blurred" dose gradient. The blurred dose gradients can be maximized by constraining the dose objective function in the static IMRT plan or by reducing geometric uncertainty during treatment with corrective verification imaging.

Internal organ motion and setup error were evaluated simultaneously for 118 individual patients with implanted fiducials and MV electronic portal imaging (EPI). A Gaussian probability density function (PDF) is reasonable for modeling geometric uncertainties as indicated by the 118 patients group. The Gaussian PDF is patient specific and group standard deviation (SD) should not be used for accurate treatment planning for individual patients. In addition, individual SD should not be determined or predicted from small imaging samples because of random nature of the fluctuations. Frequent verification imaging should be employed in situations where geometric uncertainties are expected. Cumulative PDF data can be used for re-planning to assess accuracy of delivered dose. Group data is useful for determining worst case discrepancy between planned and delivered dose. The margins for the PTV should ideally represent true geometric uncertainties. The measured geometric uncertainties were used in this thesis to assess PTV coverage, dose to OAR, equivalent uniform dose per fraction (EUD_f) and NTCP.

The dose distribution including geometric uncertainties was determined from integration of the convolution of the static dose gradient with the PDF. Integration of the convolution of the static dose and derivative of the PDF can also be used to determine the dose

including geometric uncertainties although this method was not investigated in detail. Local maximum dose gradient (LMDG) was determined via optimization of dose objective function by manually adjusting DVH control points or selecting beam numbers and directions during IMRT treatment planning. Minimum SD ($SD_{min)}$) is used when geometric uncertainty is corrected with verification imaging. Maximum SD (SD_{max}) is used when the geometric uncertainty is known to be large and difficult to manage. SD_{max} was 4.38 mm in anterior-posterior (AP) direction, 2.70 mm in left-right (LR) direction and 4.35 mm in superior-inferior (SI) direction; SD_{min} was 1.1 mm in all three directions if less than 2 mm threshold was used for uncorrected fractions in every direction.

EUD_f is a useful QA parameter for interpreting the biological impact of geometric uncertainties on the static dose distribution. The EUD_f has been used as the basis for the time-course NTCP evaluation in the thesis. Relative NTCP values are useful for comparative QA checking by normalizing known complications (e.g. reported in the RTOG studies) to specific DVH control points. For prostate cancer patients, rectal complications were evaluated from specific RTOG clinical trials and detailed evaluation of the treatment techniques (e.g. dose prescription, DVH, number of beams, bean angles). Treatment plans that did not meet DVH constraints represented additional complication risk. Geometric uncertainties improved or worsened rectal NTCP depending on individual internal organ motion within patient.

Acknowledgements

First, I would like to express my deep appreciation to my supervisor, Dr. Rob Barnett, for his excellent advice and thoughtful guidance throughout this project. His support and encouragement during my Ph.D. studies provided me with a unique perspective into the problem and gave me the right balance between independence and supervision to keep the research on track. His insight into medical physics problems has enhanced my understanding of the research work. I would like to thank my co-supervisor, Professor Jeff Chen, for providing me with the first opportunity to learn about medical biophysics, and for discussions regarding math and statistics. I would also like to thank my Ph.D. advisory committee members, Professor H. Peemoeller, Professor E. Vrscay, and Professor Q.-B. Lu, whose support and contributions were greatly appreciated. I would like to thank Dr. Jerry Battista for serving as the external examiner in my Ph.D. defence.

I would like to thank Dr. Ernest Osei for providing his developed IGRT software, without which this project would not have been possible. I would like to thank our physicists in Medical Physics Department at Grand River Regional Cancer Center (GRRCC), Dr. Paule Charland, Dr. Ernest Osei, Andre Fleck, and Dr. Bryan Schaly, for their gracious and inspiring discussions and answering my many questions in clinical aspects of the field. Thanks to Ronald Snelgrove and Grigor Grigorov for their kindness help on measurements and treatment planning. The wording of thesis by Andre Fleck was greatly appreciated. I would also like to thank Dr. James Chow, our former colleague and physicist, for his generous help. Thanks to all the Medical Physics Department staff, Denis Brochu; John Ukos; Mariusz Ogrodowczyk; Mike Gallamore; and Vanya Mathews for their selfless support and help. I would like to thank all the staff, physicians and therapists at GRRCC for their selfless support and advice over these years. The Medical Physics Department at GRRCC has been a very pleasant place to work and has made my stay at GRRCC very enjoyable.

I would like to thank my family for their encouragement and support. My parents have offered much support to help me reach my goals. My husband and my son have always been there for me to keep my motivation by their love, understanding, and support.

Finally, I would like to extend my sincere appreciation to our graduate secretary, Judy McDonnell, for all of her kindness and help. I could not have completed this thesis without everyone's support. Thank you very much!

Table of Contents

Chapter 6

Summary and Conclusions...151

List of Figures

List of Tables

List of Abbreviations

2D	Two Dimensional
3D	Three Dimensional
5F	Five-field
7F	Seven-field
AP	Anterior-Posterior
ART	Adaptive Radiation Therapy
CBCT	Cone Beam Computed Tomography
CI	Conformality Index
CM	Center of Mass
CRT	Conformal Radiation Therapy
CT	Computed Tomography
CTV	Clinical Target Volume
DMLC	Dynamic Multi-Leaf Collimator
DRR	Digitally Reconstructed Radiograph
DVH	Dose-Volume Histogram
EPI	Electric Portal Imaging
EPID	Electric Portal Imaging Device
EUD	Equivalent Uniform Dose
EUD_f	Equivalent Uniform Dose per Fraction
GPDF	Gaussian Probability Density Function
GRRCC	Grand River Regional Cancer Center
GTV	Gross Tumor Volume
Gy	Gray
HDR	High Dose Rate
ICRU	International Commission on Radiation Units and Measurements
IGRT	Image Guided Radiation Therapy
IM	Internal Margin
IMRT	Intensity Modulated Radiation Therapy
ITV	Internal Target Volume
kVCT	Kilovoltage Computed Tomography

LET	Linear Energy Transfer
Linac	Linear Accelerator
LMDG	Local Maximum Dose Gradient
LR	Left-Right
LQ	Linear-Quadratic
MD	Mean Dose
MeV	Mega Electron-volts
MLC	Multi-Leaf Collimator
MPR	Multi-planar Dose Reconstruction
MR	Magnetic Resonance
MU	Monitor Units
MV	Megavoltage
MVCT	Megavoltage Computed Tomography
NTCP	Normal Tissue Complication Probability
OAR	Organ At Risk
OMDS	Organ Motion Dose Sensitivity
PET	Positron Emission Tomography
PDF	Probability Density Function
PMDD	Percentage Mean Dose Deviation
PSA	Prostate Specific Antigen
PTV	Planning Target Volume
RMS	Root Mean Square
RTOG	Radiation Therapy Oncology Group
RTP	Radiation Therapy Planning
SD	Standard Deviation
SI	Superior-Inferior
SM	Setup Margin
TCP	Tumor Control Probability
US	Ultrasound

Chapter 1

Introduction

1.1   Overview and Thesis Outline

The goal of radiation therapy is to deliver a highly conformal and lethal absorbed dose to a prescribed target volume and to spare surrounding healthy tissue as much as possible. Using commercial treatment planning systems available presently, the patient anatomy is assumed to be static over the course of treatment (i.e. 5~6 weeks). Fundamentally, reproducibility of patient setup and internal organ motion leads to discrepancies between the planned (intended) and actual delivered dose to the patient. These discrepancies can have a significant impact on treatment outcome and should be accounted for in the treatment planning process. Dose planning, including a 3D dose calculation performed by the treatment planning system and a dose prescription from the radiation oncologist, assumes stable anatomy. During treatment delivery, however, geometric uncertainties arising from patient repositioning and internal organ motion are unavoidable. For prostate patients, anisotropic motions with magnitudes of 1–2 cm have been reported in several studies, with the greatest displacement along the superior-inferior direction (Ten Haken 1991, Schild 1993, Balter 1995, Crook 1995, van Herk 1995, Lebesque 1995, Roeske 1995, Beard 1996, Althof 1996, Melian 1997). The position of the prostate is also affected by patient positioning, e.g., supine versus prone (Stroom 1999), and by rectal and bladder distension (Ten Haken 1991, Schild 1993). Balter (2000) showed that

craniocaudal motion was largest for the prostate. Geometric uncertainty causes the target volume to move in and out of the high dose region of the radiation fields which can lead to a compromise in target dose coverage and a decrease in tumor control probability (TCP). Similar uncertainty associated with healthy organs adjacent to the target volume can lead to an increase in normal tissue complication probability (NTCP).

```
┌──────────────────────────────────────┐
│   Patient positioning & immobilization │
└──────────────────────────────────────┘
                    │
                    ▼
┌──────────────────────────────────────┐
│          Imaging for RT planning        │
└──────────────────────────────────────┘
                    │
                    ▼
┌──────────────────────────────────────┐      ┌───────────┐
│   Target & normal tissue delineation    │◄─────│    ART    │
└──────────────────────────────────────┘      └───────────┘
                    │
                    ▼
┌──────────────────────────────────────┐
│  Formulation of dose prescription with constraints │
└──────────────────────────────────────┘
                    │
                    ▼
┌──────────────────────────────────────┐
│             Inverse planning            │
└──────────────────────────────────────┘
                    │
                    ▼
┌──────────────────────────────────────────────────────┐
│  Data transfer from planning system to treatment delivery system │
└──────────────────────────────────────────────────────┘
                    │
                    ▼
┌──────────────────────────────────────┐
│          Dosimetry confirmation         │
└──────────────────────────────────────┘
                    │
                    ▼
┌──────────────────────────────────────┐
│            Verification Imaging         │
└──────────────────────────────────────┘
                    │
                    ▼
┌──────────────────────────────────────┐
│     Computer controlled dose delivery   │
└──────────────────────────────────────┘
```
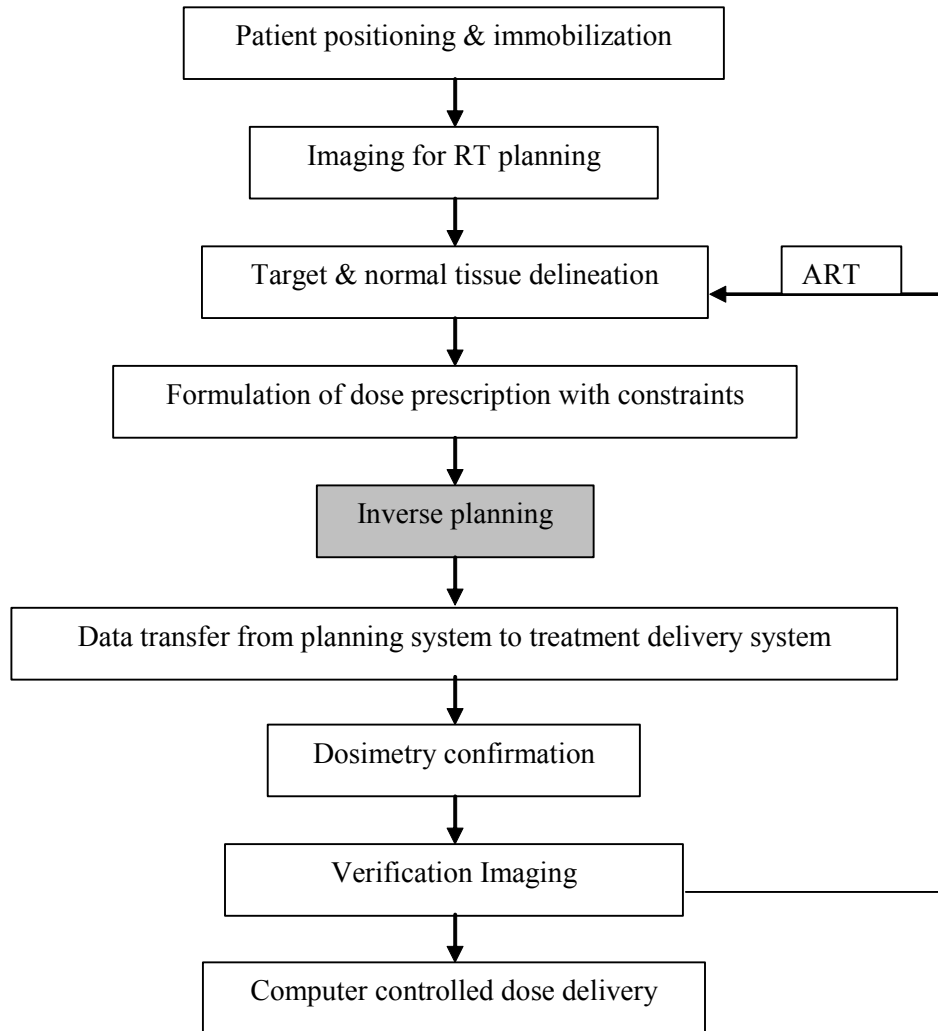
Figure 1. 1: The steps in IMRT treatment planning process.

The process of radiation therapy for malignant disease is complex and involves many steps (Van Dyk 1999, 2005) as shown in Figure 1.1. The overall process leading to

patient treatment begins with patient positioning and immobilization and includes other important component steps of imaging for target delineation, definition of dose constraints, inverse planning, dosimetry verification and finally dose delivery.

In each of the process steps there will be uncertainties that should be quantified and managed (reduced, eliminated, and/or included in the dose calculation of total absorbed dose). It is important that each step of the process is executed with the greatest accuracy possible. The success or failure of a radiation therapy treatment is highly dependent upon the accuracy of the dose delivered. Even small deviations (reductions) from the plan of the prescribed dose to the target volume can have a direct impact on treatment outcome. At the same time, small deviations (increases) in dose delivered to radio-sensitive healthy organs or tissues can significantly increase the probability of normal tissue complications. Overall, the total dose delivered should be accurate to within 5% (ICRU report 24 1976), and any potential method to increase the accuracy in the dose calculation or dose delivery should be investigated. Uncertainties of 5% or greater may jeopardize the intent of the treatment and represent significant risk to patient. The outcome of clinical trials is dependent on dose accuracy, 5% accuracy is desirable and assuming that uncertainties in each procedure are random in nature, then the required accuracy for each step is 2.5% (ICRU report 50 1993, ICRU report 62 1999, Van Dyk 1999).

Historically, radiation therapy predominantly employed parallel-opposed rectangular fields with cerrobend blocks, which remain the foundation for conformal radiation therapy (CRT). Generous margins have been applied to the target volume to compensate for general uncertainties including setup error and organ motion (ICRU report 50 1993, ICRU report 62 1999). Unavoidably, situations arise where the margins of the clinical target volume (CTV) and critical structures (rectum and bladder for prostate patient, for example) overlap. Under realistic situation involving target and organ at risk (OAR) intersection and movement, conventional treatment planning systems do not always calculate the dose accurately. Dose calculation incorporating organ motion will improve agreement between planned and delivered doses ideally leading to higher TCP and lower NTCP.

Newer paradigms for radiation therapy, for example, Intensity Modulated Radiation Therapy (IMRT), Image Guided Radiation Therapy (IGRT) and Adaptive Radiation Therapy (ART), require detailed anatomical segmentation. Unfortunately, studies of inter-observer variability in defining radiation target suggest that gross tumor volumes (GTVs) are not always reproducible (Cazzaniga 1998, Rasch 1999).

With the advent of improved medical imaging technologies for radiation therapy planning (RTP), including Computed Tomography (CT), Positron Emission Tomography (PET), Magnetic Resonance (MR), Ultrasound (US), and verification imaging technologies including Cone Beam CT (CBCT) and a-Si MV electronic portal imaging (EPI) for repositioning and re-planning guidance, it is possible to reduce the margin because of greater confidence in CTV delineation and greater confidence in delivering dose to the planning target volume (PTV). Improved medical imaging technologies, with the capability for image co-registration and fusion offer improved resolution and contrast between malignant and healthy tissues. The improved verification imaging systems lead to greater confidence in aligning treatment beams with the target. Newer technology for radiation delivery, for example, a linear accelerator (linac) with Dynamic Multileaf Collimator (DMLC), Helical Tomography, Cyberknife and High Dose Rate (HDR) Brachytherapy offer improved ability to sculpt dose with greater precision, and lead to increase confidence in the delivery of dose to the target since the radiation "travels" with the target.

Improved 3 dimensional (3D) dose calculations (optimization of objective functions, dose assessment tools including 2 dimensional (2D) dose analyses by image slice, multi-planar dose reconstruction (MPR), and dose volume histogram (DVH)), collectively demonstrate the benefits for 3D CRT. However, DVH does not provide spatial information about the dose distribution, and optimized IMRT plans do not always develop a high local maximum dose gradient (LMDG) between the PTV and OAR. The accuracy of the dose distribution based on static anatomy is limited because of exclusion of the blurring effects of geometric uncertainties (internal organ motion and setup error).

4

The assessment of planned versus delivered dose is necessary because of the impact of geometric uncertainties.

The inclusion of geometric uncertainties in dose calculations has been approached using several methods, many of them employing convolution techniques (Leong 1987, Lind 1993, Rudat 1994 1996, Bel 1996, Keall 1999, Lujan 1999a 1999b, Stroom 1999, Li 2000, McCarter 2000, McKenzie 2000a 2000b, van Herk 2000 2002, Booth 2001, O'Dell 2002). Recently Craig *et al* (2003a, 2003b) have shown that for deep seated tumors (e.g. prostate) it is reasonable to convolve the static dose distribution with a probability density function (PDF) characterizing geometric uncertainties to obtain a modified dose distribution. Using this approach, however, it is not easy to interpret the modified dose distribution in terms of magnitude and position of the motion effects. There is no direct parametric connection between the convolution integral and the static dose distribution that could be used to manage geometric uncertainties from the perspective of optimized dose (DVH does not contain spatial information). One of the main objective of this thesis is to develop a parametric connection between the convolution integral of dose with PDF; namely the dose gradient $G_0 = \partial D_0 / \partial \vec{r}$. Another important area of focus is on careful clinical assessment of the PDF using modern imaging technology and surgically implanted fiducial markers.

The thesis objectives in each chapter are shown in Table 1.1 and the flow chart of the thesis is shown in Figure 1.2. The dose distribution including geometric uncertainties was determined from the static dose gradient and motion PDF (Chapter 3, published in Jiang *et al* 2007a). Geometric uncertainty was determined from EPID images including fiducial markers for 118 patients; including a study of 20 patients with simultaneous fraction-to-fraction evaluation of setup error and organ motion (Chapter 2, published in Jiang *et al* 2007c). Geometric uncertainties were shown to reduce the static dose gradient and result in a blurred dose gradient (Chapter 3, published in Jiang *et al* 2007a, 2007b). The blurred dose gradient can be maximized by improving the LMDG in the static plan (Chapter 4, published in Jiang *et al* 2006a, 2007d) or by reducing geometric uncertainty during treatment with corrective verification imaging (Chapter 2, published in Jiang *et al* 2007c).

The rectal positional variations were evaluated by equivalent uniform dose per fraction (EUD$_f$) deviations, and NTCP changing with fraction numbers was evaluated with and without motion (Chapter 5, published in Jiang *et al* 2006b).

Table 1. 1: The topics in each chapter of the thesis.

Chapters	Topics
Chapter 1 Introduction (Objective)	PDF for description of geometric uncertainties during radiation treatment
	IMRT optimization and dose calculation incorporating PDF
	Determination of biological effects, EUD$_f$, NTCP with uncertainties
Chapter 2 IGRT	Evaluation of Gaussian PDF (MV EPID with fiducials: 118 patients)
	Bony vs. prostate motion (simultaneous fraction-to-fraction evaluation of setup error and organ motion for 20 patients)
Chapter 3 Dose Calculation Framework	Blurred dose gradient; $\dfrac{\partial D}{\partial \vec{r}} = \dfrac{\partial D_0}{\partial \vec{r}} \otimes PDF$
	Blurred dose profile; $D = \int [G_0 \otimes PDF] d\vec{r} \qquad G_0 = \dfrac{\partial D_0}{\partial \vec{r}}$
Chapter 4 LMDG & IMRT	Improving static LMDG in IMRT optimization
	Reducing uncertainty with corrective verification imaging
Chapter 5 Biological Effect of Motion	EUD per fraction (EUD$_f$)
	NTCP fraction-to-fraction (NTCP$_f$)
Chapter 6 Conclusion	Summary and conclusion
	Recommendation for future work
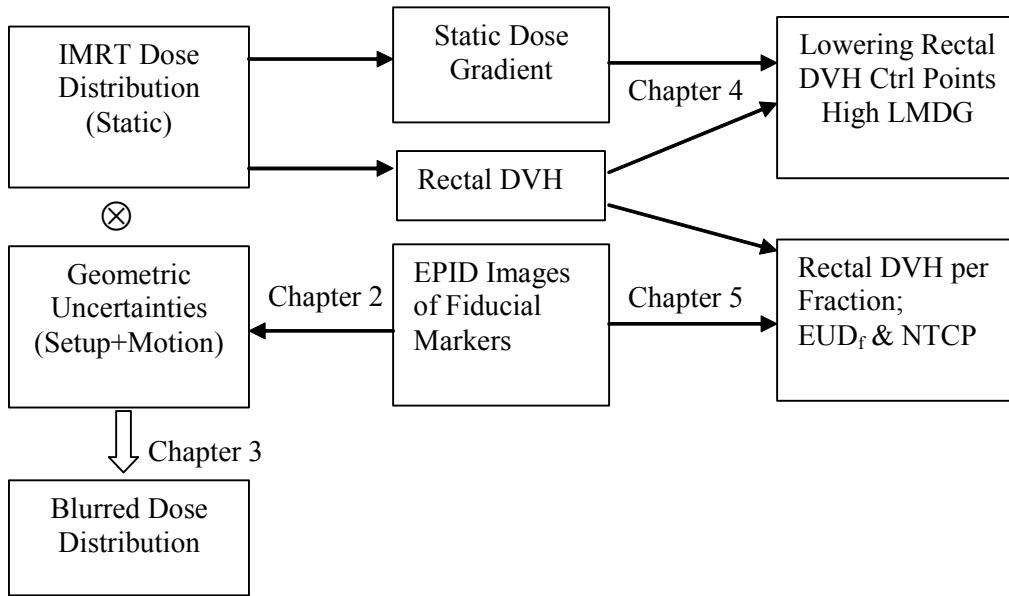
Figure 1. 2: Flow chart of the thesis.

1.2 Uncertainties in Prostate Radiation Therapy

1.2.1 Radiation and radiation biology

Radiation can be classified as directly or indirectly ionizing. All the charged particles, such as electrons, protons, α-particles and heavy charged ions are directly ionizing, that is, provided the individual particles have sufficient kinetic energy, they can directly disrupt the atom structure of absorber through which they pass and produce chemical and biological changes. Electromagnetic radiations (x- and γ- rays) are indirectly ionizing. They do not produce chemical and biological damage themselves, but when they are absorbed in the material through which they pass they give up their energy to produce fast-moving charged particles.

When an x-ray beam (i.e. a beam of photons) passes into an absorbing medium such as body tissues, some of the energy is transferred to the medium where it may produce biological damage. The energy deposited per unit mass of the medium is known as the absorbed dose. The unit of absorbed dose is Gray (Gy). The events that result in this absorbed dose and subsequent biological damage are complicated and illustrated in a simplified way in Figure 1.3 (Johns and Cunningham 1994). The first step involves the collision between a photon and some electron in the body, resulting in the scattering of some radiation and the setting in motion of a high speed electron (Figure 1.3 A). In traveling through the tissue, the high speed electron produced a track along which ionization occurs, excitation of atoms takes place, and molecular bonds are broken (Figure 1.3 B). All of these result in biological damage. Most of the energy is converted into heat, producing no biological effect. Some of the high speed electrons may suffer a collision with a nucleus and produce bremsstrahlung. This bremsstrahlung, as well as the scattered radiation, can undergo interactions in the same way as the original photon.

8

Usually, some 30 interactions are required before all the energy of the photons is converted into electronic motion. The physics of the absorption process is over in 10^{-15} second; the chemistry takes longer since the lifetime of free radicals is about 10^{-5} second; the biology takes days to months for cell killing, years for carcinogenesis, and generations for heritable damage.

X-ray photons interact with the absorber to produce high speed electrons by three important mechanisms known as the photoelectric process, Compton scattering, and pair production. The process by which x-ray photons are absorbed depends on the energy of the photons and the chemical composition of the absorbing material. The biological effects of radiation result principally from damage to DNA, which is the critical target. When any form of radiation is absorbed in biological material, the atoms of the target itself may be ionized or excited, thus initiating the chain of events that leads to a biological change. This is the direct action of radiation. It is the dominant process when radiations with high linear energy transfer (LET), such as neutrons or α-particles, are considered. Alternatively, the radiation may interact with other atoms and molecules in the cell (particularly water) to produce free radicals that are able to diffuse far enough to reach and damage the critical targets. This is the indirect action of radiation. Biological effects of x-rays may be due to direct action (the recoil electron directly ionizes the target molecule) or indirect action (the recoiled electron interacts with water to produce a hydroxyl radical, which diffuses to target molecule).
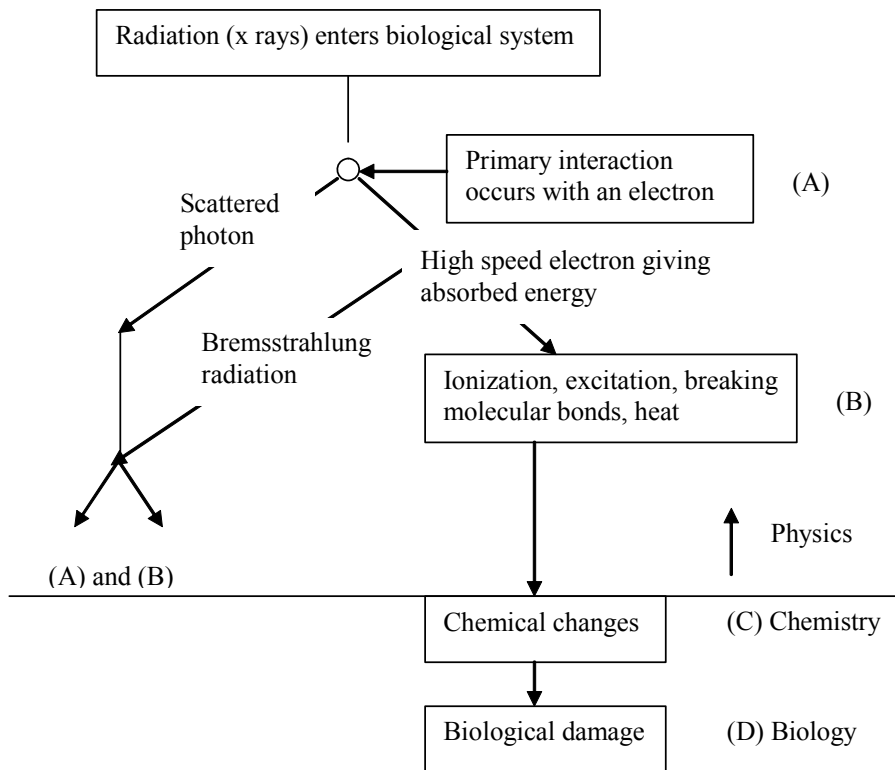
Figure 1. 3: The absorption of energy from radiation resulting in biological damage (Johns and Cunningham 1994).

1.2.2 Prostate cancer and treatment

Prostate cancer is the abnormal growth of cells in a man's prostate gland. The prostate produces semen fluid in the male. Prostate cancer is common in men older than 65. It usually grows slowly and can take years to grow large enough to cause any problems. Most cases are treatable, because they are found with screening tests before the cancer has spread to other parts of the body. Experts don't know what causes prostate cancer, but they believe that the age, family history (genetics), and race affect the chances of getting it, and diet may exert an indirect influence. About 70–75% of prostate cancers arise in the peripheral zone of the gland, mainly in a posterior location, of the remaining cases, 15%

derive from the central zone and 10–15% from the transitional zone (Qian 1997). Prostate cancer may spread locally, by direct invasion of seminal vesicles, urinary bladder or surrounding tissues (Cotran 1999).

A prostate-specific antigen (PSA) test measures the amount of prostate-specific antigen in the blood. PSA is released into a man's blood by prostate gland. Healthy men have low amounts of PSA in the blood. The amount of PSA in the blood normally increases as a man's prostate enlarges with age. PSA may increase as a result of an injury, a digital rectal exam, sexual activity (ejaculation), inflammation of the prostate gland (prostatitis), or prostate cancer. In the past, most experts viewed PSA levels less than 4 ng/mL as normal. Due to the findings from more recent studies, some recommend lowering the cutoff levels that determine if a PSA value is normal or elevated. Some researchers encourage using less than 2.5 or 3 ng/mL as a cutoff for normal values, particularly in younger patients. Younger patients tend to have smaller prostates and lower PSA values, so any elevation of the PSA in younger men above 2.5 ng/mL is a cause for concern.

Prostate cancer is often graded using the Gleason score, on a scale of 2 to 10. The Gleason score is considered a powerful tool for predicting how aggressive a tumor will be. The higher the Gleason score, the more likely the tumor is to grow rapidly and spread (metastasize) to other parts of the body. A Gleason score of 2 to 6 indicates well-differentiated tumors with cells that are expected to grow slowly and not spread readily. A Gleason score of 7 indicates moderately differentiated tumor cells. A Gleason score of 8 to 10 indicates poorly differentiated tumors with cells that are likely to grow rapidly and spread to other parts of the body.

Many kinds of cancer have staging systems that help physicians decide what treatments to choose. The stages of cancer are based on where and how far it has grown. The most common staging system for prostate cancer is the TNM system, which labels the cancer in three categories: the size of the tumor (T), the spread of the cancer to lymph nodes (N), and the spread of the cancer to other parts of the body (M, for metastasis). Besides using the TNM labels, the physician also will give the cancer a Gleason score. A Gleason score

is a way to describe differences in prostate cancer cells. Prostate cancer cells that have a low Gleason score grow more slowly than cells that have a higher score. Once the TNM and Gleason score information is collected, the physician can tell what stage the cancer is in, what treatment is best, and what the outlook is for being cured. The stages of prostate cancer are classified as following:

Stage I: T1a, N0, M0, low Gleason score (2 to 4); the cancer is still within the prostate and has not spread to lymph nodes or elsewhere in the body. The cancer was found during a transurethral resection, it had a low Gleason score (2 to 4), and less than 5% of the tissue was cancerous.

Stage II: T1a, N0, M0, Gleason score of 5 to 10; OR T1b-T2, N0, M0, any Gleason score; the cancer is still within the prostate and has not spread to the lymph nodes or elsewhere in the body, and one of the following applies: it was found during a transurethral resection and has an intermediate or high Gleason score (5 or higher), or more than 5% of the tissue contained cancer; or it was discovered because of a high PSA level, cannot be felt on digital rectal exam or seen on transrectal ultrasound, and was diagnosed by needle biopsy; or it can be felt on digital rectal exam or seen on transrectal ultrasound.

Stage III: T3, N0, M0, any Gleason score (2 to 10); the cancer has begun to spread outside the prostate and may have spread to the seminal vesicles, but it has not spread to the lymph nodes or elsewhere in the body.

Stage IV: T4, N0, M0;OR any T, N1, M0;OR any T, any N, M1 (any Gleason score); one or more of the following apply: the cancer has spread to tissues next to the prostate (other than the seminal vesicles), such as the bladder's external sphincter (muscle that helps control urination), rectum, and/or the wall of the pelvis; and/or it has spread to the lymph nodes; and/or it has spread to other, more distant sites in the body.

There are three risk levels according to the stages of prostate cancer: Favorable risk (T1-T2a): a Gleason score less than 6, and a pretreatment PSA less than 10 ng/mL; Intermediate risk (T2b or T2c): a Gleason score less than 7, or a pretreatment PSA between 10~20 ng/mL,; Unfavorable risk (T3a or higher): a Gleason score: 8 ~10, or a pretreatment PSA higher than 20 ng/mL.

If prostate cancer is truly confined to the prostate, it is curable with surgery or radiation. However, in order to benefit from curative treatment, a patient's life expectancy may need to be 10-15 years. Patients diagnosed with early stage prostate cancer must choose between "watchful waiting", more aggressive treatment with radiation or surgery (radical prostatectomy), or participation in a clinical study. Unfortunately, well-controlled clinical studies comparing these treatment approaches have not been performed. Before making treatment recommendations, physicians who treat prostate cancer consider a number of aspects about the patient's disease that help predict whether the cancer is confined to the prostate (potentially curative) and how fast the cancer will grow. These aspects include the clinical stage of the cancer, the PSA level, and the appearance of the prostate cancer cells under the microscope (the Gleason score). Patients with early stage cancer, lower PSA levels and a low Gleason score have more treatment options available and a better chance of long-term survival.

Grand River Regional Cancer Center (GRRCC) initiated a Stage I/II prospective study of radiation treatment of prostate cancer. Patients with intermediate and low-risk carcinoma of the prostate were identified for radiation treatment in this clinical trial as shown in Figure 1.4. The eligibility criteria included clinical stage T1b, T1c and T2, a Gleason score less than 8 and PSA levels less than or equal to 20 ng/ml. The goal of the study is to reduce acute and late side effects without compromising local tumor control. Dose escalation is proven to be effective for this disease, and IGRT plays an integral role in preparing these patients for accurate, reproducible treatments with daily online image verification.

Prostate cancer

```
┌─────────────────────┐
│  T1b, T1c, T2       │
│  N0, M0,            │
│  Gleason < 8        │
│  PSA ≤ 20 ng/ml     │
└─────────────────────┘
```

Low Risk

```
┌─────────────────────┐
│  T1b, T1c, T2a      │
│  Gleason ≤ 6 &      │
│  PSA ≤ 10 ng/ml     │
└─────────────────────┘
```

Intermediate Risk

```
┌─────────────────────┐
│  T2b or             │
│  Gleason 7 or       │
│  PSA > 10 ng/ml     │
└─────────────────────┘
```
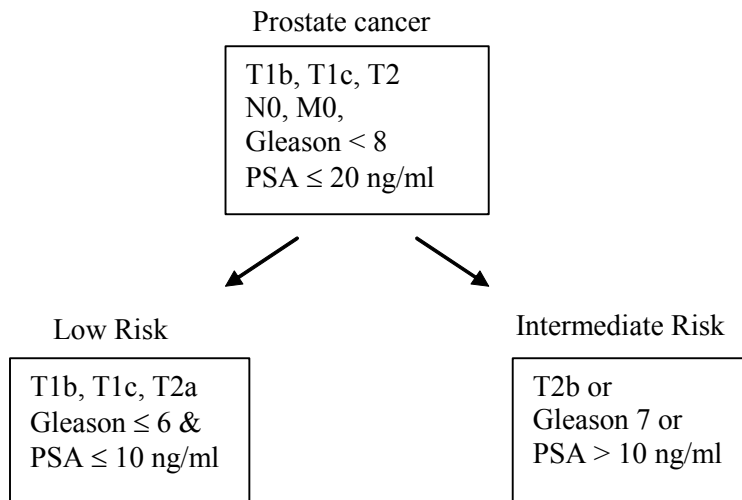
Figure 1. 4: Radiation treatment at GRRCC for low and intermediate risk prostate cancer.

1.2.3   Characterization of geometric uncertainties

Geometric uncertainties are separated into two categories: variations in the positioning of the patient's bony anatomy with respect to the beam axes (often referred to as setup errors), and variations in the position of the target within the patient with respect to the bony structures (often referred to as organ motion).

Most of the geometric uncertainty studies in external-beam radiation therapy have been performed using portal imaging to assess setup errors during treatments. Orthogonal Megavoltage and Kilovoltage imaging, with or without fiducial markers, can decrease setup error and target margins. The verification imaging, obtained before, during, or after treatment, records a patient's position at the time of radiation therapy. It can guide the radiation beam and lead to repositioning of the patient prior to irradiation if misalignments are detected. Image-guidance strategies used to reduce setup error are generally classified as either online or offline procedures. An online approach acquires

and assesses information from daily imaging, typically before every treatment fraction. Simple corrections are implemented to compensate for deviations in patient's position that exceed a predefined threshold before radiation delivery. An offline strategy refers to frequent acquisition of images without immediate intervention. When enough fractions have been administered (typically three or more), an offline statistical analysis calculates the systematic (mean) and random (standard deviation) components of the patient's setup error. A correction for systematic error can be implemented for the remaining treatment fractions. Online correction strategies achieve a larger reduction in geometric errors compared with offline approaches, but require spending more effort and time at treatment delivery and require a higher imaging dose. With offline and online approaches, clinicians can re-plan an individual's treatment during the radiation therapy course to account for patient-specific information acquired with image guidance. This practice is referred to as adaptive radiation therapy (ART). The reported magnitude of setup error is most certainly influenced by the particular setup technique performed at the particular institution.

Many authors have reported on the uncertainty in the location of the prostate relative to bony anatomy. It is difficult to give any concrete comparison from the various studies because of the differences in methods and analysis employed by the authors. The characterization of prostate motion is difficult, and the small numbers of patients limit the scope of conclusions that can be drawn from any particular study. The reported range of organ motion varied by a factor of nearly 10 (Jaffray 1999). In a review of organ motion studies, Kutcher (1995) *et al* suggest that the larger number of data sets should be acquired to better characterize the motion and its dependence on other factors. Investigators have recommended caution in interpreting the results of organ motion studies. The variability in the reported results makes interpretation difficult. It is expected that the discrepancies among these studies are due to uncontrolled variables, such as changes in intra-abdominal pressure due for example to gas in the bowel, filling of the bladder, unspecified conditions, the use of immobilization cradles or the position of the patient.

1.2.4   Managing uncertainties with safety margins: ICRU formalism

One of the important factors that has contributed to the success of 3D CRT is the standardization published in the International Commission on Radiation Units and Measurements (ICRU) Reports 50 and 62 (ICRU report 50 1993, ICRU report 62 1999). The reports gave the radiation oncology community a consistent nomenclature and a methodology for image-based treatment planning in which the physician specifies the volumes of tumor: GTV; clinical target volume (CTV): the volumes of suspected microscopic spread; and PTV: the marginal volumes necessary to account for setup variations and organ motion.

ICRU Report 62 defined PTV by introducing the concept of an internal margin (IM) to take into account variations in size, shape, and position of the CTV in reference to the patient's anatomic reference points, and also the concept of a setup margin (SM) to take into account all uncertainties in patient-beam positioning in reference to the treatment machine coordinate system. IM uncertainties are caused by physiologic variations (filling of rectum, motion etc) and are difficult or almost impossible to control from a practical point of view. SM uncertainties are related largely to technical factors that can be dealt with by more accurate setup and immobilization of the patient and improved mechanical stability of the machine. The internal target volume (ITV) represents the movements of the CTV referenced to the patient coordinate system and preferably should be rigidly related to bony structures.
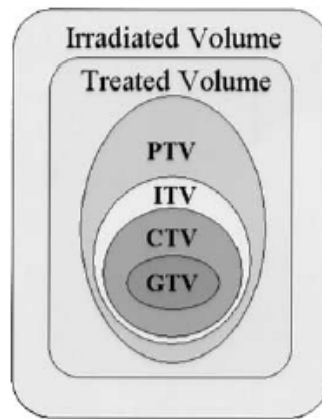
Figure 1. 5: Schematic illustration of the volumes defined by ICRU Report 62: GTV, CTV, ITC, PTV, treated volume, and irradiated volume.

GTV, CTV, ITC, PTV, treated volume and irradiated volume defined by ICRU Report 62 are illustrated in Figure 1.5. Report ICRU 62 defined two dose volumes: the treated volume and the irradiated volume. The treated volume is the tissue volume that is planned to receive at least a dose specified by radiation oncology as being appropriate to achieve the purpose of the treatment; the irradiated volume is the tissue volume that receives a dose that is considered significant in relation to normal tissue tolerance. Purdy (2002, 2004) reviewed the development of the current ICRU volume definitions, and discussed the issues and compromises required when using these definitions in 3DCRT and IMRT planning.

Safety margins can be decided based on geometric considerations. The simplest of these is to statistically select a margin as some number of standard deviations (SDs) of motion outside the target volume. The more sophisticated approach is presented by van Herk (2002) *et al*, in which they concluded that there is a substantial difference in systematic errors as compared with random errors, leading to an overall margin that is about a factor of 2 larger than that proposed by Goitein (1983). McKenzie *et al* (2002) propose a margin around OAR that is half the size of that which they propose to place around the target volume.

Large margins result in a high level of confidence that the CTV is adequately covered during treatment. Narrower margins and more conformal dose distributions are helpful to reduce the dose to the normal tissues and complications, but may on the other hand risk violation of the PTV concept. IMRT dose distributions can be shaped to conform much more closely to the PTV and to avoid OAR, thus introducing sharp dose gradients on the edge of the PTV. IMRT treatments are more sensitive to geometric uncertainties (Jaffray *et al* 1999). The uncertainties may result in tumor underdose or normal tissue overdose. Factors that primarily affect positional uncertainty in target and OAR are errors in target delineation, patient positioning or setup errors, and internal organ motion.

Although much attention in recent years has focused on organ motion and setup error, errors in delineating the gross and clinical target volumes should also be considered when determining planning target volume margins. A number of studies (Roach *et al* 1996, 1997, 1999, Tai 2002) have shown that there can be large differences in image interpretation among physicians and institutions. A lack of delineation protocols and understanding of radiological anatomy are frequent and important sources of error. It is known that the shape and size of the GTV can depend significantly on the imaging modality (Roach *et al* 1996, 1997, 1999). Roach *et al* (1996) compared the delineated prostate volumes using both CT and MRI for a series of patients and found significant volume differences in approximately one third of the cases, depending on the imaging modality used. Rasch *et al* (1997) concluded that MRI derived target volumes had less inter-observer variation than CT-only derived target volumes. In another study, Rasch *et al* (1999) compared GTVs defined using both CT and MRI, the target volume defined using CT and MRI was different than the volume defined using CT alone.

With regard to organ motion, a review by Langen *et al* (2001) provided the most comprehensive compilation of organ motion data. Inter-fraction organ motion studies have focused mainly on the treatment of prostate cancer (Balter 1995, Roeske 1995, van Herk 1995, Althof 1996, Tinger 1998, Jiang 2007c) as shown in Table 1.3, whereas intra-

fraction motion studies have focused on variations caused by respiratory motion (Balter 1998, Hanley 1999) for disease in the thoracic and upper abdominal regions.

Table 1. 2: Prostate motion specified as one SD (mm) in the AP, LR and SI directions.

Prostate Motion (1 SD) (mm)	AP	LR	SI
Jiang *et al* , seeds (2007c)	2.6	1.4	3.0
Alasti *et al*, seeds (2001)	5.8	-	3.3
Althof *et al*, seeds (1996)	1.5	0.8	1.7
Antolak *et al*, CT (1998)	3.6	0.7	3.6
Balter *et al*, seeds (1995)	2.3	0.9	1.9
Crook *et al*, seeds (1995)	4.1	1.5	5.0
Litzenberg *et al*, CT (2002)	2.4	1.9	2.1
Melian *et al*, CT (1997)	4.0	1.2	3.1
Roeske *et al*, CT (1995)	3.9	0.7	3.2
Rudat *et al*, CT (1996)	3.7	1.9	-
Schiffner *et al*, CT (2007)	2.1	0.9	2.4
Tinger *et al*, CT (1998)	2.6	0.9	3.9
Van Herk *et al*, CT (1995)	3.8	1.3	2.4
Vigneault *et al*, seeds (1997)	3.5	1.9	3.6
Wu *et al*, seeds (2001)	2.3	-	2.1

The setup uncertainty is due to an inability to control all factors that influence the setup, such as weight loss, discomfort, tension, inconsistent full or empty of bladder and rectum etc. These factors may cause patient to a poor setup; and large setup error could lead to significant errors in dosimetric coverage of the target volume and possible overdosing of normal tissues in the dose escalation with conformal treatments. Herman (2001) surveys the clinical uses of electronic portal imaging device. Although the most widespread use has been to verify and correct positioning of skeletal anatomy, it has been increasingly used in prostate localization and correction with implanted fiducials.

The relationship between targeting uncertainty and choice of treatment margin has been reviewed by Kutcher (1995) *et al*. The margin used to create the PTV should not just be based strictly on target geometric uncertainty considerations, the OAR should also be taken into account. The margin is the result of tradeoffs that balance concerns for potential geometrical miss versus unacceptable toxicity. A serious limitation currently present with some IMRT planning systems occurs when a PTV overlaps with an OAR. The basis for choosing a margin between a tumor and OAR should not just be purely physical considerations, but also a biological consideration. An analysis using TCP and NTCP would be a natural way of approaching this problem. Herring (1970) *et al* summarized the sensitivity of tumor control and normal tissue complication rates to dosimetric variations. The dose delivered over the course of treatment should be within ± 5%. Achieving this level of accuracy and precision requires that each step of the treatment process much be better than 5%. This requirement places stiff tolerances on both the precision of the clinical dosimetry and the geometric precision in delivery and planning. To achieve and maintain the desired level of precision, it is recommended that a system of treatment delivery be constructed that considers both dosimetric and geometric uncertainty factors. However, it is uncertain whether TCP/NTCP models correctly represent dose-response under conditions of inhomogeneous dose distributions often encountered in IMRT, especially in the case of when some part of the normal tissue is exposed to a small region of high dose (i.e. overlap with the tumor). Therefore, any optimization result based on biophysical modeling must be interpreted with great caution.

1.3   Image Guided Radiation Therapy (IGRT)

1.3.1   Setup error and organ motion

External-beam radiation therapy is a major treatment modality for prostate cancer. The treatment course typically consists of many fractions over several weeks. Geometric and anatomic variations occur throughout the treatment process. These uncertainties include setup error and organ motion. The prostate gland is located between the rectum and the bladder, the contents of which may change from day to day. The prostate position as well as its shape can change from fraction-to-fraction because of filling and emptying of the bladder and rectum.

Previous studies that utilized multiple CT scans (Roeske 1995, Antolak 1998, Deurloo 2005) during the treatment course showed that the organ motion is largely of random nature, although some evidence suggests radiation-induced changes occurring during a treatment course (Mechalakos 2002). In addition, setup errors based on marks placed on skin or immobilization device can be larger because the target depth for prostate cancer is greater than that for other tumor sites. These uncertainties can be either compensated for by use of safety margins or reduced by use of image guidance.

To compensate for uncertainties, the ICRU recommends use of margins in treatment planning (ICRU report 50 1993, ICRU report 62 1999). Setup error can be measured by a comparison of megavoltage (MV) portal images, obtained from an EPID, with reference digitally reconstructed radiographs (DRRs) based on bony structures (Wong 1995, Herman 2001). The uncertainties caused by prostate motion are more complicated. Studies have shown that prostate motion can be up to a few centimeters from fraction-to-fraction (Balter 1995, Crook 1995). Both inter-fraction and intra-fraction organ motion

can have a significant impact on treatment delivery if they are not accounted for. Prostate motion cannot be easily detected by use of an EPID because of the low soft-tissue contrast. Radiopaque markers implanted inside the prostate gland have been used to help localize the moving target by use of EPID (Litzenberg *et al* 2002, Herman *et al* 2003, Jiang *et al* 2007c). This is the technique used in this work.

Advancements in linear accelerator (Linac) design, especially the introduction of kilovoltage X-ray tubes and flat-panel detectors make CBCT available at GRRCC recently. CBCT offers many opportunities for image-guided radiation therapy (IGRT). Jaffray (2002) surveyed 3 dimensional (3D) image-guided treatment systems and describes their early clinical experience. The importance of IGRT was emphasized by Millender and colleagues (2004) in a series of obese men with prostate cancer. Factors to compare correction technologies include accuracy, workload and patient tolerance etc. For example, online corrections may be preferred if they can be performed rapidly. The time required for measurement and correction can affect accuracy because of patient discomfort and internal organ motion. Large skin doses can occur with frequent kilovoltage image guidance in some circumstances.

1.3.2 Data acquisition: DRR and electronic portal imaging device (EPID)

In our study, patients were instructed to arrive for the planning CT one week after implantation with a full bladder and empty rectum. Three tattoos are then placed on the anterior, right and left lateral pelvis after the CT scan. On each treatment day patients are positioned using laser alignment to the marks on their skin, as well as the immobilization device. The therapist acquires one pair of orthogonal EPIs using the AP and LR setup fields and these constitute the comparison image set. Using both pairs of images, on-line repositioning of patients is accomplished through image matching using Varian Portal-Vision software. A total of 4878 electronic portal images from 118 patients were acquired

over the course of the study. The data were used to analyze center of mass seed displacements relative to the isocenter. The daily on-line repositioning of the patients (calculation of the repositioning displacements) was accomplished through image matching using Varian Portal-Vision software. In order to study the displacement of bony anatomy relative to the isocenter and prostate relative to bony anatomy, an in-house built localization software (Proloc) was used to get the data of forty simulated DRRs and 1284 EPIs for 20 prostate patients. The software is capable of determining mismatch between EPI and DRR using either seeds or bony anatomy. In 'seed mode' the three positions of the projected seeds are selected on both the DRR and the EPI and the software compares the selected positions on the EPI to the same positions on the DRR and then determines the required displacement in the anterior-posterior (AP), left-right (LR) and superior-inferior (SI) directions. Using the same set of patient images and in 'bony anatomy mode', two reproducible bony anatomy pair points are selected on both the DRR and EPI. The software once again aligns the points on the two sets of images and determines the required displacement in the AP, LR and SI directions.

1.3.3 Statistical analysis of IGRT image data

High geometrical precision and accuracy is a prerequisite for a safe clinical application of conformal radiation therapy. Several factors contribute to the overall treatment accuracy. The error was used to describe any deviation between planned and delivered treatment. The statistical analysis of pool data for all the fractions of the patient group was use to obtain Gaussian PDF (GPDF) with mean and standard deviation (SD) (Rudat 1996). Another way to express error involves the group mean and SD of all patients' means (van Herk 2004). For each patient, the mean and SD of the daily measurements are first obtained per patient. The group mean (M) is the mean of individual patients' means; the SD of the individual patients' means (Σ) and the root mean square (RMS) of the individual patients' SDs (σ) were used to characterize the systematic error and random error.

As mentioned previously, a total of 4878 electronic portal images from 118 patients were extracted over the course of the study. The mean (M), standard deviation (Σ) and RMS (σ) of gold seed displacement relative to isocenter were studied and analyzed, which combined the setup error and organ motion. Data from the 20 patients were evaluated for setup error and prostate motion fraction-to-fraction simultaneously. Three data sets: seed displacement relative to beam isocenter, bony displacement relative to beam isocenter, and prostate displacement relative to bony anatomy, were analyzed and compared.

1.4 IMRT Optimization and Dose Gradients

1.4.1 Prostate IMRT protocol

Dose escalation through 3D-CRT is widely recognized as an effective treatment approach in the management of prostate cancer. Improvements in local control have been shown when doses 76 Gy are applied (Lu 1995, Hanks 1998 1999 2000, Horwitz 2001, Zelefsky 1998 2002a) compared to doses in the conventional range (70Gy). This benefit is particularly evident for patients with intermediate and high-risk prognostic factors, but has also been shown for patients with favorable prognostic factors (Vicini 2001, Zelefsky 2002a). Late rectal toxicity with rectal bleeding is a well-known complication of high-dose 3D-CRT (Hartford 1996, Michalski 2000, Skwarchuk 2000, Shu 2001, Chism 2003). The biological mechanisms of radiation-induced damage are still not entirely understood and have been the topic of an extensive review (Denham 2002). Several reports have clearly indicated a significant dose–volume dependence of late rectal injury (the so-called volume effect) (Cheng 1999, Jackson 2001b, Wachter 2001, Fiorino 2002b, Huang 2002b, Chism 2003).

IMRT may prove efficacious by enabling consideration of dose escalation, by reducing margins and radiation exposure to dose-limiting normal tissues (Zelefsky 2002a, 2002b). IMRT offers a great flexibility to deliver dose to any desired volume. Organs at risk may potentially be effectively spared while still reaching high target dose coverage. However, it is difficult to exploit this flexibility when the margin is in the volume of intersection of PTV and OAR, such as the case of prostate. In order to keep rectal toxicity at acceptably low levels, knowledge of the dose volume relationship within a specific patient population must be acquired for a certain treatment setup, so that appropriate treatment constraints may be confidently applied (Lyman 1987, Kutcher 1996). DVHs have been used as an invaluable tool to evaluate the quality of a treatment plan. The DVH constraints for PTV and OAR in IMRT optimization are shown in Figure 1.6. The type includes: the minimum dose @ 100% volume DVH; maximum dose @ 0% volume DVH; minimum and maximum DVH applies to percentage volume of PTV and OAR. DVH data from these studies clearly indicate that the percent volume of rectum exposed to doses above 60–70 Gy plays a crucial role in determining radiation-induced rectal morbidity. It may also be expected that the anatomical definition of the rectum and variations in contouring may have a significant impact on the relationship between rectal DVH and late treatment morbidity (Fiorino 2002a). Although DVHs are important planning parameter and are linked TCP and NTCP, they do not contain spatial information about the dose distribution and are therefore not as effective as the dose gradient (Jiang *et al* 2007a). The convergence of the optimization algorithm will be determined by specific constraints in the objective function; however dose gradient is easier to interpret as a "limiting" parameter. Dose gradient analysis in this study is completely general and is independent of optimization algorithm.
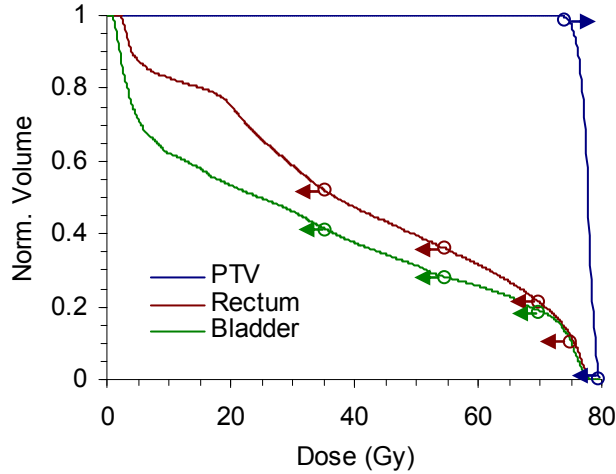
Figure 1. 6: DVH constraints for PTV and OAR in IMRT for optimization.

1.4.2 Dose gradients in IMRT dose distribution

In practice, IMRT treatment planning is performed using a proprietary optimization algorithm and a custom optimization objective function including weighted dose constraints and DVH control points for the PTV and OARs. The DVH is a valuable tool for plan evaluation and optimization in the 3D treatment planning; also DVHs are linked to TCP and NTCP. However, the DVH curve cannot provide spatial dose information about the distribution of dose and are therefore not as effective as the dose gradient. For a given planning protocol, e.g. RTOG 0126 (Michalski 2004), the IMRT solutions from different institution and commercial treatment planning system will not be the same and it is therefore important to continue to specify the spatial dose distribution, including dose gradients as an indicator of how conformal the dose coverage actually is (Jiang *et al* 2007a). The dose gradient is the rate change of dose profile along specific direction (the slope of the dose fall in that direction). Relating the targeting uncertainty to dosimetric variation depends on the gradients in the dose distribution produced in the patient; the most significant variations are at the periphery of the target volume. Novel beam delivery

systems allow highly conformal dose distributions to be produced within the patient. IMRT dose distributions are shaped to conform more closely to the PTV and avoid normal tissues, introducing large gradients at the boundary of PTV and normal structures. The steeper the dose gradients outside the PTV, the more sensitive the treatment will be to geometric uncertainties. The basic strategy is sketched in Figure 1.7. Differential dose effects can be achieved between tumor and normal tissue, using strong dose gradients.
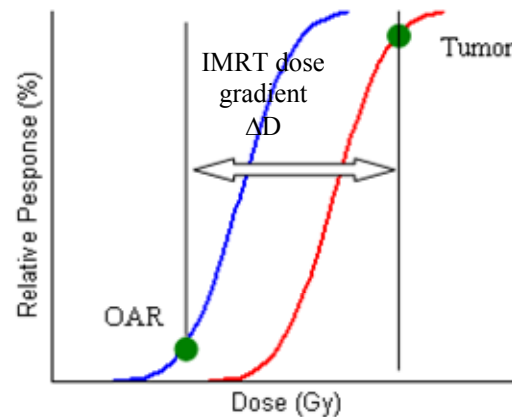
Figure 1. 7: Tissue response for tumor and OAR.

1.4.3 The impact of geometric uncertainties on dose gradients

The effect of organ motion and positional uncertainties on the dose distribution can be estimated by convolving of the 'static' dose distribution initially obtained from the treatment planning system, with a PDF describing the geometric uncertainty of the anatomy. This approach was first proposed by Leong (1987) and subsequently applied by many investigators (Lind 1993, Rudat 1994 1996, Bel 1996, Keall 1999, Lujan 1999a 1999b, Stroom 1999, Li 2000, McCarter 2000, McKenzie 2000a 2000b, van Herk 2000

2002, Booth 2001, O'Dell 2002, Jiang *et al* 2007a). Although the convolution method is a well-known and generally accepted method in radiation therapy, the limitations of a convolution method for modeling geometric uncertainties in radiation therapy must be noted (Craig 2003a, 2003b). Convolution requires several assumptions, this including that the patient is treated with an infinite number of fractions, each delivering an infinitesimally small dose; also convolution assumes shift invariance of the dose distribution, while internal inhomogeneities and surface curvature lead to violations of this assumption. Convolution can accurately estimate plan evaluation parameters for treatments of approximately 20 or greater fractions. In this study, the fraction numbers are over 30 fractions. The errors are largest near the surface due to the discontinuous nature of the dose distribution. In clinical examples, errors are small for a deep-seated tumor or critical organ, such as with prostate patients. Errors due to the presence of inhomogeneities appear negligible (Craig 2003a, 2003b).

Most of the organ motion studies give the mean and standard deviation of motion in three orthogonal coordinate directions (Balter 1995, Crook 1995, Roeske 1995, van Herk 1995, Althof 1996, Beard 1996, Melian 1997, Dawson 1998, Zelefsky 1999). Doses at points along the anterior-posterior line through the isocenter were used to define the anterior and posterior doses for each patient, and the same method was used for the lateral and superior inferior directions. Geometric uncertainties can be incorporated in the treatment planning process provided that PDF of the geometric uncertainties can be estimated. In this work, dose gradients were obtained in the transverse and sagittal planes and analyzed to find the relationships between dose gradient and organ motion dose sensitivity (OMDS), TCP and NTCP.

1.5   Rectal DVH Control Points and Dose Gradient

1.5.1   Prostate IMRT treatment planning

IMRT Treatment plans were created for fifteen prostate patients and planned for supine patient treatment using a 6 MV photon beam from Varian 21EX linear accelerator (Varian Medical Systems, Palo Alto, CA). The prostate IMRT inverse treatment planning was optimized with a coplanar, isocentric five-field (5F: 0°, 72°, 144°, 216°, 288°) and seven-field (7F: 40°, 80°, 110°, 250°, 280°, 310°, 355°) techniques. An escalated 82 Gy prescription dose (2 Gy per fraction) was used for all IMRT plans. DVH control points for the PTV and OARs were adapted from RTOG 0126 (2004). The relative weights and DVH control points were adjusted for OARs for the IMRT plans. All patients were planned using the same objectives and constraints for PTVs and bladder but different for rectum as shown in Figure 1.8. Rectal DVH control points were lowered down as much as possible without compromising PTV. For each PTV, 3D uniform margins of 10 mm were used and compared with non-uniform margins of 5mm in posterior direction and 10mm margins in other directions.
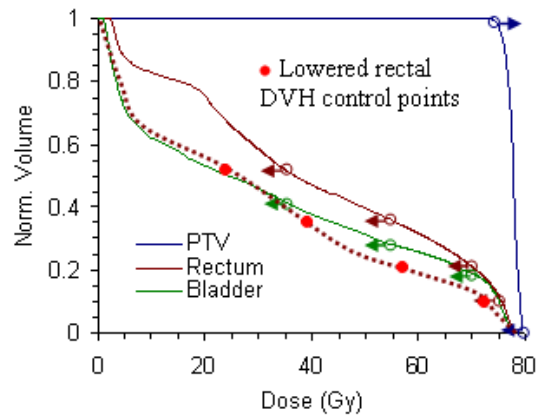
Figure 1. 8: Lowered rectal DVH control points in IMRT for optimization.

1.5.2 Local maximum dose gradient (LMDG)

The dose gradient is defined as the derivative of the dose profile along specific direction. The dose gradient used in this study is the absolute dose gradient (Gy/cm), and is determined at the isocenter along a specific direction in the sagittal plane in vicinity of posterior directions as shown in Figure 1.9. The magnitude of the dose gradient will tell how fast the dose falls in the specific direction. The local maximum dose gradient is the maximum dose gradient along the dose profile as shown in Figure 1.10, which was used to find the relationships with rectal dose, mean dose and NTCP.
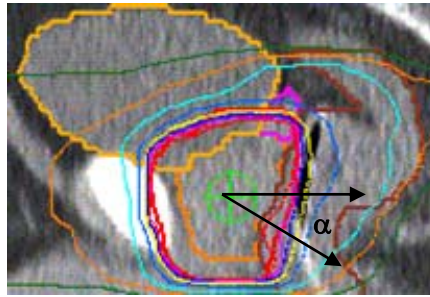
Figure 1. 9: The dose profile in sagittal plane in vicinity of posterior direction.
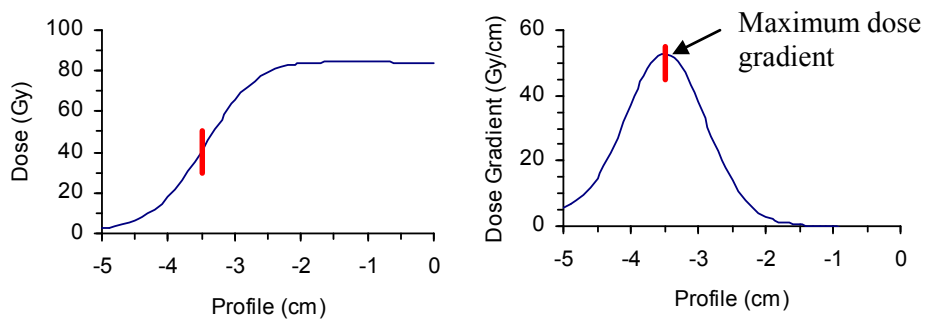
Figure 1. 10: Maximum dose gradient along a dose profile.

1.5.3 The impact of LMDG on NTCP

The IMRT prostate treatment plan uses specific control points in the rectum and bladder DVH curves to set the treatment dose level (Yan 2000, Martinez 2001). The target dose is prescribed to meet the predetermined rectum and bladder constraints based on different dose volume limitations of rectum and bladder. A lack of knowledge about safe dose volume constraints may lead to inappropriate dose delivery with IMRT: excessively

cautious rectum sparing may increase the risk of missing the target, whereas the irradiation of large fractions of rectum may result in patients' experiencing moderate/severe bleeding. A precise understanding of the tolerance of rectum in prostate treatment is essential because it determines the dose to the target.

The relationships between rectal dose volume data and clinically observed rectal complications have been investigated and reported. However, few studies specify the spatial dose distribution, such as dose gradient as an indicator of how conformal the dose coverage actually is and its effect to the target and normal tissue (Jiang *et al* 2006a, 2007a, 2007b). No one has previously focused on dose gradient as end points of commercial optimization protocols. For a given planning template, e.g. RTOG 0126 (Michalski 2004), the IMRT solutions from different commercial planning system will not be the same and it is therefore important to specify the dose gradient as an indicator of how conformal the dose coverage actually is. Although DVHs are important planning parameter and are linked to TCP and NTCP, they do not contain spatial dose distribution information and are therefore hypothesized to be less effective than the dose gradient presented in this work.

1.6   Cumulative Rectal Dose Considering Rectal Movement

1.6.1   Rectal movement in AP direction

Repeated portal images and gold seeds data were used to characterize daily prostate patient organ motion for 20 prostate patients (Jiang *et al* 2007c). The geometric uncertainties of prostate and rectum were assumed to be rigid body displacement; the calculation of rectal dose is based on a rigid-body model of localization uncertainty

involving translations of the prostate and rectum relative to a fixed dose distribution. The rectum was shifted in AP direction according to the prostate AP motion. IMRT plans for these 20 prostate patients were made with prescribed dose $D = 78$ Gy (2 Gy per fraction) using 15MV photon beam. PTV includes the prostate plus a 10 mm margin in the anterior, left-right, superior-inferior directions, and 7mm in posterior direction. The DVH of one fraction plan was obtained using the Pinnacle[3] treatment planning system for five-field (5F: 0°, 72°, 144°, 216°, 288°) and seven-field (7F: 40°, 80°, 110°, 250°, 280°, 310°, 355°) IMRT. The possible rectal DVHs considering rectal movement in every fraction were used to calculate the rectal equivalent uniform dose in every fraction.

1.6.2 Fractional EUD (EUD$_f$)

When considering non-uniform dose distributions, the DVH must be converted to an effective homogeneous dose to total volume as shown in Figure 1.11. The EUD algorithm uses the power-law relationship (Niemierko 1997), and the EUD in each fraction is called fractional equivalent uniform dose (EUD$_f$) (Jiang *et al* 2006b). The EUD$_f$ for the rectum was calculated for each fraction according to the rectal AP movement over the course of treatment and used to calculate the NTCP for the rectum for the course of treatment. This model can produce the cumulative dose for the rectum incorporating motion, and the effect of the rectal motion on the cumulative rectal dose and risk can be assessed during the course of treatment.

$$EUD = \left(\sum_i v_i D_i^{\ a} \right)^{\frac{1}{a}}$$
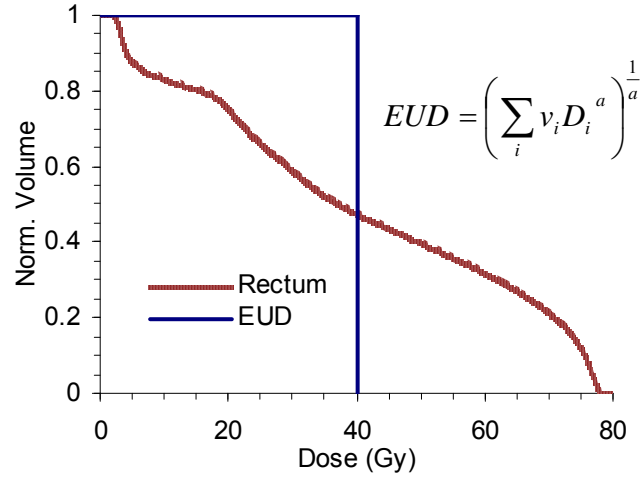
Figure 1. 11: Rectal DVH and EUD.

1.6.3 Evaluating rectal NTCP fraction-to-fraction

DVH of the rectum is affected by a number of uncertainties and limitations; for example, the dose delivered to normal structure is conventionally assessed using dose distribution calculated from a single CT scan taken prior to the planning treatment scan. Complication arising from treatment is usually evaluated in terms of dose-volume histogram and NTCP. While dose distribution delivered to the rectum for prostate patient over the course of treatment is different from planned dose distribution because of the uncertainties such as patient setup error, rectal movement with respect to the bony anatomy, the delineation of the rectum, and the filling of rectum etc (Urie 1991, Webb 1997, Fiorino 2002, Stasi 2006) and it is necessary to study the impact of organ motion on the rectal cumulative dose.

Advanced planning and delivery techniques make dose escalation possible to spare normal tissues while maintaining target coverage. Dose escalation is further encouraged by the study results that higher target doses improve local control without increasing normal tissue toxicity (Zelefsky, 1998). However, the fluctuation of the internal organ

motion with respect to the bony anatomy fraction-to-fraction is associated with this multi-fractional treatment. Rectal movement causes considerable dose uncertainty over the course of treatment and leads to the differences between planned dose distribution and the dose distribution that is actually delivered to the rectum. The most important limitation of analyzing dose to the rectum lies in the fact that the rectum moves during the course of treatment, both by distorting and by moving bodily (i.e. in the AP direction).

Studies of patients with multiple CT scans taken during treatment for prostate cancer (Balter 1995, Mageras 1996, Melian 1997, Lebesque 1995, Roeske 1995, van Herk 1995) showed that the rectum can move 1 cm in the anterior-posterior direction with respect to the bony anatomy. Recently, ART using both online and offline correction schemes have been used for compensation of patient setup errors and organ motion (Lo¨f 1998, Yan1998). The calculation of dose is typically based on a rigid-body model of localization uncertainty involving translations (Killoran *et al* 1997) of the entire patient relative to a fixed dose distribution. Although the rectal movement is obvious for the rectum during a course of treatment for prostate cancer, it is not clear what kind of influences these variations might have on the predictive value of NTCP for the course of treatment. Few study reported the dosimetric consequences of the rectal movement. In this study, the rigid body model and serial portal imaging data were used to reproduce the cumulative dose distribution to the rectum considering internal organ motion using the fractional treatment plan method for prostate patients.

The uncertainties of the internal organ motion result in variation of the delivered dose and can be evaluated fraction-to-fraction using EUD_f. The rectal positional variations can be measured from portal imaging with gold seeds for prostate patients and expressed as EUD_f deviations. This evaluation is performed by comparison of the dose-volume histogram per fraction, the rectal EUD_f considering organ motion, and NTCP, with and without considering the internal organ motion.

Chapter 2

IGRT Patient Study: Tracking Prostate Motion with Implanted Fiducials and MV EPI

Minimization of setup errors and localization of the prostate within the patient are critical components of three-dimensional (3D) conformal radiation therapy (CRT) of prostate cancer with escalated dose. Setup error and organ motion were studied and analyzed for 118 patients who were treated with image-guided radiation therapy (IGRT) using electronic portal image (EPI) and implanted three gold seeds within the prostate, in which 20 patients were analyzed for setup error and prostate motion. Setup errors and gold seed displacements were determined from bony anatomy and gold seeds mismatch between the EPI and the simulation digitally reconstructed radiograph (DRR) respectively. Prostate motion relative to bony anatomy was determined by the difference between gold seed displacement and bony anatomy displacement. Daily on-line repositioning of patients was accomplished through image matching using Varian Portal-Vision software. The setup error and organ motion were compared fraction-to-fraction statistically. Image-guided implanted gold seeds play a vital role in radiation therapy and will continue to be a reliable tool for prostate localization and minimization of setup errors. The reported positional variances are independent of treatment technique, and can be used to determine PTV margins using recipes reported in the literature.

2.1   Introduction

Advances in radiation therapy technology enable higher precision treatments; however, as dose distributions become more conformal they may become more sensitive to treatment uncertainties, such as setup errors and organ motion. The developments in imaging modalities and computer algorithms have made quantitative measurements of treatment uncertainties possible, which have led to new strategies for reducing as well as incorporating uncertainties into the treatment planning process. The number of studies has increased significantly since the advent of electronic portal imaging device (EPID), which have become an important tool for studying setup error. Computed tomography (CT) scanners are also becoming commonplace, permitting studies of uncertainty in organ location based on repeat CT scans. Kilo-voltage or Mega-voltage cone beam computer tomography (CBCT) or kilo-voltage on-board imaging (OBI) systems are currently being employed for target volume localization.

During treatment, the patient is aligned on a flat couch using the skin tattoos. The reproducibility of "virtual isocenter" is based on the agreement between the relative position of the anatomy at treatment and that of CT simulation. Daily alignment with lasers on external skin tattoos, and a weekly set of portal films for bony anatomy alignment has been a standard technique to reduce setup errors during radiation therapy. However, the outer patient skin markers are not accurate fiducial reference for internal structures, and hence more accurate position verification is based on internal fiducial markers. The use of radio-opaque gold seeds implanted in the prostate and visualized daily using EPIDs has therefore been employed to reduce both setup error and organ position variations and continue to provide accurate and efficient method for prostate localization (Wu *et al* 2001, Aubin *et al* 2004, Van den Heuvel *et al* 2006, Jiang *et al* 2007c).

Interest in setup errors and organ motion has grown quickly over the last decades, driven by medical needs and technological advances. Setup errors have been of continuing

interest in radiation oncology over the past decades (Alasti *et al* 2001, Nederveen *et al* 2002, Rudat *et al* 1996). The number of setup studies has further increased significantly since the advent of EPIDs, which have become an important tool for studying setup error. Rational protocols that balance cost and efficacy have been developed to reduce and control setup errors (Kutcher *et al* 1995, Hurkmans *et al* 2001).

Organ motion is inherently more difficult to correct than setup error. Organ motion refers to the variation of organ position and shape relative to the skeletal anatomy. During a single treatment, intra-fraction organ motion can be caused by breathing, heartbeat, swallowing, and peristaltic motion. Between treatments, inter-fraction organ motion may be caused by variable filling of the bladder and rectum, weight gain or loss, and other factors. The reported range of prostate motion varied significantly and comparison between studies is complicated due to different imaging procedures and tracking methods used by various researchers. Ten Haken *et al* (1991) have compared in 50 patients of CT-based treatment plans and showed a range from 0 to 2 cm and an average of 0.5 cm of prostate movement, mostly in the anterior and/or superior direction. Melian *et al* (1997) performed four serial CT scans over a 5 ~ 6 week period on each of 12 patients. Target shifts of 0 to 3.0 cm in the anterior-posterior (AP) were observed and were correlated primarily with bladder filling. Forman *et al* (1993) examined patients who received CT scans on a weekly basis over the treatment course. An initial study of five patients showed an average prostate and seminal vesicle movement of 1.7 cm (range 0 to 3.5 cm), primarily in the AP direction. Beard *et al* (1996) examined movement of the prostate and seminal vesicles, for 12 patients who underwent two CT scans 4 weeks apart in the supine position. The greatest movement was observed in the AP direction, up to 1.6 cm with a median value of 0.45 cm, and appeared to correlate with bladder and rectal filling.

There are large discrepancies in the reported results of prostate motion. Although some of the reported results are preliminary, there appears to be agreement that AP movement is more pronounced, and that movement correlates with bladder and rectal filling. There is clearly a need for additional studies with larger patient populations to better characterize organ motion and the influence of factors such as organ size and treatment technique.

The aim of this study is to analyze the interfraction setup error, gold seed displacement, and prostate motion for prostate patients, who were treated with IGRT at Grand River Regional Cancer Center (GRRCC), using three gold seeds implanted within the prostate and every day portal imaging. 118 prostate patients were analyzed for gold seed displacements relative to the isocenter, in which 20 patients were analyzed for setup error and prostate motion. Setup errors and gold seed displacement were determined from bony anatomy and gold seeds mismatch between the EPI and the DRR respectively. Prostate motion relative to bony anatomy was determined by the difference between gold seeds and bony anatomy displacement. Daily on-line repositioning of patients was accomplished through image matching using Varian Portal-Vision software. Setup error, gold seed displacement and prostate motion among patients and fractions were compared and analyzed statistically.

2.2   Methods and Materials

2.2.1   Patients

Patients with intermediate and low-risk prostate cancer were identified for radiation treatment in this clinical trial. IGRT plays an integral role in preparing these patients for accurate, reproducible treatments with daily online image verification. The eligibility criteria included clinical stage T1B, T1C and T2, N0, M0, a Gleason score less than 8 and prostate-specific antigen (PSA) levels less than or equal to 20. Three gold seeds were implanted in these patients trans-rectally in the prostate via a biopsy needle under ultrasound guidance. Gold seeds were cylindrical shape with 1.2 mm in diameter and 3 mm in length (Northwest Medical Physics Equipment, a Med-Tec Company). This procedure assumes that the seeds are stable and do not move within the prostate (Pouliot 2003).

2.2.2 CT planning and treatment planning

The planning CT scan (Philips AcQsim CT, Philips Medical Systems, Cleveland Inc.) was acquired one week after implantation and treatment usually begins a few days later. Patients were instructed to arrive for the CT procedure with a full bladder (drinking 2 glasses of water approximately one hour prior to the appointment) and with an empty rectum (asked to void before the appointment). Patients lie in a supine position on a solid flat carbon fiber couch top. An immobilization device is place below the knees. The pelvis area is scanned at increments of 3 mm. Three tattoos are then placed on the anterior, right and left lateral pelvis after the CT scan. All patients' treatment planning was done using the pinnacle treatment planning system (Philips Pinnacle version 7.4 TPS, Milpitas, CA) using 15MV photon beams. When the CT images have been imported into the treatment planning system, the prostate gland (clinical target volume (CTV)) was contoured by the radiation oncologist. The planning target volume (PTV) was created by expanding the CTV by 7 mm on the posterior direction and 10 mm in all other directions. The organs at risk (OAR) included the rectum, the bladder and femoral heads are also contoured. After the treatment planning one pair of orthogonal (AP and LR) DRRs are constructed in which the seeds and bony anatomy's position can be located. This image set constitutes the reference image pair and are exported from the treatment planning system to the treatment software together with the patient treatment plan.

2.2.3 Patient repositioning

The patients are immobilized and treated in the supine position. On each treatment day patients are positioned using laser alignment to the skin tattoos and immobilization device. The therapist acquires one pair of orthogonal EPIs using the AP and LR setup fields and these constitute the comparison image set. The portal images are taken using Varian Oncology Systems a-Si flat panel electronic portal imager (Varian Medical Systems, Palo Alto, CA) mounted on a dual energy Linac 2100EX accelerator. The

imager has a sensitive area of 512 by 384 pixels with a pixel size of 0.784 mm. All images are acquired using about 3-4 MU of radiation exposure. Using both pairs of images, on-line repositioning of patients is accomplished through image matching using Varian Portal-Vision software.

2.2.4   Data analysis

Data from 118 patients were used to study gold seed displacements relative to the isocenter, in which 20 patients were used to study bony anatomy displacements relative to the isocenter and prostate motion relative to bony landmarks. Setup error is defined as the bony anatomy mismatch between the simulated DRR and the daily EPI. To quantify seed displacements, setup errors and prostate motion, statistical data such as the mean, standard deviations (SD) were calculated for the seeds, bony anatomy and prostate displacement. The quantification of these displacements was performed using the EPI obtained during treatment and the simulated DRR. The images enabled us to detect the displacement of both bony anatomy and seeds. The displacement of both seeds and bony anatomy was calculated relative to an initial position, which is taken from the location of these internal structures as imaged during CT scanning. Comparing these structures on both the DRR and EPI requires that both images are represented in the same coordinate system and the projection of the isocenter of the treatment beam was chosen during treatment planning as the origin.

Table 2.1 shows specification and computation of the group mean (M), the standard deviation of all the means (Σ) and the root mean square (RMS) (σ) of all the patients' standard deviations.

Table 2.1: The group mean (M), the standard deviation of all the means (Σ) and the root mean square (RMS) (σ) of all the patients' standard deviations.

	Patient1	Patient2	Patient3	…	
Day1	D11	D21	D31	…	
Day2	D12	D22	D32	…	
Day3	D13	D23	D33	…	
…	…	…	…	…	
Mean	$\overline{M1}$	$\overline{M2}$	$\overline{M3}$	…	M = Group Mean $\longrightarrow \pm \Sigma = SD$
SD	σ2	σ2	σ3	$\longrightarrow$	$\sigma_{rms} = \sqrt{(\sigma_1^2 + \sigma_2^2 + \cdots + \sigma_p^2)/p}$

The set-up error is the difference between the actual and intended position of the patient that is irradiated, with respect to the treatment beams during treatment. The intended or reference patient position is recorded on a reference image (DRR). On the reference image, anatomical structures, radio-opaque markers and the outline of the field which is used to generate the image are seen. The term match structure will be used when referring to the markers or structures which are used to match the treatment portal image with the reference image. In this paper, bony setup error or seed displacement is the difference between the measured position of a bony anatomy or seeds as defined by an EPID image and the reference position as defined by DRR respectively. Prostate displacement relative to bony anatomy is the difference between the seeds position relative to the isocenter and the bony anatomy position relative to the isocenter. For each patient, the mean and SD of the daily setup error, seed displacement or prostate displacement is the patient's setup error, seed displacement or prostate motion respectively.

2.3   Data Collection and Analysis

2.3.1   Seed displacements analysis: 118 patients

Seed displacements relative to the isocenter combine both setup error and prostate motion. The pooled statistical data of the mean and standard deviation for seed displacements relative to the isocenter for all the fractions of 118 patients in AP, LR and SI directions are shown in Figure 2.1. In this study, the meaning of positive and negative in different direction is defined as following: the AP: Anterior ("-"), Posterior ("+"); LR: Left ("-"), Right ("+"); SI: Superior ("-"), Inferior ("+"). The frequency distribution of the seed displacement relative to the isocenter shows a normal distribution in all three directions. LR direction is narrow; AP and SI directions are much broader than LR direction; the predominant displacement was found in the posterior direction.
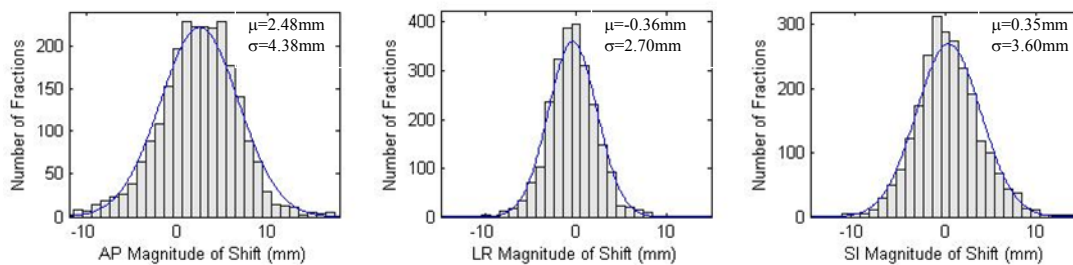
Figure 2.1: Pooled statistical data of seed displacement relative to isocenter with mean (μ) and standard deviation (σ) in AP, LR and SI directions.

Table 2.2 shows the group mean, standard deviation of all the means and RMS of SDs of all patients for the whole population. The data shows a preference of seed displacement in the posterior direction.

Table 2.2: Group mean (M) and standard deviation of all the means (Σ) and RMS (σ) of all SDs for seed displacements relative to the isocenter in a population of 118 patients in AP, LR and SI directions.

118 Patients	Seed displacement: 1 SD (mm)		
	AP	LR	SI
Mean (M)	2.05	-0.46	-0.97
SD (Σ)	2.65	1.74	1.86
RMS (σ)	3.16	1.91	2.10
$E_t = \sqrt{\Sigma^2 + \sigma^2}$	4.12	2.58	2.81
Pooled (Seeds)	4.38	2.70	3.60

Seed displacement relative to isocenter distribution over the entire course of treatment (2439 fractions) for all 118 patients is shown in Figure 2.2. Figure 2.2a) gives the distribution in the AP direction, Figure 2.2b) in the LR direction and Figure 2.2c) in the SI directions. The predominant distributed points above zero in AP distribution indicate preference displacements in the posterior direction, the LR and SI distribution has equally distributed points above and below zero, indicating no preference displacements in LR and SI directions. The distribution does not narrow with treatment fraction, which means that the displacement persisted through out the entire course of treatment.

The cumulative distribution of seed displacement relative to isocenter of the 118 patients in AP, LR and SI directions is shown in Figure 2.3. Figure 2.3a) is the distribution in the AP, LR and SI directions, whereas Figure 2.3b) is the distribution in the anterior, posterior, left, right, superior and inferior directions. The cumulative distribution of seed displacement was largest in the AP direction, and smallest in the LR direction. Most of the displacements in the AP direction were found to be in the posterior direction (74%) as opposed to 26% displacements in the anterior direction. In the AP direction, 49% of the displacements were smaller than 3mm, 38% within 3mm ~ 7mm, 10% within 7mm ~ 10mm and 3% larger than 10mm; In the LR direction, 83.6% of the displacements were smaller than 3mm, 15% within 3mm ~ 7mm, 1% within 7mm ~ 10mm and 0.4% larger

44

than 10mm. In the SI direction, 70% of the displacements were smaller than 3mm, 25% within 3mm ～ 7mm, 4% within 7mm ～ 10mm and 1% larger than 10mm.

The mean from individual patients as a function of SD for seed displacement relative to isocenter is shown in Figure 2.4. Figure 2.4a), 2.4b) and 2.4c) show the scatter plots in the AP direction (Pearson correlation coefficient r = - 0.22), LR: r = 0.05 and SI: r = 0.05, respectively. Most of patients means are positive (in the posterior direction, above the x-axis) in figure 2.4a), and superior direction (below x-axis) in figure 2.4c). In the anterior and inferior direction, the weak tendency of large mean corresponding to large standard deviation was observed in figure 2.4a) and 2.4c). The dominant seed displacement in posterior and superior direction was also shown in the histograms of individual patient's mean and SD of seed displacement relative to reference image for all the 118 patients in AP, LR and SI directions in Figure 2.5. The histograms of individual patient's standard deviation shows the AP displacement is largest in this patient group.
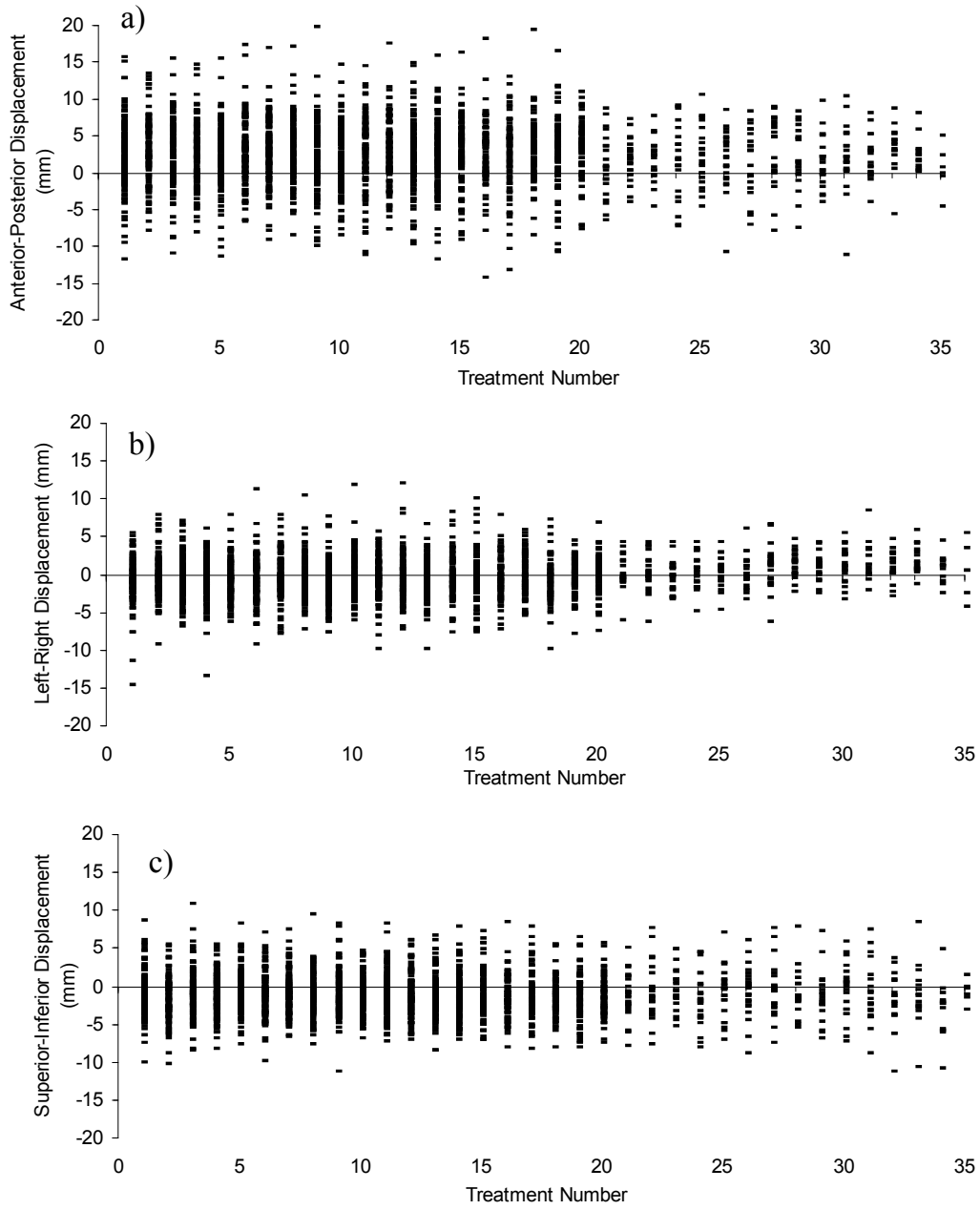
Figure 2.2: Seed displacement relative to isocenter distributed over the entire course of treatment for all 118 patients; (a) AP (b) LR and (c) SI.

46
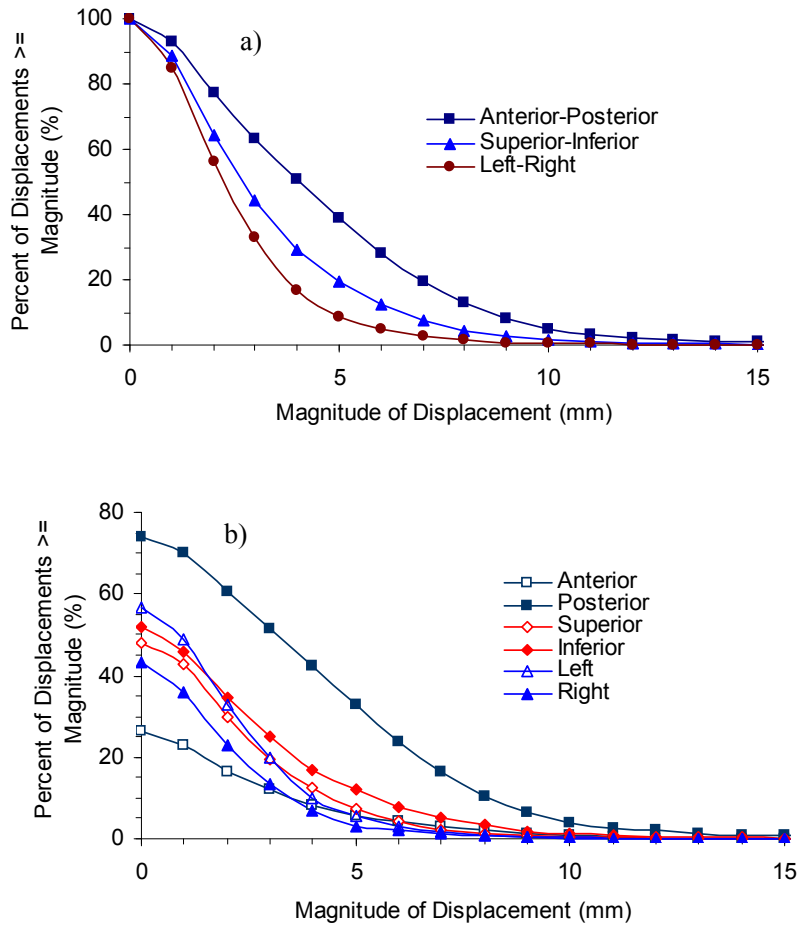
Figure 2.3: Cumulative frequency distribution of seed displacement relative to isocenter for 118 patients in AP, LR and SI directions; (a) AP, LR and SI directions (b) anterior, posterior, left, right, superior and inferior directions.
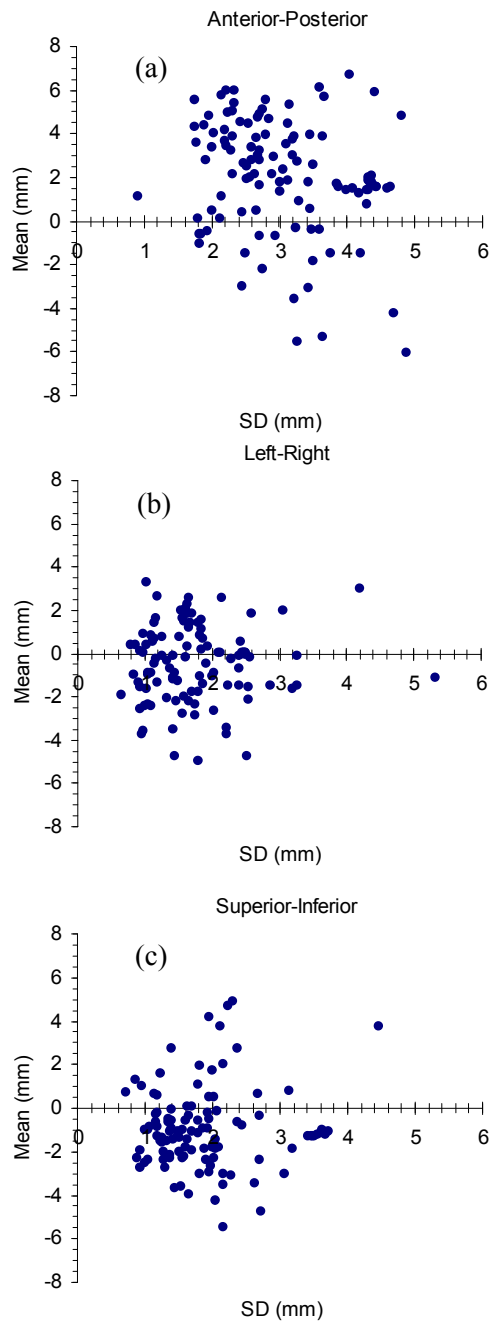
Figure 2.4: Scatter plot of the mean from individual patients as a function of SD for seed displacement relative to isocenter for 118 patients; (a) AP: r = - 0.22 (b) LR: r = 0.05 and (c) SI: r = 0.05.
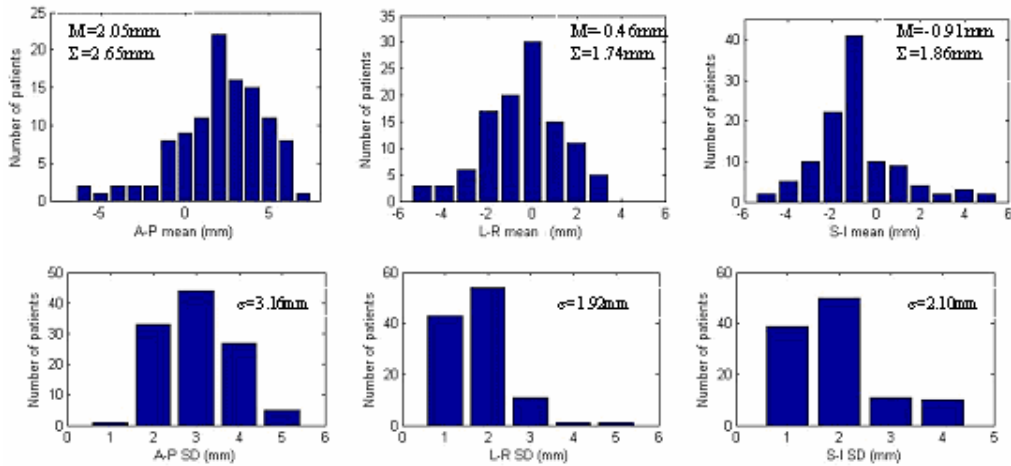
Figure 2.5: The histograms of individual patient's mean and SD of seed displacement relative to reference image for all the 118 patients in AP, LR and SI directions.

2.3.2   Setup error analysis for 20 patients

Some studies report setup errors measured after corrections are applied according to a protocol during the time the patients were treated (Hunt 1995, Hanley 1997). No data are given about the original setup errors. The data used in this study are the original setup errors *before* the corrections are applied.

The pooled statistical data of the mean and standard deviation of setup error for 20 patients in AP, LR and SI directions are shown in Figure 2.6. The frequency distribution of setup error shows a normal distribution in all three directions. LR direction is narrow; AP and SI directions are much broader than LR direction. The predominant displacement was found in posterior direction.

The cumulative frequency distribution of setup error in three directions is shown in Figure 2.7. The cumulative distribution of setup error was smallest in the LR direction. 88.3% of the setup errors were smaller than 3mm, 11.2% within 3mm ～ 7mm, and 0.5%

within 7mm ∼ 10mm. In the AP direction, 68% of the setup errors were smaller than 3mm, 28% within 3mm ∼ 7mm, and 4% within 7mm ∼ 10mm. In the SI direction, 78.1% of the displacements were smaller than 3mm, 18.8% within 3mm ∼ 7mm, and 3.1% within 7mm ∼ 10mm. The mean setup errors are 1.2 ± 3.3mm in AP, -0.1 ± 2.2mm in LR, -0.8 ± 2.9mm in SI. When separated into the various directions, the mean setup errors are 2.5 ± 2.2 anterior, 3.0 ± 2.2 posterior, -2.5 ± 2.0 superior, 2.2 ± 1.6 inferior, 1.7 ± 1.3 left and 1.8 ± 1.4 right.
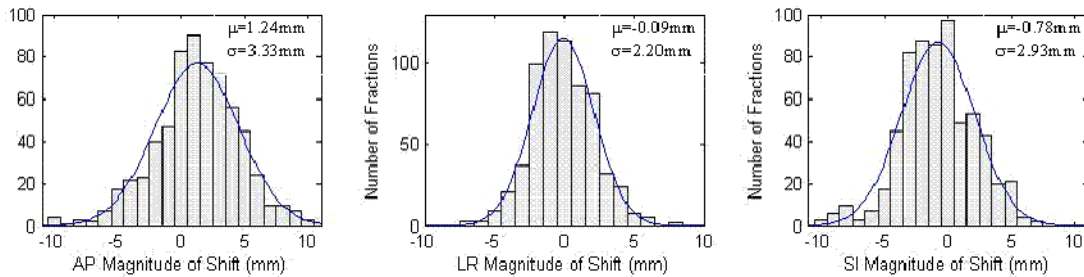
Figure 2.6: Pooled statistical data of setup error with mean and standard deviation in AP, LR and SI directions.
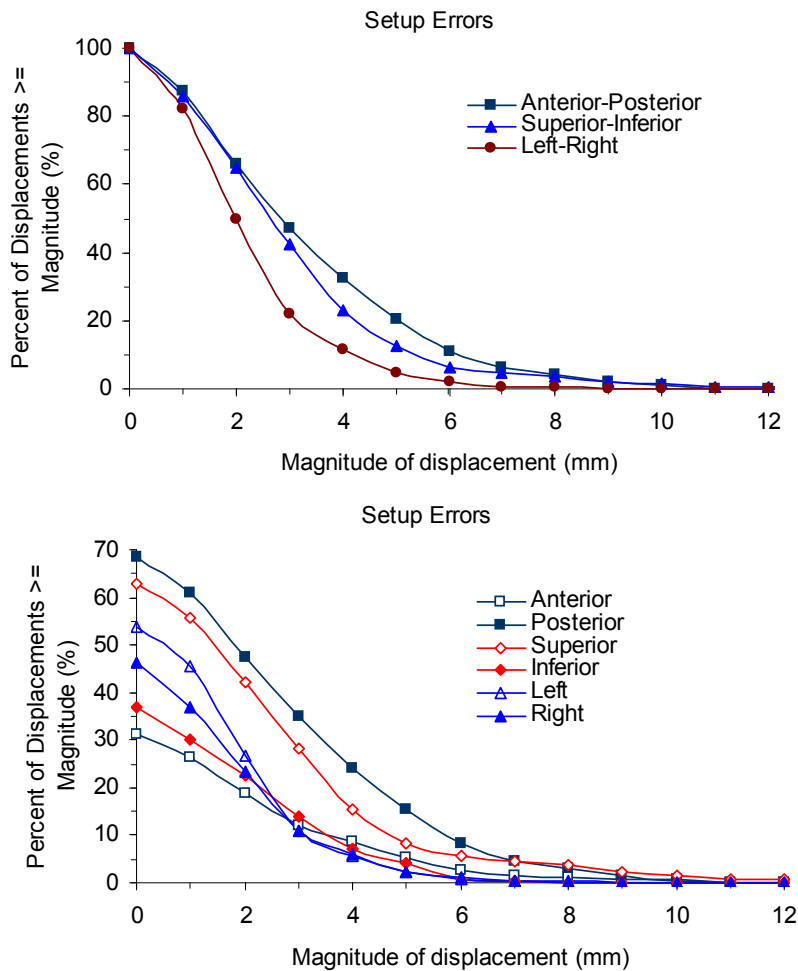
Figure 2.7: Cumulative frequency distribution of setup error for 20 patients in the AP, LR and SI directions; (a) AP, LR and SI directions (b) anterior, posterior, left, right, superior and inferior directions.

2.3.3　Prostate motion analysis for 20 patients

The pooled statistical data of the mean and standard deviation of prostate motion for 20 patients in AP, LR and SI directions are shown in Figure 2.8. The frequency distribution of organ motion shows a normal distribution in all three directions. LR direction is narrow; AP and SI directions are much broader than LR direction.
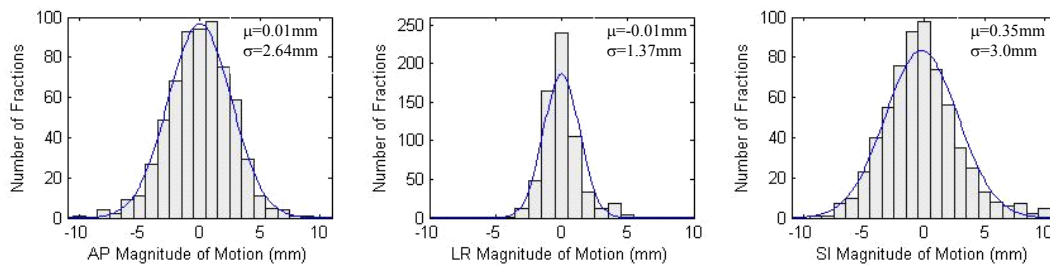
Figure 2.8: Pooled statistical data of prostate motion with mean and standard deviation in AP, LR and SI directions.

The cumulative frequency distribution of prostate motion in three directions is shown in Figure 2.9. The cumulative distribution of prostate motion was smallest in the LR direction with 96% of the organ motion smaller than 3mm, 4% within 3mm ～ 7mm. In the AP direction, 83.5% of the prostate motion was smaller than 3mm, 15.3% within 3mm ～ 7mm, and 1.2% within 7mm ～ 10mm. In the SI direction, 75.9% of the displacements were smaller than 3mm, 20.6% within 3mm ～ 7mm, 3.1% within 7mm ～ 10mm and 0.4 larger than 10mm.
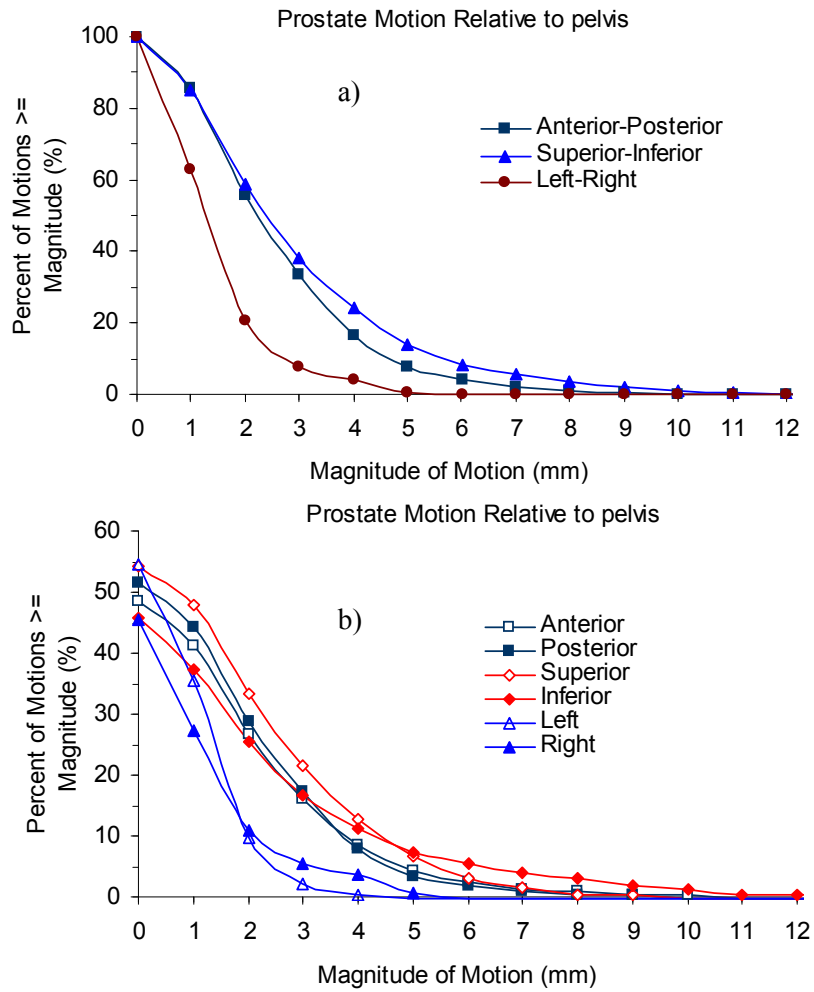
Figure 2.9: Cumulative frequency distribution of prostate motion relative to pelvis for the 20 patients in the AP, LR and SI directions; (a) AP, LR and SI directions (b) anterior, posterior, left, right, superior and inferior directions.

2.3.4 Comparing setup error and organ motion for 20 patients

Table 2.3 shows the statistical data for setup error and prostate motion for 20 patients in three directions. For prostate motion, the mean is zero in the AP and LR directions, and -0.2 mm in SI direction. There is no preference motion in three directions; while for setup error, dominant setup error was found in posterior direction and superior direction. There is larger setup error compared to organ motion in the AP directions. The observations are consistent with the findings of Alasti *et al* (2001).

Table 2.3: M, Σ and σ for setup error and prostate motion for 20 patients in the AP, LR and SI directions.

20 Patients	Statistical value	1 SD (mm)		
		AP	LR	SI
Setup Error	Mean:M	1.20	-0.12	-0.82
	SD (Σ)	2.17	1.35	2.55
	RMS (σ)	2.62	1.78	1.64
	$E_s = \sqrt{\Sigma^2 + \sigma^2}$	3.40	2.23	3.03
	Pooled (Bony)	3.33	2.20	2.93
Prostate Motion	Mean:M	0.00	-0.02	-0.16
	SD (Σ)	1.36	1.05	2.44
	RMS (σ)	2.22	0.91	1.95
	$E_m = \sqrt{\Sigma^2 + \sigma^2}$	2.60	1.39	3.12
	Pooled (Prostate)	2.64	1.37	3.00
Total	$E_t = \sqrt{E_s^2 + E_m^2}$	4.28	2.63	4.35
	Pooled (Seeds)	4.18	2.40	3.61

Scatter plots of bone anatomy versus seed displacements for 20 patients are shown in Figure 2.10. All displacements are relative to the isocenter. The x-axis depicts

displacements of seed displacement relative to isocenter, whereas the y-axis shows bony displacement relative to isocenter. Figures 2.10a), 2.10b) and 2.10c) show the scatters of the displacements for all fraction in AP, LR and SI directions respectively. Figures 2.10d) and 2.10e) show the individual patient mean and SD in AP, LR and SI directions. The correlation between seed displacements and bony anatomy is highest in the LR direction (Pearson's correlation coefficient $r = 0.83$). In the AP direction the correlation coefficient ($r = 0.78$) is smaller compared to the LR direction and the correlation coefficient ($r = 0.58$) is lowest in the SI direction. Nederveen's et al (2002) reported correlation coefficient between seed and bone displacements of 0.71 in the AP direction, 0.92 in the LR direction, and 0.46 in the SI direction. The correlation coefficient of mean between bony landmark and seed displacements are 0.87 in AP, 0.76 in LR and 0.56 in SI. Nederveen et al (2002) reported a correlation coefficient of 0.86 in AP, 0.91 in LR, and 0.08 in SI direction. A similar correlation for the SD revealed correlation coefficients of 0.83, 0.92, and 0.55 in AP, LR and SI directions, respectively.

The organ motion and setup error from the 20 patient studies are shown in Figure 2.11. The error bars indicate one standard deviation. The mean of AP, LR and SI prostate motion and setup error for the 20 patients was calculated by averaging all displacements over all fractions for each patient. The mean of prostate motion varied from –3.2 to 2.4mm in AP, -1.7 to 3.4mm in LR, -4.4 to 7.2mm in SI, with SD changing from1.2 to 3.3mm in AP, 0.4 to 1.5mm in LR, 1.2 to 2.4mm in SI directions respectively. While the mean of setup error varied from –3.6 to 4.4mm in AP, -2.2 to 2.3mm in LR and –7.6 to 3.7mm in SI, with SD changing from 1.2 to 4.8mm in AP, 0.6 to 2.5mm in LR, 1.0 to 2.6mm in SI directions respectively. The setup errors in the AP direction were larger in magnitude than those in the SI and LR directions, while the setup error in the LR direction was smallest. The dominant setup errors were found in the posterior direction and superior direction for the AP and SI setup errors respectively.

A comparison of cumulative frequency distribution of prostate motion and setup error for 20 patients in the anterior, posterior, left, right, superior and inferior directions is shown in Figure 2.12. There is larger setup errors compared to organ motion in the posterior and

superior directions, while larger prostate motion compared to setup error was found in the anterior and inferior directions. Alasti *et al* (2001) reported larger prostate motion compared to the setup errors in both AP and SI directions. A little bit difference was found in LR direction for both setup error and organ motion.

Scatter plots of prostate motion versus setup error are shown in Figure 2.13. The mean of prostate motion versus setup error for every patient in the AP, LR and SI directions are shown in Figure 2.13 (d); and the SD of prostate motion versus setup error in the AP, LR and SI directions are shown in Figure 2.13 (e). There is no correlation between prostate motion and bony shift. Prostate motions relative to bone, and bone displacements relative to isocenter as function of treatment number also showed that prostate motion is independent to bony shift in Figure 2.14.

The resultant displacement was obtained by adding three displacements in quadrature: $R = \sqrt{AP^2 + LR^2 + SI^2}$. The resultant displacement for seed displacements relative to isocenter, setup error and prostate motion for the pooled data of 20 patients are shown in Figure 2.15. If corrections were applied with resultant displacement bigger than 5 mm, for tracking the seeds from localization of fiducial markers, 61% of the fractions have resultant displacement larger than 5mm in the 20 patient groups; while for localization of bony landmarks alone, 37% of fractions are displaced by more than 5mm. For internal organ motion relative to bony anatomy, 23% of the fractions have displacement larger than 5mm. The just use of daily EPI alignment of bony anatomy would still result in 23% of fractions larger than 5mm because of internal organ motion.
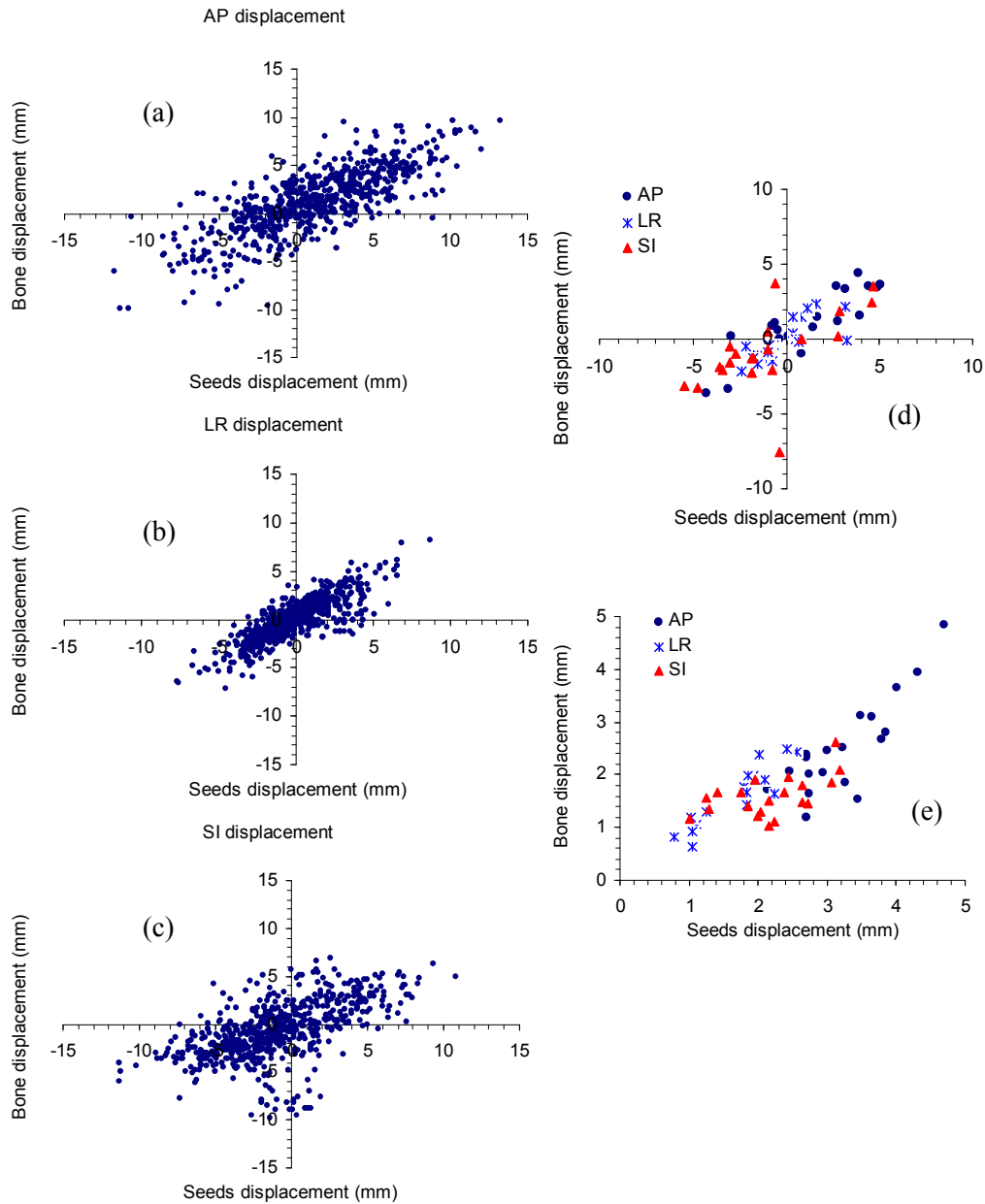
Figure 2. 10: Scatter plots of bony landmark versus seed displacement relative to isocenter. (a) AP: r = 0.78 (b) LR: r = 0.83 (c) SI: r = 0.59 (d) The mean of 20 patients in the AP, LR and SI directions: r = 0.87, 0.76, 0.60 in AP, LR and SI directions, respectively (e) SD in the AP, LR and SI directions: r = 0.83, 0.92, 0.55 in AP, LR and SI directions, respectively.

57
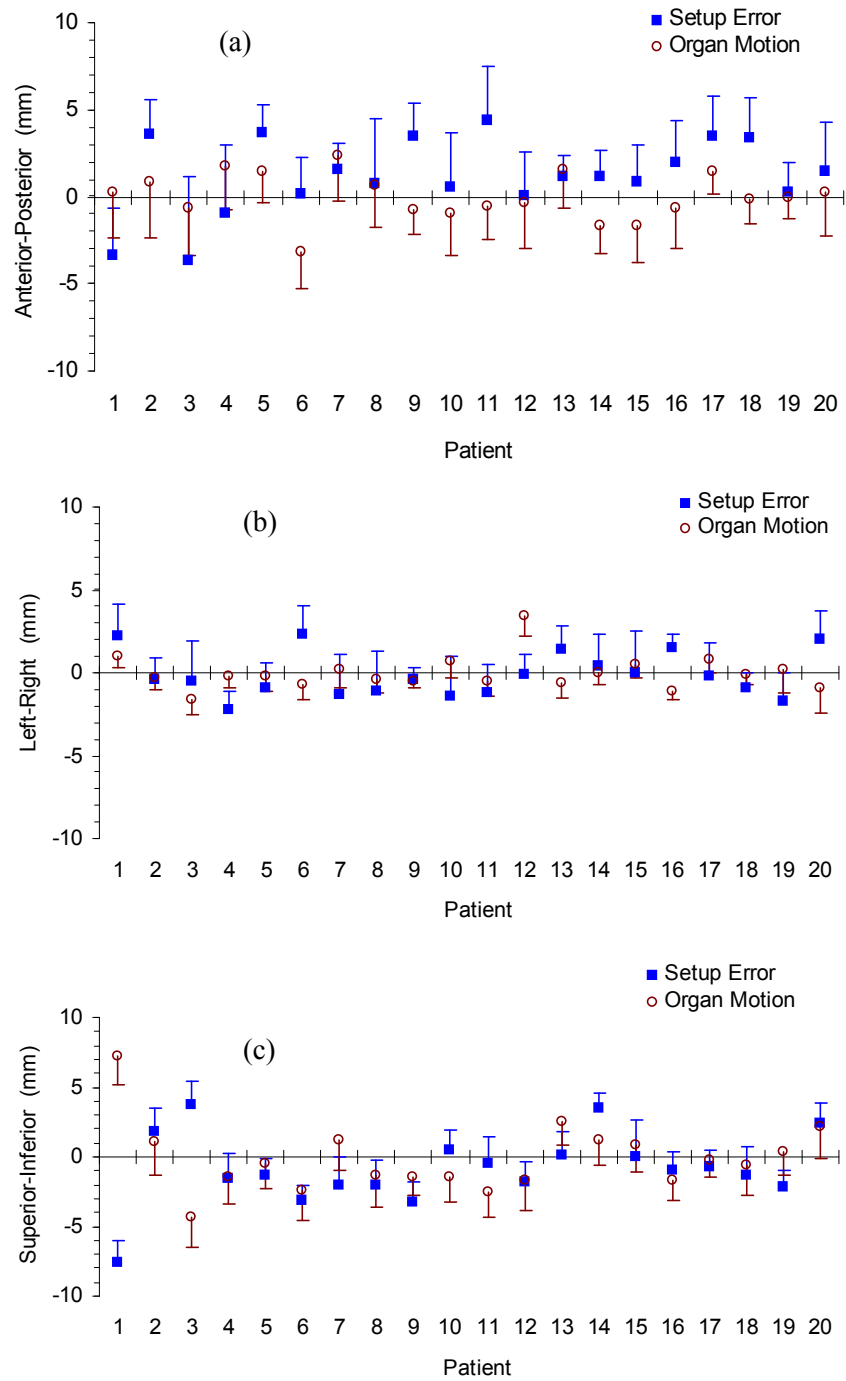
Figure 2.11: Prostate motion and setup error and for the 20 patients in the AP, LR and SI directions. The error bars indicate one SD. (a) AP direction (b) LR direction and (c) SI direction.
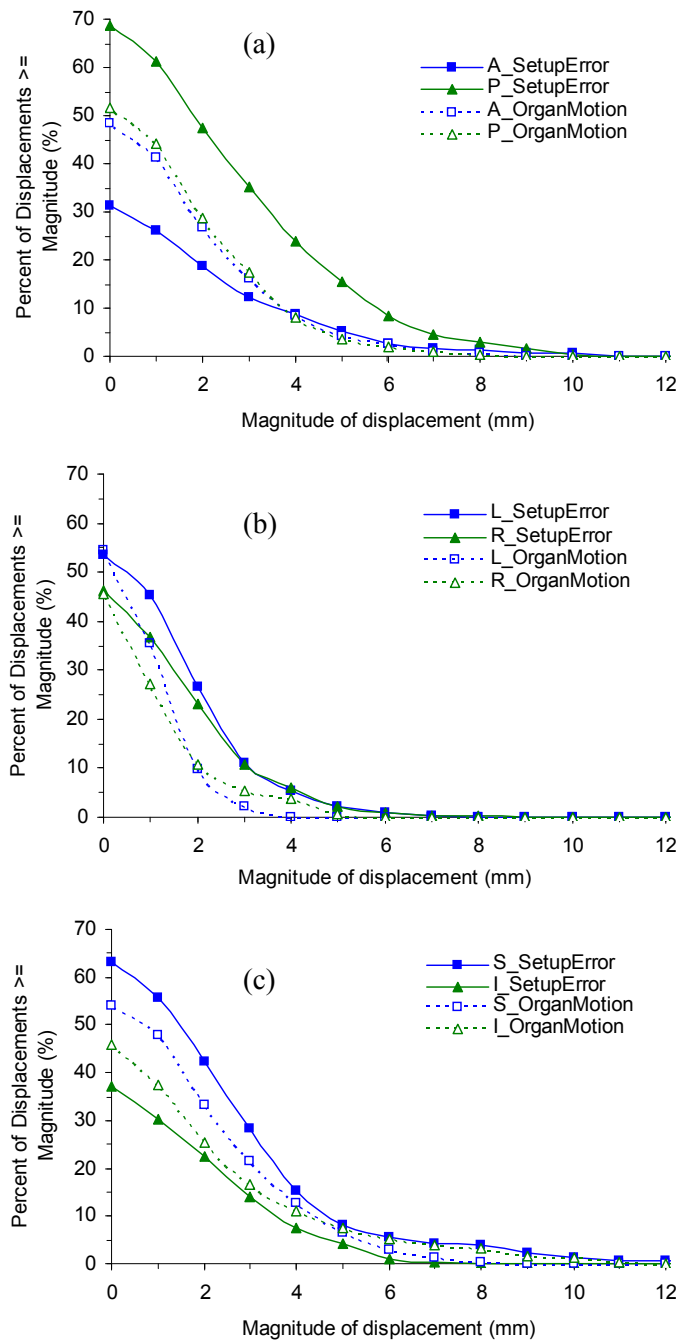
Figure 2.12: A comparison of cumulative frequency distribution of prostate motion and setup for 20 selected patients. (a) Anterior and Posterior directions (b) Left and Right directions, and (c) Superior and Inferior directions.

59
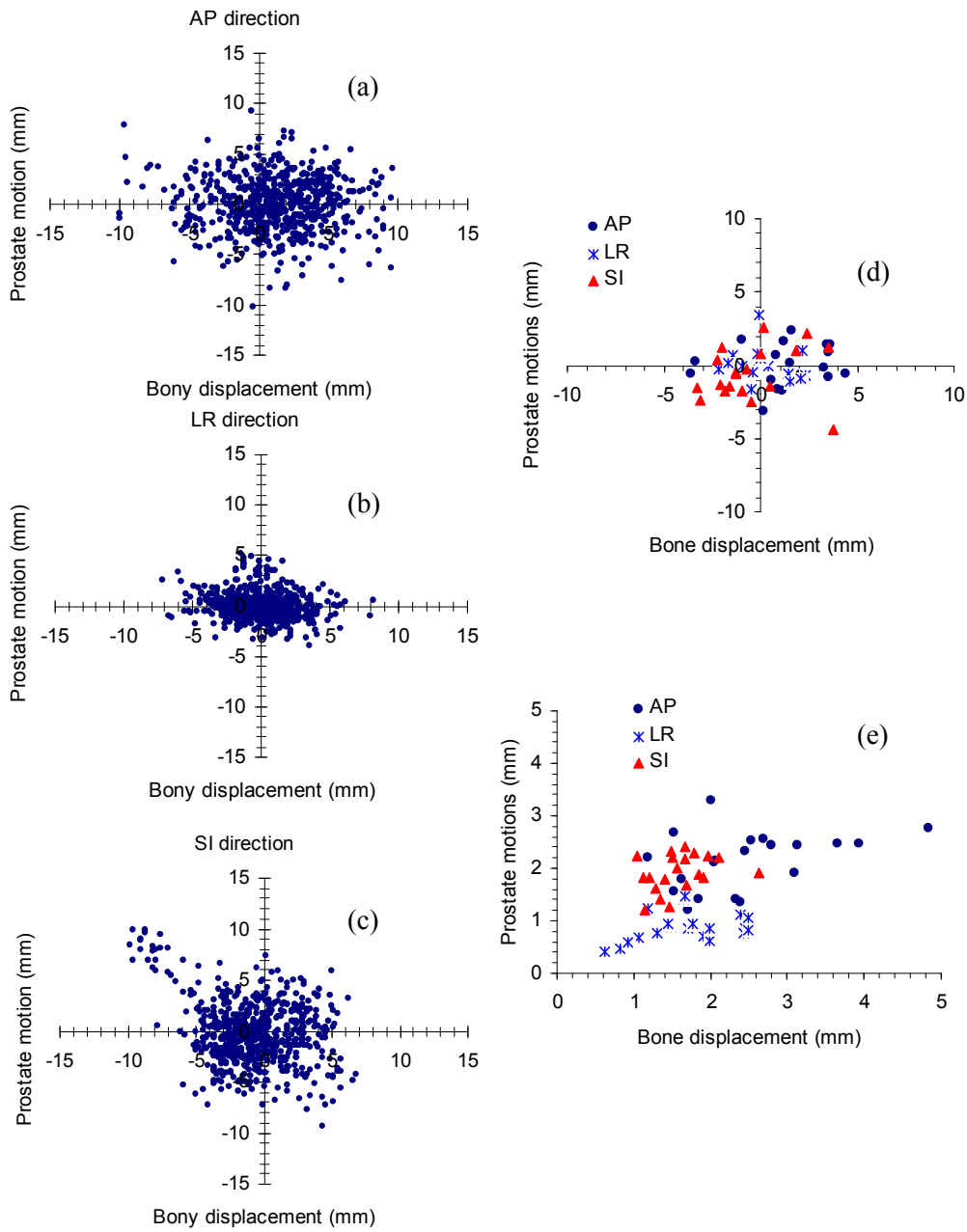
Figure 2. 13: : Scatter plots of prostate motion versus setup error (a) AP: r = -0.03 (b) LR: r = -0.16 (c) SI: r = -0.27 (d) The mean of prostate motion versus setup error for 20 patients in the AP, LR and SI directions: r = 0.15, -0.12, -0.34 in AP, LR and SI directions, respectively (e) SD of prostate motion versus setup error in the AP, LR and SI directions: r = 0.38, 0.35, 0.31 in AP, LR and SI directions, respectively.
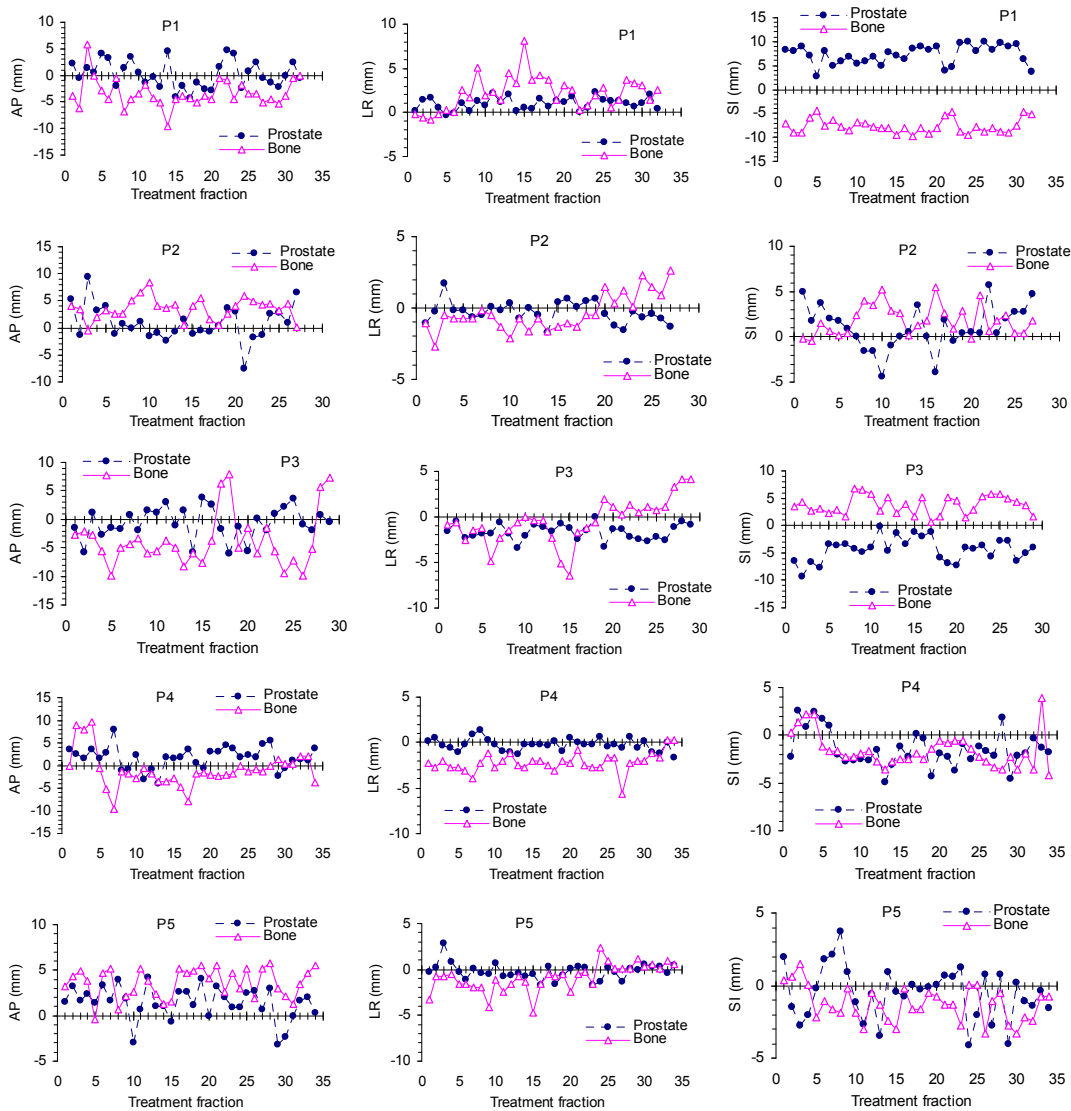
60

Figure 2.14: Prostate motion relative to bone, and bone displacement relative to isocenter as a function of treatment number.

Figure 2.14: Prostate motion relative to bone, and bone displacement relative to isocenter as a function of treatment number.
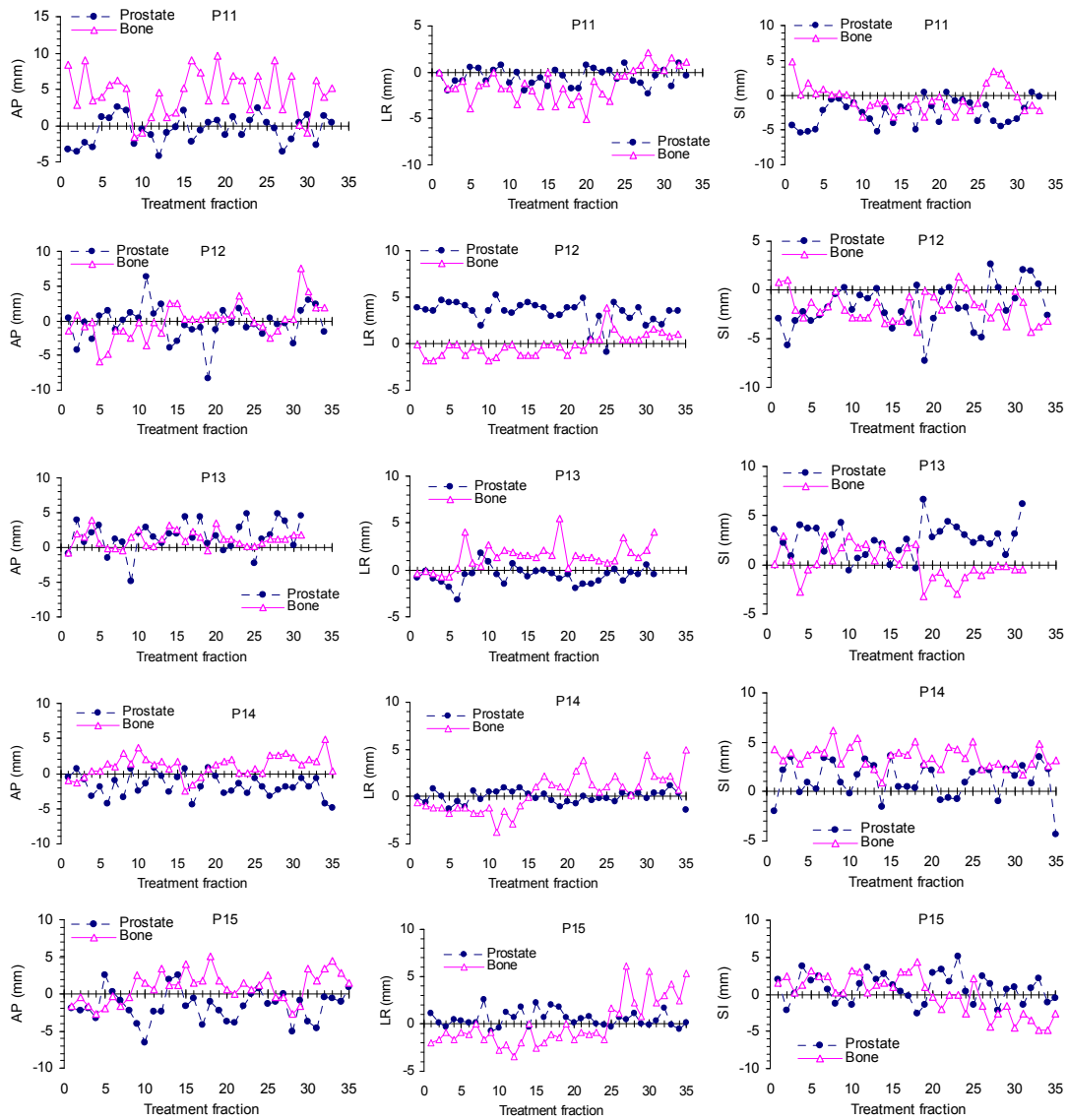
Figure 2.14: Prostate motion relative to bone, and bone displacement relative to isocenter as a function of treatment number.

Figure 2.14: Prostate motion relative to bone, and bone displacement relative to isocenter as a function of treatment number.
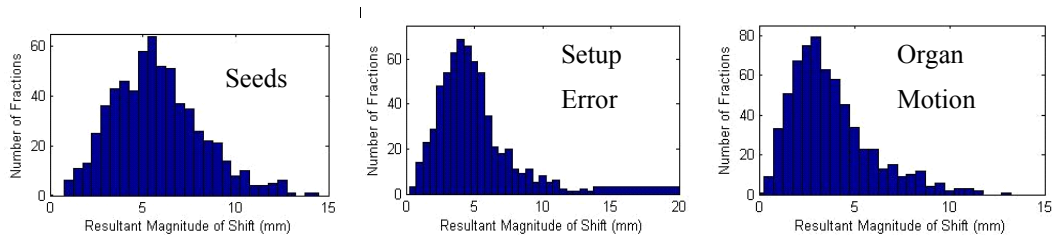
Figure 2.15: The resultant $R = \sqrt{AP^2 + LR^2 + SI^2}$ for seed displacements relative to isocenter, setup error, and prostate motion for the pooled data of 20 patients.

2.3.5 The effect of body size on setup error

The predominance of setup error in the anterior-posterior direction found in the study may be mainly due to the use of skin markers to determine the isocenter height in combination with the use of the pelvic bones as a match structure. The movement of the skin markers used for patient positioning relative to the pelvic bones, results in a setup error. The skin movement might be due to respiration, weight loss, patient's relaxation or body size. This movement is expected to be small in the LR and SI directions and more pronounced in the AP direction. The correlation of body size and setup error was analyzed. The body size was characterized by the maximum separation in AP direction. The mean, SD and AP setup error (defined as absolute mean plus two SDs) for AP setup error with the relationships of body size for 20 patients are shown in Figure 2.16. The mean of AP setup errors were divided into two parts by x-axis, for most of the patients, the means of setup error are positive (above the x-axis in posterior direction), the correlation coefficient is 0.27, while for the patients with negative means (below the x-axis in anterior direction), the correlation coefficient is - 0.46 as shown in Figure 2.16 a). The correlation coefficient between body sizes and SD is 0.43 in Figure 2.16 b); however the correlation coefficient of body size with AP setup error (absolute mean plus two SDs)

is 0.51. For the 10 patients with large setup errors in this 20 patients group, the correlation coefficient between the AP setup error and AP separation is 0.82 as shown in figure 2.16 d). There is the tendency that the larger body size leads to larger AP setup error. This result is consistent with Luchka (1997)'s study, who reported setup errors for an obese patient which were much larger than for normal patients.
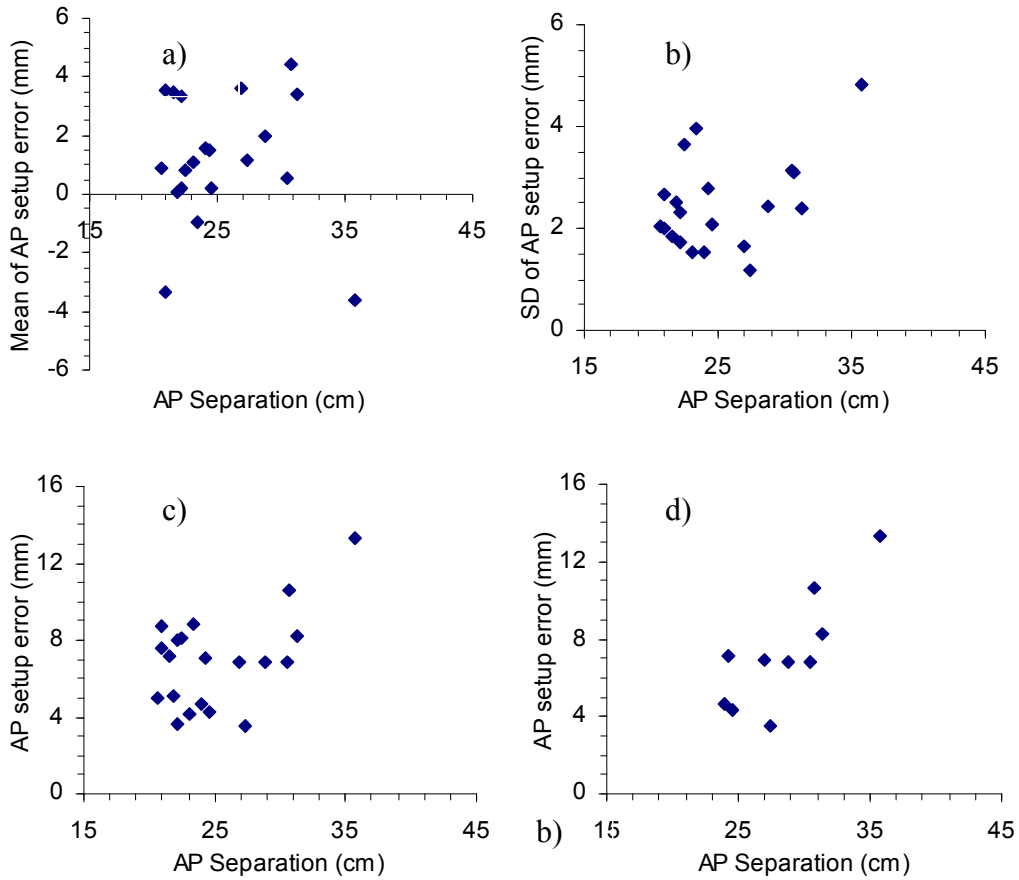
Figure 2.16: The mean, SD and AP setup error (absolute mean plus two SDs) versus AP separation for 20 patients (a) mean (b) SD: r = 0.43 (c) mean plus two SDs: r = 0.51 (d) 10 patients with larger AP separation: r = 0.82.

2.3.6 The effect of bladder and rectal volumes on prostate motion

The relationships of the mean of prostate AP motion with bladder volume and rectal volume are shown in Figure 2.17. The correlation coefficient of the mean of prostate AP motion with bladder volume is - 0.34. There is the tendency that the mean of AP motion is in anterior direction (negative) for larger bladder. The largest bladder volume (patient 6, bladder volume: 578.16 cm^3) results in the most of the motion in anterior direction (Mean = -3.15mm), which may be the reason that the bladder volume reached the maximum capacity during the CT scanning and relative smaller for the course of treatment comparing to the planning bladder volume. The correlation coefficient of the mean of prostate AP motion with rectal volume is 0.35. The tendency is opposite to the relationship between AP motion and bladder volume because the opposite position the rectum relative to prostate comparing the bladder position relation to prostate.
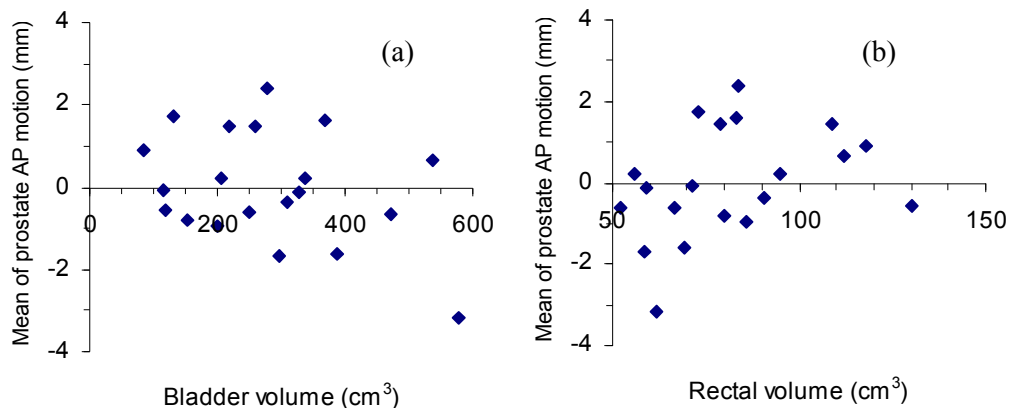
Figure 2.17: The mean of prostate AP motion versus volume (a) bladder: r = -0.34 and (b) rectum: r = 0.35.

The relationships of the mean of prostate AP motion with bladder volume and rectal volume for the AP motion bigger than 5mm are shown in the Figure 2.18. The correlation coefficient of the mean of prostate AP motion with bladder volume is -0.47, while the correlation coefficient of the mean of prostate AP motion with rectal volume is 0.44.
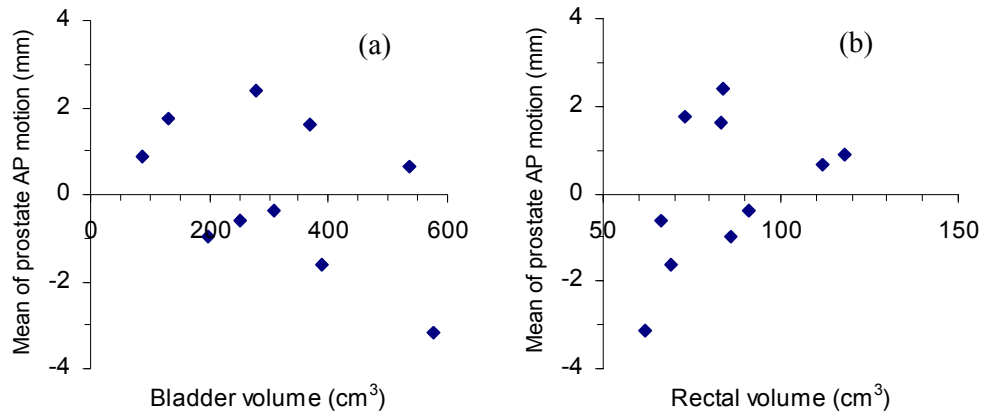
Figure 2.18: The mean of prostate AP motion versus volume for the AP motion bigger than 5mm (absolute mean plus two SDs) (a) bladder: r = -0.47 and (b) rectum: r = 0.44.

The relationships of the SD of prostate AP motion with bladder volume and rectal volume for the AP motion bigger than 5mm are shown in the Figure 2.19. The correlation coefficient of the SD of prostate AP motion with bladder volume is -0.67. The bladder was asked to be full during CT scan and everyday treatment. The smallest bladder has the largest SD (Patient 2, Bladder volume = 85.82 cm^3, SD = 3.28 mm). SD decreased with increasing bladder volume, however the SD increase again when bladder is too full. The correlation coefficient of the mean of prostate AP motion with rectal volume is 0.60. During CT scan and everyday treatment, the rectum should be emptied. The SD increased with increasing rectal volume.
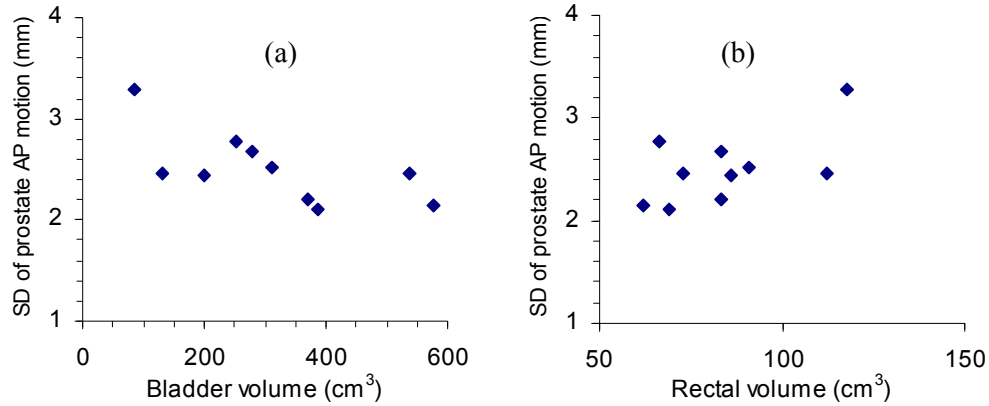
Figure 2.19: SD of prostate AP motion versus volume for AP motion bigger than 5mm (absolute mean plus two SDs) (a) bladder: $r = -0.67$ and (b) rectum: $r = 0.60$.

Figure 2.20 shows the relationships of the prostate AP motion (defined as absolute mean plus two SDs) with bladder volume and rectal volume for the AP motion bigger than 5mm. Except patient 7 (Bladder volume = 278.88 cm^3, Rectal volume = 83.44 cm^3, AP motion = 7.74 mm), the rest of patients show that too smaller or larger bladder volume will result in the larger AP motion because of the bigger bladder volume variation between the planning CT scan and everyday treatment. Same result was found in Figure 2.20 b) for the rectum.
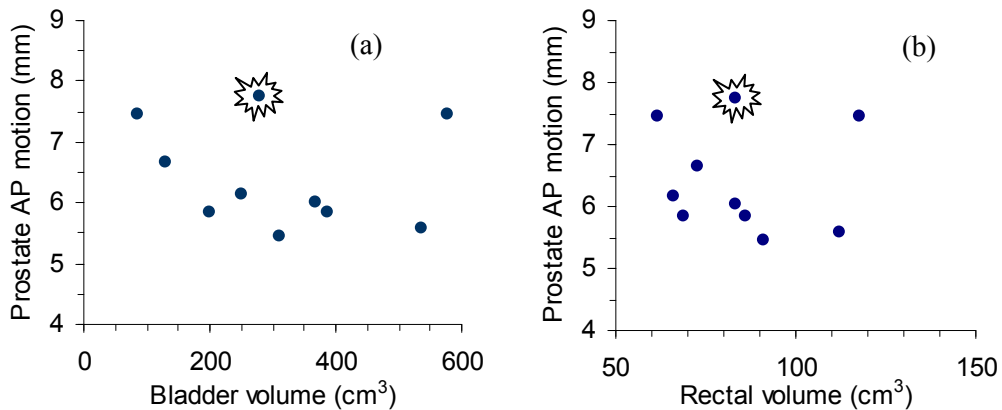
Figure 2.20: Prostate AP motion (absolute mean plus two SDs) versus volume for AP motion bigger than 5mm (a) bladder and (b) rectum.

69

There is no obvious correlation between the prostate motion and prostate volume, also no obvious correlation between the prostate motion and maximum AP separation of the body size as shown in the Figure 2.21.
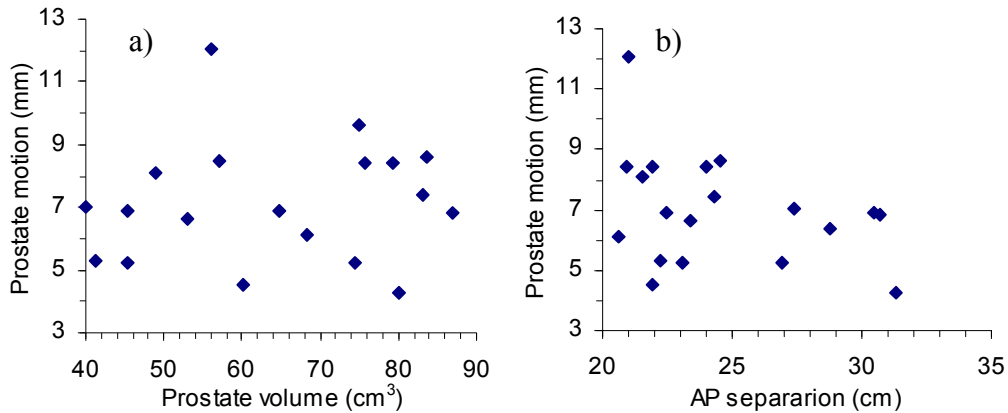
Figure 2.21: Prostate motion (R = $\sqrt{AP^2 + LR^2 + SI^2}$) versus volume (a) prostate (b) maximum AP separation of the body.

2.3.7 Comparing the results with other researchers

The setup errors (1 SD) in this study compared with other researchers in the literature are shown in Table 2.4, and range from 1.8 to 7.3 mm in AP direction, 1.4 to 8.8 mm in SI direction, lateral direction is smallest.

Hanley *et al* (1997) did a retrospective analyzes of port films of 50 patients. Patient positioning uncertainty was determined using port film from three projections: two oblique, and one lateral. A total of 1239 port films and 300 simulator films were analyzed for the study. The distribution of setup errors for the population of patients were 1.9 mm, 2.0 mm and 1.7 mm, in the AP, LR and SI directions, respectively. Alasti *et al* (2001)

also analyzed a total of 2549 portal images from 33 patients. Data from 23 patients were analyzed for setup errors and 10 were analyzed for prostate motion. Setup errors were characterized by standard deviations of 1.8 mm in AP and 1.4 mm in SI directions. The setup errors in our research are found to be predominant in the AP direction. This agrees with the work by Dunscombe *et al* (1993), Hunt *et al* (1995), and *Alasti et al* (2001) who showed similar largest displacement in the AP direction and least in the LR direction; however the researches from Althof *et al* (1996), Rudat *et al* (1996), van Herk *et al* (2004) showed the largest displacement in the SI direction. The uncertainties of the skin markers used for patient positioning relative to the pelvic bones result in setup error. The skin markers' variation might be due to respiration, weight loss, patient's relaxation or body size. This movement is expected to be small in the LR and SI direction and more pronounced in the AP direction.

The prostate displacement occurs independently from the bony anatomy and compared results are shown in Table 2.5. The repositioning the patient using bony anatomy only slightly contributes to a better target positioning. The range of prostate motion was different from different researchers and the comparison among studies is complicated due to different procedures employed by different researchers. Organ motion was reported to be the result of pressure from bowel gas and the filling of rectum and bladders (Roeske *et al* 1995, Melian *et al* 1997). Additionally, the high variability was noted in many of the studies because of different patient population sizes, different bladder sizes (full vs. empty), and different number of measurements, methods of measurements, and time interval between measurements (Balter *et al* 1995, Roeske *et al* 1995, van Herk *et al* 1995, Melian *et al* 1997, Vigneault *et al* 1997, Alasti *et al* 2001, Wu *et al* 2001). Melian *et al* (1997) studied the variation of bladder and rectum filling in 12 patients and found 0 ∼ 3.0 cm AP shifts, correlated with filling. Balter *et al* (1995) used weekly orthogonal radiographs to measure prostate motion and observed translational of a maximum of 7.5mm with typical range between 0 ∼ 4 mm, predominantly in AP and SI direction. In agreement with their results, our results show the largest motion in the AP direction and the smallest motion in the LR direction; and too smaller or larger bladder volume will result in the larger AP motion because of the bladder volume inconsistency between the planning CT scan and everyday treatment.

Table 2.4: Setup error specified as one standard deviation (mm) in the AP, LR and SI directions.

Setup Error (1 SD) (mm)	AP	LR	SI
Results from this study	3.3	2.2	2.9
Alasti *et al* (2001)	1.8	-	1.4
Althof *et al* (1996)	2.4	3.1	3.2
Antolak *et al* (1998)	5.1	4.0	2.3
Dong (1995)	2.3	2.7	2.1
Dunscombe *et al* (1993)	5.2	4.0	4.1
Hanley *et al* (1997)	1.9	2.0	1.7
Hunt *et al*, EPID (1995)	5.3	5.5	5.3
Hunt *et al*, film (1995)	7.3	5.2	5.3
Jones *et al* (1995)	3.1	2.5	2.2
Rudat *et al* (1996)	4.9	3.1	5.4
Tinger *et al* (1998)	3	3.1	2.1
van Herk *et al* (2004)	2.3	3.9	8.8
Vigneault *et al* (1997)	2.5	2.1	2.5

Table 2.5: Prostate motion specified as one standard deviation (mm) in the AP, LR and SI directions.

Prostate Motion (1 SD) (mm)	AP	LR	SI
Results from this study, seeds	2.6	1.4	3.0
Alasti *et al*, seeds (2001)	5.8	-	3.3
Althof *et al*, seeds (1996)	1.5	0.8	1.7
Antolak *et al*, CT (1998)	3.6	0.7	3.6
Balter *et al*, seeds (1995)	2.3	0.9	1.9
Crook *et al*, seeds (1995)	4.1	1.5	5.0
Litzenberg *et al*, CT (2002)	2.4	1.9	2.1
Melian *et al*, CT (1997)	4.0	1.2	3.1
Roeske *et al*, CT (1995)	3.9	0.7	3.2
Rudat *et al*, CT (1996)	3.7	1.9	-
Schiffner *et al*, CT (2007)	2.1	0.9	2.4
Tinger *et al*, CT (1998)	2.6	0.9	3.9
Van Herk *et al*, CT (1995)	3.8	1.3	2.4
Vigneault *et al*, seeds (1997)	3.5	1.9	3.6
Wu *et al*, seeds (2001)	2.3	-	2.1

2.4 Chapter Summary

Daily electronic portal images with gold seeds provided an effective way to verify and correct the position of targets immediately prior to radiation delivery. There is a direct correlation of patient size and magnitude of setup error where, the larger a patients body, the larger the potential setup error. Prostate motion occurred independently from bony anatomy displacement during treatment, and correlated with bladder and rectal filling. Margins, though reduced in size after correcting setup error by bony anatomy based

position verification, are still needed to account for internal organ motion. If corrections were applied with resultant displacement bigger than 5 mm, for tracking the seeds from localization of fiducial markers, 61% of the fractions have resultant displacement larger than 5 mm in the 20 patient groups; while for localization of bony landmarks alone, 37% of fractions are displaced by more than 5 mm. For internal organ motion relative to bony anatomy, 23% of the fractions have displacement larger than 5 mm. The use of daily EPI alignment of bony anatomy would still result in 23% of fractions larger than 5 mm because of internal organ motion. The margin is determined according to the specific setup technique: for a conventional beam setup without image guidance, both setup error and organ motion should be considered; for correction of daily bony setup error by EPID, a margin should be considered to account for internal organ motion; for correction of fiducial markers, a margin is still needed to account for intra-fraction organ motion during treatment and other uncertainties. Margin is also determined by treatment techniques: for a four-beam box, 95% coverage is required according to the ICRU-62 (ICRU 1999) report; for IMRT with correction of inter-fraction tumor motion, 4 mm margin should be used for intra-fraction motion and other uncertainties because of high dose gradient. Significant reduction in both setup error and organ motion can be achieved by on-line target-based position verification using gold seeds image-based verification or recently employed cone beam CT. The dosimetric effects of organ motion on the rectum were quantified in other chapter.

Permission to reproduce copyright material in Chapter 3

PERMISSION TO REPRODUCE AS REQUESTED
IS GIVEN PROVIDED THAT

(a) the consent of the author(s) is obtained

(b) the source of the material including author/editor, title, date and publisher is acknowledged.

IOP Publishing Limited
Dirac House
Temple Back
BRISTOL   12/10/07
BS1 6BE   Date   Rights & Permission

Please include mention of the journal's homepage at: www.iop.org/journals/pmb and provide a link-back to the article's abstract on our website from the electronic version of your thesis.

Thank you!

Chapter 3

The Effect of Organ Motion in a Region of High Dose Gradient

The aim in this chapter was to investigate the effects of geometric uncertainties on intensity-modulated radiation therapy (IMRT) treatment planning of prostate patients using dose gradients and probability density function (PDF) of geometric uncertainties. Spatial dose distributions were generated from a Pinnacle[3] planning system using a co-planar, five-field IMRT technique. Five types of beam plans were created for each patient using equally spaced beams but shifting the angular displacement of the beam set by 15°. Dose profiles taken through the isocenter in anterior-posterior (AP), left-right (LR) and superior-inferior (SI) directions for IMRT plans were analyzed by exporting RTOG file data from Pinnacle. The convolution of the "static" dose distribution $D_0(x,y,z)$ and Gaussian PDF, denoted as $P(x,y,z)$, was used to analyze the combined effect of repositioning error and internal organ motion. The percentage mean dose deviation (PMDD) was defined as dose difference between the mean dose (MD) of the blurred dose profile from isocenter to the edge of PTV and the mean dose of the whole planning target volume (PTV). The PMDD depended on the dose gradient and organ motion PDF. Organ motion dose sensitivity (OMDS) was defined by the rate of change in PMDD with standard deviation (SD) of Gaussian PDF and was found to increase with the maximum dose gradient in anterior, posterior, left and right directions. Due to common inferior and superior field borders of the field segments, the sharpest dose gradient occurred in the inferior or both superior and inferior directions. Thus, prostate motion in the SI direction produced the greatest dose difference. The PMDD is within 2.5% when SD is less than

5mm, but the PMDD is over 2.5% in inferior direction when SD is higher than 5 mm in inferior direction. Verification of prostate organ motion in the inferior directions is essential. The margin of the PTV significantly impacts on the confidence of tumour control probability (TCP) and level of normal tissue complication probability (NTCP). Smaller margins help to reduce the dose to normal tissues, but may compromise the dose coverage of the PTV. Lower rectal NTCP can be achieved by either smaller margin or steeper dose gradient between PTV and rectum. With the same dose volume histogram (DVH) control points, the rectum had lower complication in the seven-field technique because of the steeper dose gradient between the target volume and rectum. The relationship between dose gradient and rectal complication can be used to evaluate IMRT treatment planning. The dose gradient analysis is a useful tool to evaluate IMRT treatment plan and can be used for QA checking of treatment plan for prostate patients.

3.1   Introduction

In conformal radiation therapy (CRT) and IMRT, the organ motion and positional uncertainty of the clinical target volume (CTV) is managed by adding margins to form a PTV to ensure the desired tumor dose coverage (ICRU report 50 1993, ICRU report 62 1999). This approach generally leads to increased NTCP. The use of IMRT is increasing rapidly due to promising clinical outcomes (Webb 1993, 1997, 2000, 2004, 2006, IMRT group 2001, Palta and Mackie 2003). IMRT provides more degrees of freedom for shaping dose distribution to produce highly conformal dose coverage of PTV and significantly reducing the dose to adjacent organ at risk (OAR). However, as the dose gradient at outside edge of PTV increases, the impact of setup error and internal organ motion uncertainties will be much higher.

Some specific studies in organ motion are highlighted: Mageras *et al* (1996) randomly sampled organ motions from a database of serial CT images previously acquired over the course of radiation therapy for a population of patients; these motions are then mapped

onto the patient being planned. Yan *et al* (1999) retrospectively reconstructed the dose delivered to the patient during the initial treatment fractions by acquiring multiple on-line CT images. Fontenla *et al* (2001a, 2001b) proposed a model for incorporating the effects of organ motion into the calculation of dose in a statistical fashion based on serial imaging measurements of organ motion. In Craig's study (2003c, 2005); impact of geometric uncertainties on treatment techniques was evaluated for prostate cancer. Schaly *et al* (2004, 2005a, 2005b) used a dose warping technique to assess the impact of image-guided radiation therapy (IGRT) strategies that correct patient setup errors and inter-fraction organ motion. However, no one has previously focused on absolute dose gradients as optimization parameters of commercial optimization algorithms and few studies gave the quantification relationship between the effects of organ motion on dose gradients. In this study, the effects of dose gradient along the anterior-posterior, superior-inferior and left-right directions of internal organ motion were analyzed and quantified for the first time.

Although DVHs are important planning parameter and are linked to TCP and NTCP, they do not contain spatial information about the distribution of dose and are therefore not as effective as the dose gradient. The dose gradient is the rate change of dose profile along specific direction (the slope of the dose fall in that direction). Complete dose profile is required to assess impact for internal organ motion. The maximum dose gradient is the steepest part of the dose profile at outside edge of PTV and produces the largest effect on the target dose for the internal organ motion.

To assess the impact of patient repositioning and internal organ motion on IMRT treatment plans, a dose gradient analysis is performed on spatial dose profile through the dose distribution (i.e. a linear voxel sequence). Dose gradient analysis is completely general and is independent of optimization algorithm. The method in this study can be easily adapted to arbitrary internal organ motion. Fundamental to this technique is directional gradient and probabilistic (density function) characterization of motion and determination of the blurred dose gradients along directions relevant to the motion. The analysis of the dose gradient is a powerful tool to evaluate IMRT treatment plan in light of geometric uncertainty.

3.2 Methods and Materials

3.2.1 Patient and treatment planning data

In this study, IMRT Treatment plans are created for fifteen prostate patients, covering a range of prostate target volumes from 17.3 cm^3 to 87.1 cm^3, and different overlap of PTV with rectum and bladder. The prostate, seminal vesicles, bladder, rectum, and femoral heads of the prostate patients were contoured by the therapist using CT data. Two PTVs for each patient are generated: PTV1 includes the prostate and seminal vesicles plus a 10 mm margin; PTV2 includes the prostate only plus 10 mm margin. For each PTV, 3D uniform margins of 2, 5, 8, and 10 mm were used.

3.2.2 IMRT treatment planning and objective functions

All cases were planned for supine patient treatment using a 6 MV photon beam from Varian 21EX linear accelerator (Varian Medical Systems, Palo Alto, CA). All were devised for coplanar treatment with the long axis of the patient couch parallel to the axis of the treatment machine gantry rotation. Plans were produced for each patient using equally spaced beams but shifting the angular displacement of the beam set by 15°. The prostate IMRT inverse treatment planning was optimized with a coplanar, isocentric five-field technique, involving five plans with different beam angles as shown in Table 3.1. Five and seven coplanar beams were used for comparison.

An escalated dose of 82 Gy in 2 Gy per fraction was prescribed for all IMRT plans. The DVH control points for the PTV and OAR were adapted from RTOG 0126 (Michalski

2004). The minimum and maximum dose to the target and maximum dose to the OARs are parameters in the optimization cost function, DVH control points and the weights are specified for the PTV and OAR. The weights and DVH control points of the PTV and OAR were adjusted and changed to satisfy the RTOG guideline for IMRT plans. All patients were planned using the same objectives and constraints. A 3D dose distribution was calculated using the Pinnacle inverse treatment planning system (Pinnacle 2001, 2002).

Table 3. 1: Gantry angles for 5 coplanar and 7 coplanar plans.

Plan	Gantry angle (^{o})						
5 coplanar							
plan1	0	72	144	216	288		
plan2	15	87	159	231	303		
plan3	30	102	174	246	318		
plan4	45	117	189	261	333		
plan5	60	132	204	276	348		
coplanar							
5B_1	0	72	144	216	288		
5B_2	35	110	180	250	325		
7 coplanar							
7B_1	0	51	102	153	204	255	306
7B_2	40	80	110	250	280	310	355

3.2.3 TCP and NTCP

TCP was calculated by logistic regression equation:

$$TCP = \frac{\exp(a + bD)}{1 + \exp(a + bD)} \tag{3.1}$$

where D is dose, a and b are related to D_{50} and γ_{50}. Okunieff *et al* (1995) summarized clinical data for a variety of tumors and reported parameters that can be related to slope and dose to control 50% of tumors. The multi-institutional data for the tumor control grades T2–T4 were used (for grade T4: $TD_{50} = 41.78$Gy and $\gamma_{50} = 0.66$, for grade T3: $TD_{50} = 46.29$Gy and $\gamma_{50} = 0.42$, for grade T2: $TD_{50} = 45.18$Gy and $\gamma_{50} = 0.34$), where TD_{50} (Gy) and γ_{50} (%%) are the dose and normalized slope at the point of 50% probability control.

NTCP is calculated using the Lyman-Burman-Kutcher algorithm (Lyman 1985, Burman 1991, Kutcher 1991).

$$NTCP = \frac{1}{\sqrt{2\pi}} \int_{-\infty}^{t} e^{-\frac{x^2}{2}} dx \tag{3.2}$$

$$t = \frac{D - TD_{50}(v)}{mTD_{50}(v)} \tag{3.3}$$

where $v = V/V_{ref}$ and $TD_{50}(v) = TD_{50}(1)v^{-n}$, as suggested by Burman et al. (1991), TD_{50} of 80 Gy, n of 0.12, and m of 0.15 were use for rectum.

3.2.4 Convolution of dose gradient with geometric uncertainty

In this paper, the static dose distribution D_0 is convolved with a PDF describing the geometric uncertainty P. The result is the blurred dose distribution that is expected to be delivered in the presence of this uncertainty.

$$D(\bar{r}) = D(x, y, z) = \iiint D_0(x - x', y - y', z - z')P(x', y', z')dx'dy'dz' \tag{3.4}$$

where *x*, *y*, and *z* refer to coordinates in the left-right (LR), anterior-posterior (AP), and superior-inferior (SI) directions, respectively. The dose profiles are determined across the isocenter in the LR, AP and SI directions by exporting RTOG files from Pinnacle and analyzed by MATLAB.

For simplicity, equation (3.4) is denoted as:

$$D(\bar{r}) = \iiint D_0(\bar{r} - \bar{r}')P(\bar{r}')d\bar{r}' \tag{3.5}$$

Taking the derivative is well defined by convolution (Arfken 1995),

$$\nabla D(\bar{r}) = \iiint \nabla D_0(\bar{r} - \bar{r}')P(\bar{r}')d\bar{r}' \tag{3.6}$$

where $\bar{r}$ is the vector, denotes x, y and z. The term $\nabla D_0(\bar{r})$ is the static dose gradient G_0; $\nabla D(\bar{r})$ is the blurred dose gradient G; P is the PDF (motion kernel). The simplified form can be expressed:

$$\nabla D = \nabla D_0 \otimes P \tag{3.7}$$

where $\otimes$ denotes the convolution operator, given a reference point $\bar{a} \in R^3$; the blurred dose can be expressed as:

$$D(\bar{r}) = D(\bar{a}) + \int_C \nabla D(\bar{r})d\bar{r} = D(\bar{a}) + \int_C [\nabla D_0 \otimes P]d\bar{r} \tag{3.8}$$

Where C is the line from $\bar{a}$ to $\bar{r}$; same methodology can also be applied for the derivative of motion kernel:

$$D(\bar{r}) = \iiint D_0(\bar{r}')P(\bar{r} - \bar{r}')d\bar{r}' \tag{3.9}$$

82

$$\nabla D = D_0 \otimes \nabla P \tag{3.10}$$

$$D(\bar{r}) = D(\bar{a}) + \int_C \nabla D(\bar{r}) \, d\bar{r} = D(\bar{a}) + \int_C \left[D_0 \otimes \nabla P \right] d\bar{r} \tag{3.11}$$

By integrating equation (3.7), the blurred dose including organ motion was obtained in equation (3.8), which explicitly identifies the fundamental components influencing the blurred dose which are dose gradient and motion kernel. The static dose profile and dose gradient are shown in Figure 3.1; and the Gaussian PDF with SD and derivative of PDF are shown in Figure 3.2. The blurred dose can be expressed by the integration of either the static dose gradient convolved with the PDF as shown in Figure 3.3 or the integration of the static dose convolved with the derivative of the PDF as shown in Figure 3.4. That is, the blurred dose gradient can be determined from the convolution of the static dose gradient with PDF in Figure 3.3 or determined from the convolution of the static dose with derivative of PDF in Figure 3.4. For the section of the profile where the dose gradient is near zero (inside the PTV), there will be minimal impact on the blurred dose for the internal organ motion, while for the section of the profile at outside edge of PTV where the dose gradient is the steepest, there will be maximal impact for internal organ motion. The contribution of the convolution of static dose with the derivative of PDF will have maximal impact on the blurred dose when the dose changes sharply outside edge of PTV. The algorithm used in Figure 3.4 is the edge detection used in imaging process. The blurred dose profile inclusion of geometric uncertainties can be obtained by integration of blurred dose gradient as shown in Figure 3.3 and Figure 3.4. The steps used in calculating blurred dose distribution including geometric uncertainties are shown in Figure 3.5.
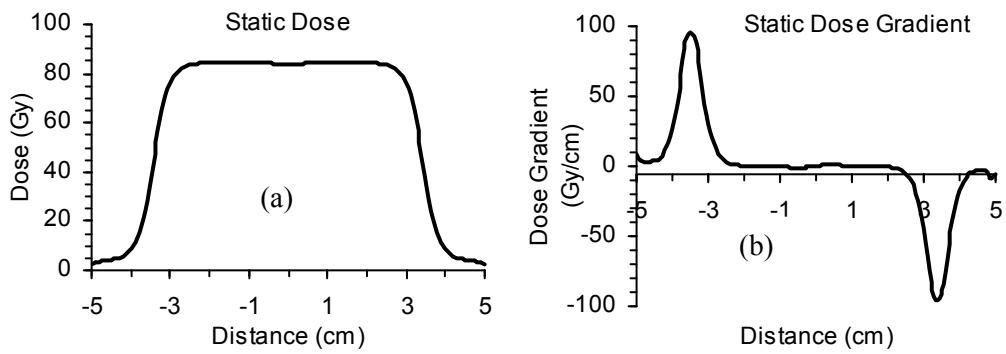
Figure 3. 1: (a) Static dose profile (b) corresponding static dose gradient.
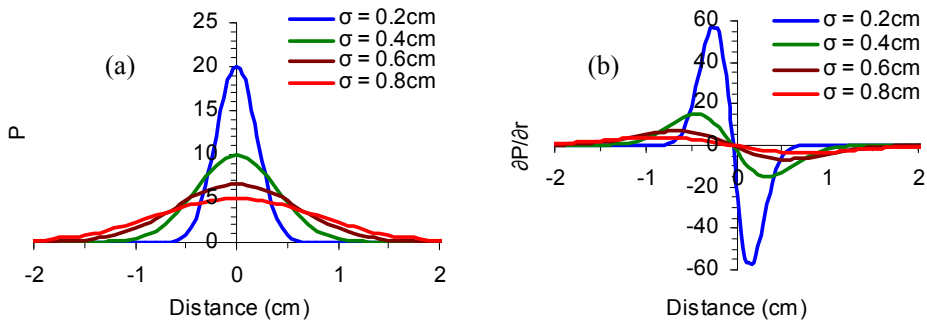
Figure 3. 2: (a) Gaussian PDF with SD (b) derivative of PDF.
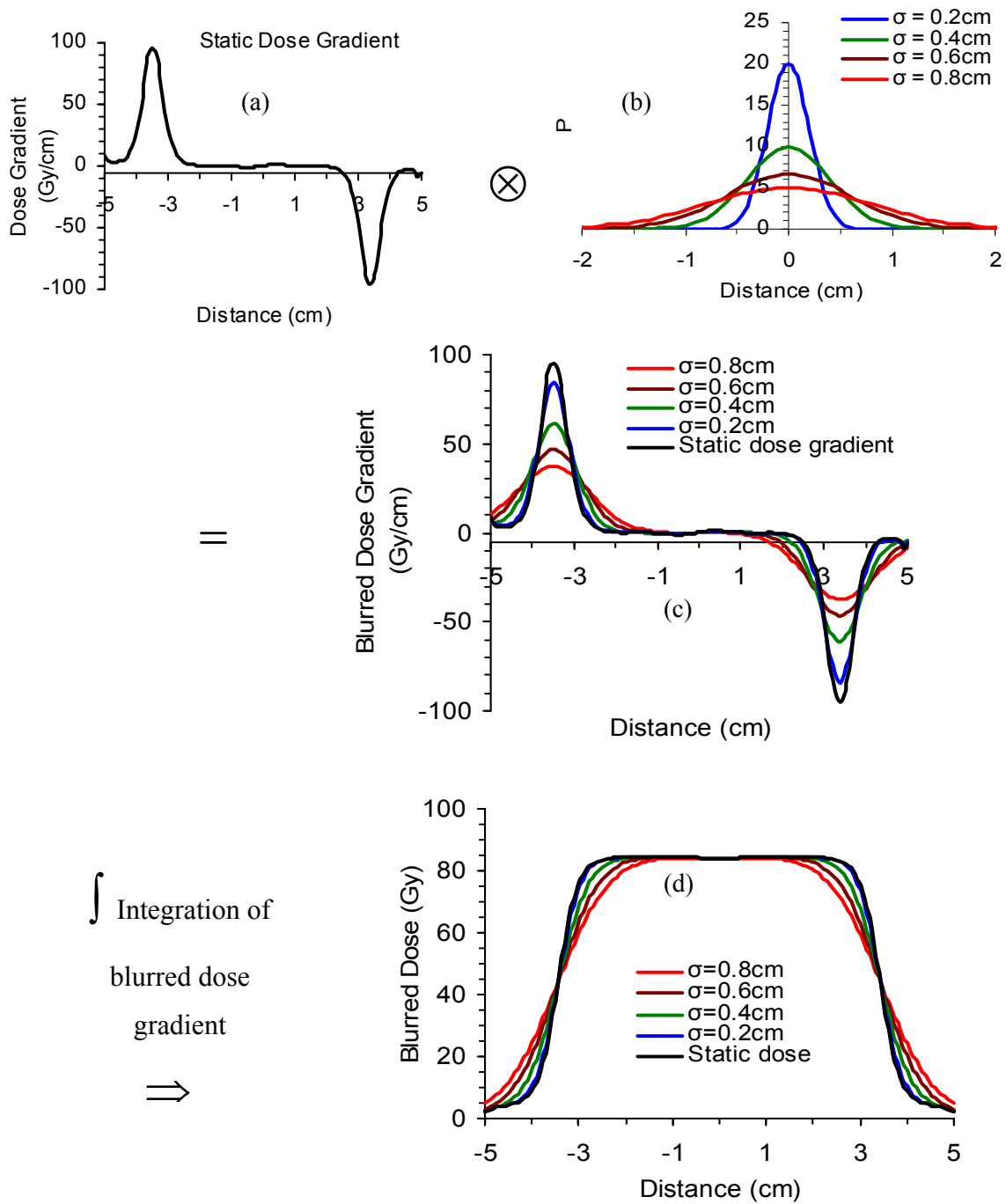
Figure 3. 3: The blurred dose gradient (c) is determined from the convolution of the static dose gradient (a) with PDF (b). The blurred dose including geometric uncertainties (d) is determined from the integration of blurred dose gradient (c).
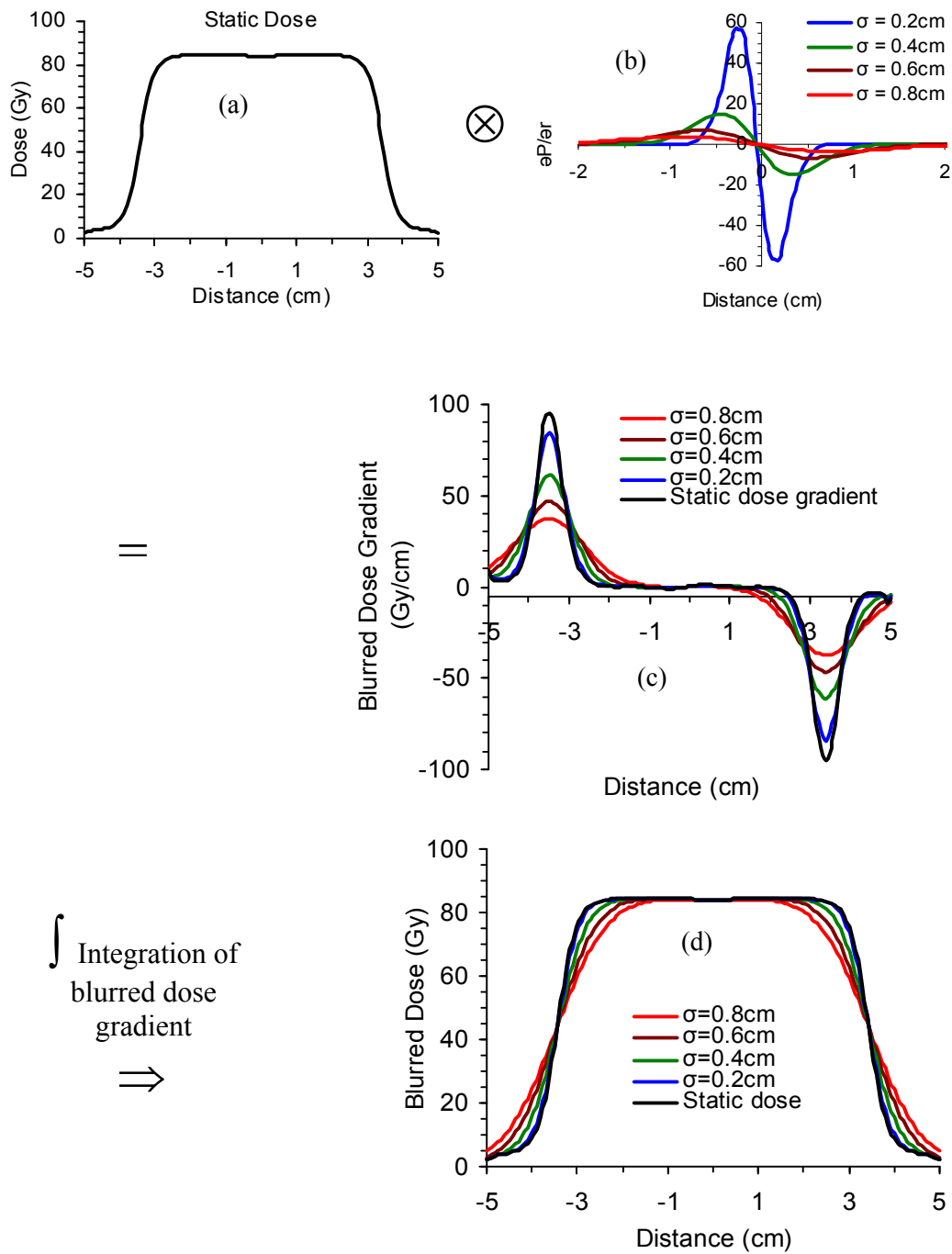
Figure 3. 4: The blurred dose gradient (c) is determined from the convolution of the static dose (a) with derivative of PDF (b). The blurred dose including geometric uncertainties (d) is determined from the integration of blurred dose gradient (c).

```
   ┌─────────────┐                        ┌─────────────┐
   │ Static dose │                        │     PDF     │
   └──────┬──────┘                        └──────┬──────┘
          │ Derivative                           │ Derivative
          ▼                                       ▼
 ┌──────────────────┐                   ┌──────────────────┐
 │ Static Dose Gradient │               │ Derivative of PDF │
 └────────┬─────────┘                   └────────┬─────────┘
          │ Convolution                          │ Convolution
          ▼                                       ▼
      ┌───────┐                             ┌───────────┐
      │  PDF  │                             │ Static dose │
      └───┬───┘                             └─────┬─────┘
          ⇓                                       ⇓
 ┌──────────────────┐                   ┌──────────────────┐
 │ Blurred dose gradient │              │ Blurred dose gradient │
 └────────┬─────────┘                   └────────┬─────────┘
          │ Integration                          │ Integration
          ▼                                       ▼
 ┌──────────────────────┐               ┌──────────────────────┐
 │ Blurred dose distribution │          │ Blurred dose distribution │
 └──────────────────────┘               └──────────────────────┘

   (a) Equation (3.6) ∼ (3.8)              (b) Equation (3.9) ∼ (3.11)
```
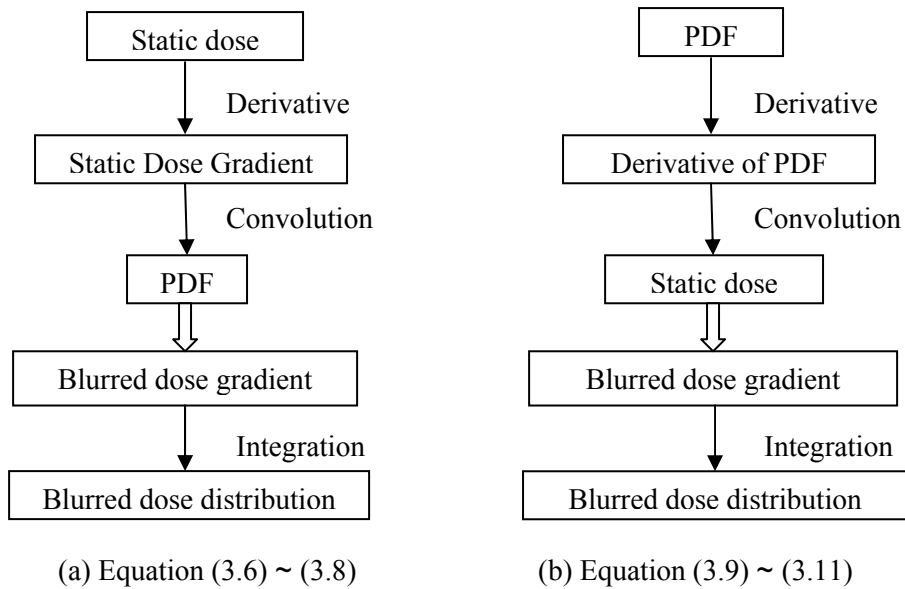
Figure 3. 5: Steps used in calculating the blurred dose distribution including geometric uncertainties.

Most of the organ motion studies give the mean and SD of motion in three orthogonal coordinate directions (Althof 1996, Balter 1995, Beard 1996, Crook 1995, Dawson 1998, Melian 1997, Roeske 1995, van Herk 1995, Zelefsky 1999). Doses at points along the anterior-posterior line through the isocenter were used to define the anterior-posterior doses for each patient, and the same method was used for the lateral and superior-inferior directions. The blurred dose gradient depends on the characteristics of the motion kernel as described by P and static dose gradient G_0.

PMDD in different directions was defined as deference between the mean dose of the dose points of blurred dose profile from isocenter to the edge of PTV and the mean dose of the whole PTV for the static dose distribution:

$$PMDD_i = \frac{MD_i - MD_0}{MD_0} \times 100\% \tag{3.12}$$

where MD_i is the mean dose of dose points of the blurred dose profile from isocenter to the edge of PTV, the i represents one of the directions: left, right, anterior, posterior, superior or inferior. MD_0 is the mean dose of the whole PTV for static dose distribution as shown in Figure 3.6.
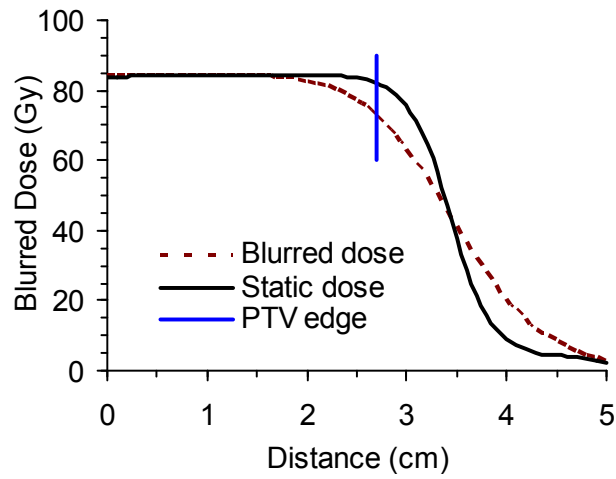
Figure 3. 6: MD_i is the mean dose of dose points along the blurred dose profile from isocenter to the edge of PTV (dashed line).

$PMDD_i$ changes with the SD (σ) of the PDF. The SD can be obtained from the IGRT data. The PDF is patient specific. The population SD and patient specific SD were listed in Chapter 2. The slope of $PMDD_i$ changing with σ defines the organ motion dose sensitivity (OMDS),

$$OMDS_i = \frac{PMDD_{i1} - PMDD_{i2}}{\sigma_1 - \sigma_2} \times 100\% \tag{3.13}$$

3.3 Results

3.3.1 Target dose profile and convolution

The dose profile across isocenter in AP, LR and SI directions for five-beam IMRT plans can obtained by exporting RTOG file data from the Pinnacle system. The resolution or dose voxel size is a user-defined parameter (typically 0.25 cm in all directions) which is specified prior to IMRT optimization. Increasing the resolution (i.e. reducing the dose voxel size) increases the time required for dose computation and optimization. The dose profile can also be obtained from the Pinnacle scripts directly. Different beam angle selections have direct influences on the dose distribution and profiles, as shown in Figure 3.7.
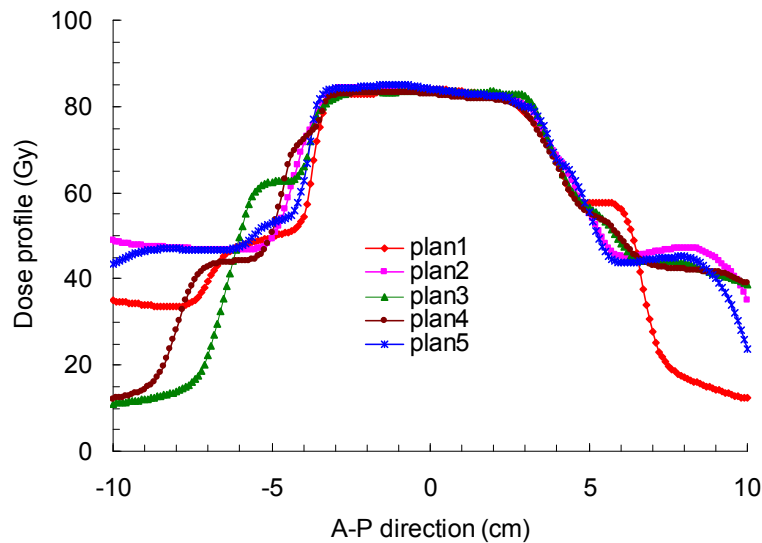
Figure 3. 7: Static dose profiles along isocenter in A-P direction for five types of IMRT plans.

A Gaussian kernel is widely used and supported with a significant body of published data (Ten Haken 1991, Schild 1993, Balter 1995, Crook 1995, van Herk 1995, Lebesque 1995, Roeske 1995, Beard 1996, Althof 1996, Melian 1997, Vigneault 1997, Dawson 1998, Zelefsky 1999, Craig 2003a, 2003b). In this study, a Gaussian PDF with clinically realistic SDs for patient organ motion and repositioning uncertainty in three orthogonal coordinate directions were obtained in Chapter 2. Motion caused blurring dose distribution and thereby to a less conformal dose distribution in Figure 3.8 (five-field plan1; SI direction profile).
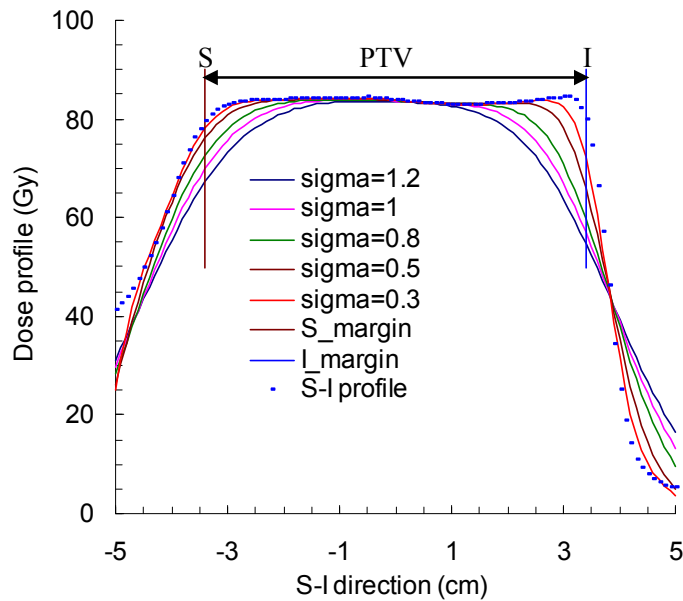
Figure 3. 8: Dose profile along the SI direction and profiles with organ motion (Gaussian distribution with standard deviation sigma = 0.3, 0.5, 0.8, 1 and 1.2).

Organ motion changes the dose distribution within the target volume. Because portions of the target volume can, in some cases, move outside of the high dose region that was planned to encompass them, a dose profile across this region of interest displays a broadening that is similar to an enlarged beam penumbra. Motion leads to a less steep

dose gradient and an enlarged dose profile penumbra at the edge of target. The amount of dose profile penumbra changing depends on the SD sigma and the dose gradient in the motion direction. The dose gradient is significantly deteriorated when internal organ motion is considered. When two dose profiles are compared, the difference between the dose with and without considering the organ motion is much greater for the sharper dose gradient as shown in Figure 3.8. The steepest gradient appears in the inferior direction (right) of the IMRT plan, while the dose gradient in superior direction (left) is not as sharp as that in inferior direction.

3.3.2   Maximum Dose gradient

The dose distribution falls steeply in the inferior direction for all the patients. Figure 3.9 shows the dose gradients results for the same patient used in Figures 3.7 and 3.8 for one treatment plan.   The steepest gradient appears in the inferior direction of the IMRT planning. For five IMRT plans with different beam angles, the sharpest dose gradient appears in the inferior direction; as well, for five beam and seven beams, the inferior direction has the sharpest dose gradient as shown in Figure 3.10. In the case of a small prostate, sharp dose gradient appears in both in the superior and inferior directions.
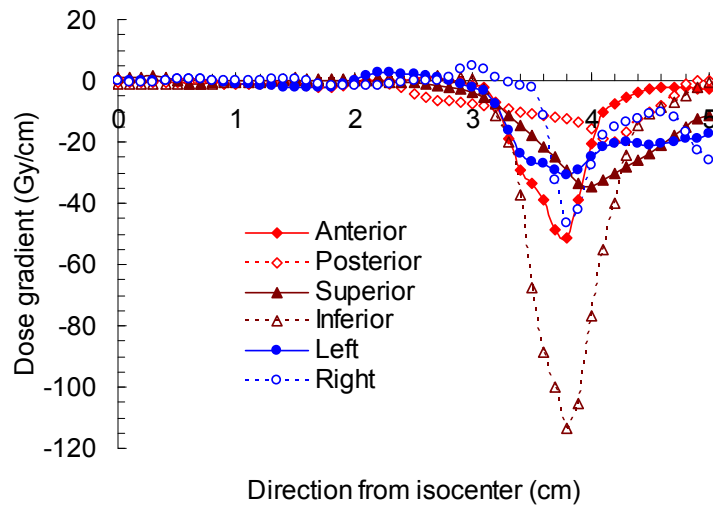
Figure 3. 9: The static dose gradient (G_0) from isocenter to anterior, posterior, superior, inferior, left, and right directions for five beam IMRT plan (0°, 72°, 144°, 216°, 288°).
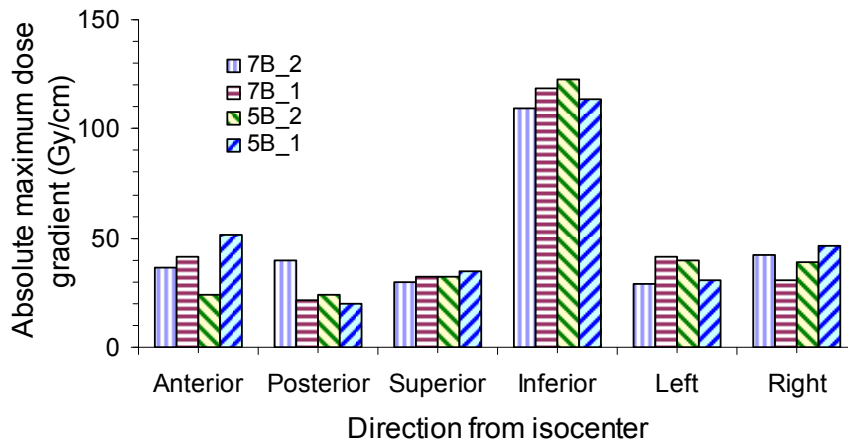
Figure 3. 10: Absolute maximum dose gradient for different IMRT techniques.

3.3.3 Organ motion dose sensitivity (OMDS)

The potential reduction in PTV dose coverage occurring at the edge of the PTV becomes a greater risk to the target with a sharper dose gradient. The motion sensitivity in anterior, posterior, left, right, superior and inferior directions with various dose gradients are evaluated by dose points along these directions within the PTV. PMDD was calculated from the dose difference between mean dose from isocenter to different directions within the PTV for the blurred dose profile and the mean dose within whole PTV for the static dose profile. The PMDD appears mostly in posterior direction for static dose distribution because of sparing the rectum intersection part of the IMRT planning as shown in Figure 3.11. The rate change of PMDD is much higher in the inferior direction when internal organ motion is considered because of the higher dose gradient in inferior direction. The inferior direction has the sharpest dose gradient; therefore the motion has the most effect on dose profile in this direction.
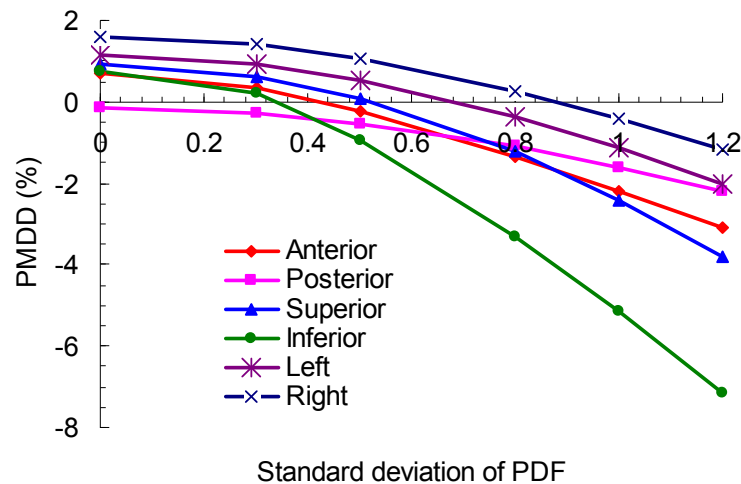
Figure 3. 11: PMDD versus SD of PDF (Equation 3.12 in text).

In general, a sharper dose gradient leads to a bigger dose difference on the edge of PTV. The PMDD varies quasi-linearly with the maximum dose gradient between standard deviation equals 0.5 cm and 1 cm. The organ motion dose sensitivity is defined as the PMDD slope between values of $\sigma = 0.5$ cm and $\sigma = 1$ cm; OMDS increases with the maximum dose gradient in anterior, posterior, left and right directions as shown in Figure 3.12. Dose gradients in superior and inferior directions are much higher than the left, right, anterior and posterior directions, due to common inferior and superior field borders of the field segments, the sharpest dose gradient will occur in the inferior direction or both the superior and inferior penumbrae. Thus, prostate motion in the SI direction produces the highest dose difference. From Figure 3.12, the OMDSs in superior and inferior directions are higher compared with other four directions. The PMDD with SD of organ motion are listed for three patients as representatives due to limited space, with small (17.3 cm^3), medium (51.6 cm^3) and large prostate (87.1 cm^3) volume when SD equals 0.5 cm and 1 cm in Tables 3.2 and 3.3 respectively. Distribution into small, medium and large prostate volume was done to observe possible trends in terms of impact of internal organ motion.
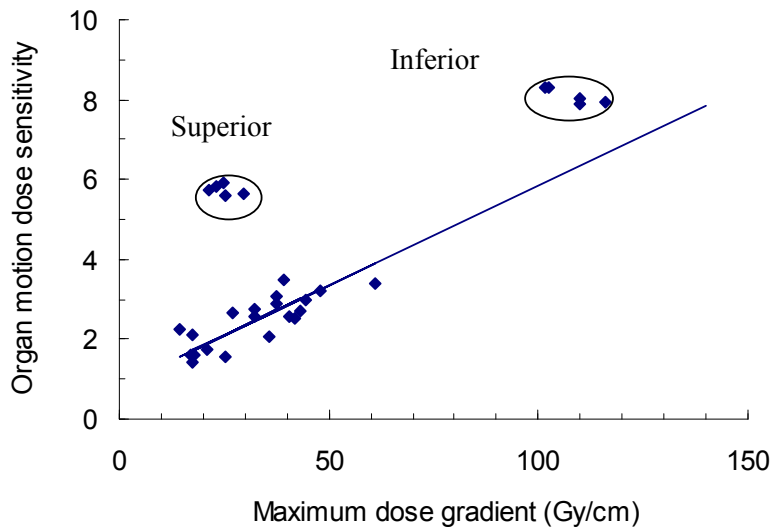
Figure 3. 12: The organ motion dose sensitivity (Equation 3.13) versus maximum dose gradient.

Table 3. 2: PMDD with organ motion (standard deviation=0.5 cm).

	Anterior	Posterior	Superior	Inferior	Left	Right	Combined effect
			Small prostate				
plan1	-0.3074	-0.2099	-1.3919	-1.2652	0.5320	-0.3867	-0.5049
plan2	1.0520	1.4079	-0.3317	-4.1806	1.9472	0.4968	0.0653
plan3	0.3960	-0.0227	-0.5723	-3.3583	0.3174	0.6685	-0.4286
plan4	0.8164	0.6231	-0.1907	-4.6110	1.1735	0.7713	-0.2362
plan5	-0.7123	0.6447	-1.1247	-2.1548	1.1746	0.3219	-0.3084
			Medium prostate				
plan1	-0.2309	-0.5280	0.0621	-0.9273	0.5473	1.0540	-0.0038
plan2	0.6963	-1.0049	-1.5420	-0.4614	0.2392	1.0668	-0.1677
plan3	0.0822	0.2264	-0.7634	-1.0548	0.2287	0.9703	-0.0518
plan4	0.2637	-1.3195	-0.6622	-0.3986	0.8790	0.4557	-0.1303
plan5	1.3458	-0.5359	-0.0618	-0.2317	1.3497	0.9489	0.4692
			Large prostate				
plan1	-0.8052	0.2641	0.2582	-0.1442	-0.3429	0.0610	-0.1182
plan2	1.3287	-0.3737	-1.0387	-1.3441	0.3811	0.5032	-0.0906
plan3	-0.7501	-0.8990	-0.8315	-2.0708	-0.2589	0.4913	-0.7198
plan4	-0.5289	-1.5026	-1.1749	-1.6552	0.2414	0.0893	-0.7552
plan5	0.7035	0.1506	-0.7529	-0.6844	0.3283	0.6097	0.0591

Table 3. 3: PMDD with organ motion (standard deviation=1 cm).

	Anterior	Posterior	Superior	Inferior	Left	Right	Combined effect
			Small prostate				
plan1	-2.0706	-0.8252	-4.3194	-8.3127	-0.6288	-1.7378	-2.9824
plan2	-0.4433	0.8291	-3.6323	-10.8452	0.5730	-0.5839	-2.3504
plan3	-0.7728	-0.4655	-3.6226	-10.3785	-0.5959	-0.4859	-2.7202
plan4	-0.1744	0.0891	-3.3109	-11.3708	-0.0410	-0.3323	-2.5234
plan5	-1.9575	0.0387	-3.9888	-8.8874	-0.1531	-0.9647	-2.6521
			Medium prostate				
plan1	-2.2125	-1.6023	-2.4045	-5.1601	-1.1344	-0.3995	-2.1522
plan2	-0.7891	-1.9366	-3.6474	-4.3970	-1.8611	-0.2200	-2.1419
plan3	-1.1295	-0.8888	-2.7875	-4.9513	-1.3697	-0.2273	-1.8924
plan4	-0.9688	-2.3458	-2.8256	-4.3181	-0.7776	-0.8393	-2.0125
plan5	-0.3996	-1.4091	-2.3929	-4.0964	-0.0167	-0.7164	-1.5052
			Large prostate				
plan1	-2.5377	-0.6100	-2.6984	-4.1174	-1.6334	-1.3100	-2.1512
plan2	-0.1187	-1.0833	-3.9053	-5.3519	-1.3138	-0.5328	-2.0510
plan3	-1.8072	-1.7094	-3.7472	-6.0106	-1.8708	-0.7618	-2.6512
plan4	-1.6618	-2.2881	-3.9881	-5.7985	-1.1006	-1.2016	-2.6731
plan5	-0.8391	-0.6528	-3.5482	-4.8273	-1.0130	-0.8719	-1.9587

3.3.4 Effects of dose profile on rectum
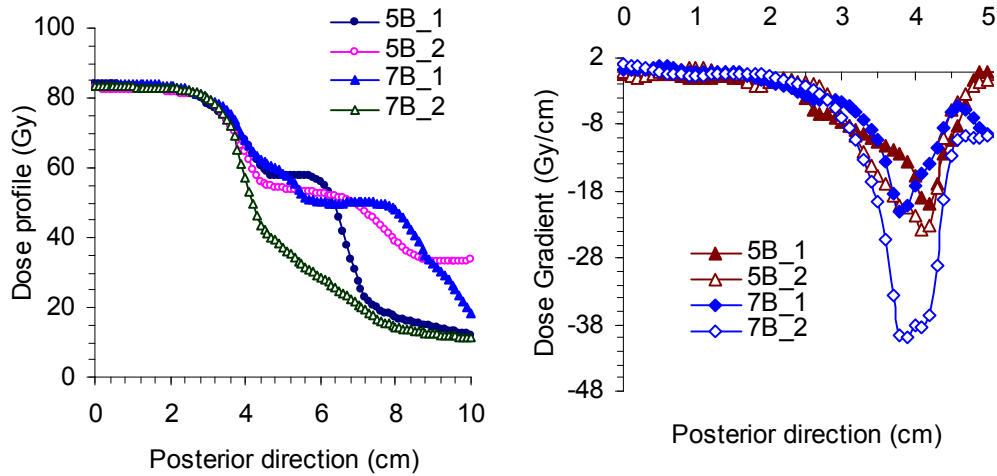
Figure 3. 13: Dose profiles and gradients for different IMRT planning techniques.

Although sparing of both the rectum and bladder was considered during treatment planning; only the effects on rectum have been evaluated in detail in this study. Rectum sparing can be gained through reducing the margin of the PTV. However, CTV coverage is still important, and any PTV margin reduction should be facilitated by reduction of geometric uncertainties. The use of posterior margins of 1 cm to define the PTV in prostate treatment implies that portions of the anterior rectum will regularly receive the full prescription dose. Advances in IMRT have allowed greater separation between tumor control and normal tissue complications through improved dose distributions with steep dose gradients.

Table 3. 4: Average NTCP with different margins and techniques.

NTCP (%)	10mm	8mm	5mm	2mm
5B_1	17.7	16	14.7	9.7
7B_2	14.7	13.3	9.7	5.0

Different IMRT techniques are compared and the dose profile and gradient in posterior direction are shown in Figure 3.13. These technologies are exploited to maintain the escalated tumor dose constant but yielding different level of rectal complications. With the same DVH control points and different beams and beam angles, the rectum has less complication risk with the steepest dose gradient between the target volume and rectum in technique 7B_2 (40°, 80°, 110°, 250°, 280°, 310°, 355°).

Technique 7B_2 has the sharpest dose gradient in posterior direction causing lower complications. The average NTCP for rectum for all the patients with different margins and two techniques are shown in Table 3.4. The margin was significantly associated with level of rectal complications. NTCP changes from 17.7% for a 10 mm margin to 9.7% for a 2 mm margin. However the results also revealed that the ability of IMRT techniques to reduce rectal complications depended on the techniques used. NTCP changes from 17.7% to 14.7% for a 10 mm margin, from 14.7% to 9.7% for a 5 mm margin for 7B_2 technique compared to 5B_1 technique because of the steeper dose gradient in 7B_2 technique. Margins are reduced for 7B_2 technique compared to 5B_1 technique to get the similar NTCP.

The limitation of analyzing doses to the rectum lies in the fact that the rectum moves during the course of treatment, either by expanding or contracting, and by bulk motion in the anterior-posterior direction. The rectum can move 1 cm in the anterior-posterior direction with respect to the bony anatomy (Jackson 2001a). Geometric uncertainties can be assumed by rigid body translations of the patient anatomy. The rectum is assumed to be moved rigidly 1 cm in the anterior-posterior direction. The rectum has lower mean dose for 7B_2 (40°, 80°, 110°, 250°, 280°, 310°, 355°) compared to the other three techniques as shown in Figure 3.14. When the rectum moves in the high dose region, MD increases; while the rectum moves out the high dose region, MD decreases and decreases more sharply for the 7B_2 technique.
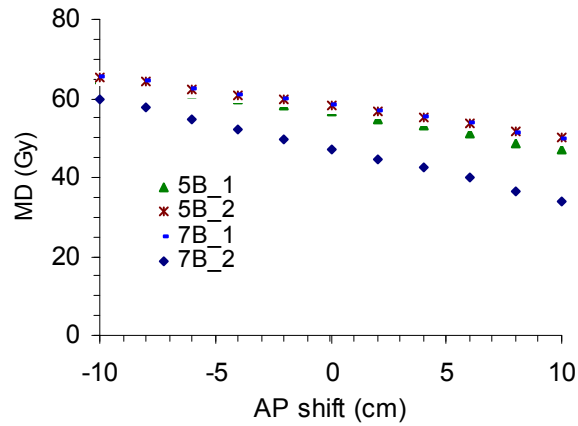
Figure 3. 14: Rectal mean dose versus AP shift.
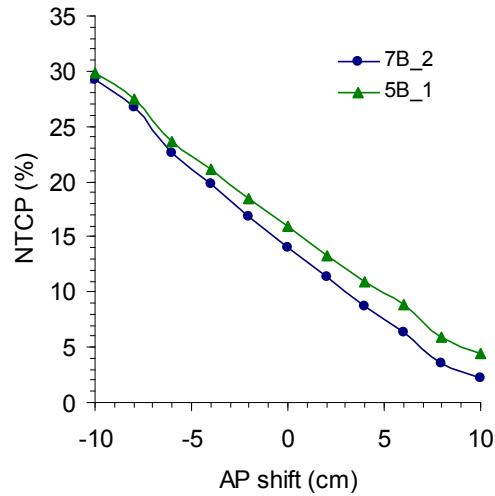
Figure 3. 15: Rectal NTCP versus AP shift.

In Figure 3.15, with escalated higher prescribed dose and sharper dose gradient in posterior direction, the slope of NTCP reduction due to rectal motion from anterior to posterior direction, is sharper for 7B_2 technique compared to 5B_1 technique because of the sharper dose gradient in the posterior direction for 7B_2 technique.

99

3.3.5 The effect of geometric uncertainty on dose profile

The patient was planned with a tight 2mm PTV margin, and then convolved with a PDF from the specific patient's IGRT data. The patient-specific PDF could be selected and the patient plan was evaluated. Table 3.5 showed the 20 patients' prostate motion with mean and standard deviation in three directions. The first column showed the patient number and total fraction number for the patient. Prostate motion relative to bony anatomy in LR direction is less than those of AP and SI directions. The PDFs of Patient #6 and patient #7 were selected to evaluate the percentage dose difference in AP direction, especially on the edge of target (cold spot). Figure 3.16 showed the percentage dose difference compared with prescription dose within PTV in AP direction. For patient #6, most of the motions are in the anterior direction, the dose difference is - 4.2 % in anterior direction; while for patient #7, most of the motions are in posterior direction, the dose difference is -3.5 % in posterior direction. Figure 3.17 showed the percentage dose difference compared with prescription dose within PTV in SI direction. For patient #1, most of the motions are in the inferior direction, the dose difference reached – 44.7 % in inferior direction; while for patient #3, most of the motions are in superior direction, the dose difference is – 5.1 % in superior direction. Figure 3.18 showed the result of patient #13, with the mean equals 2.6 mm in inferior direction, the dose difference is – 7.4 %. The inferior motion caused the most dose difference because of the sharpest dose gradient in the inferior direction.
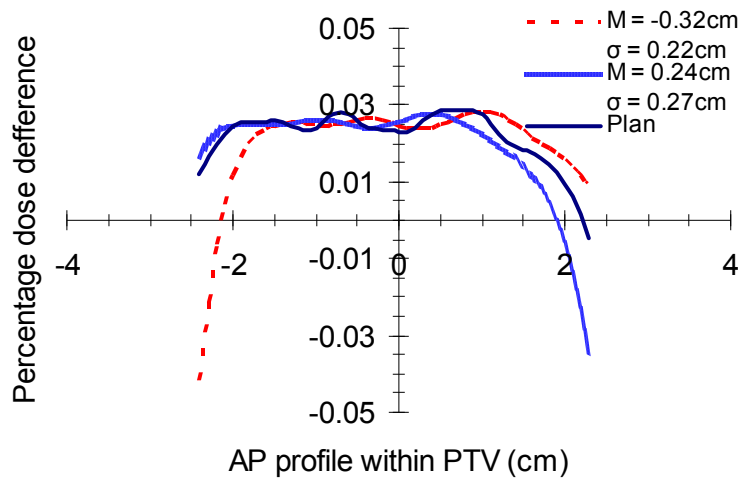
Figure 3. 16: The dose difference for static 7F IMRT plan with a tight 2mm margin compared to the prescription dose within the PTV in AP direction. Static dose profile and profiles convolved with the PDFs of patient #6 (red) and patient #7 (blue).
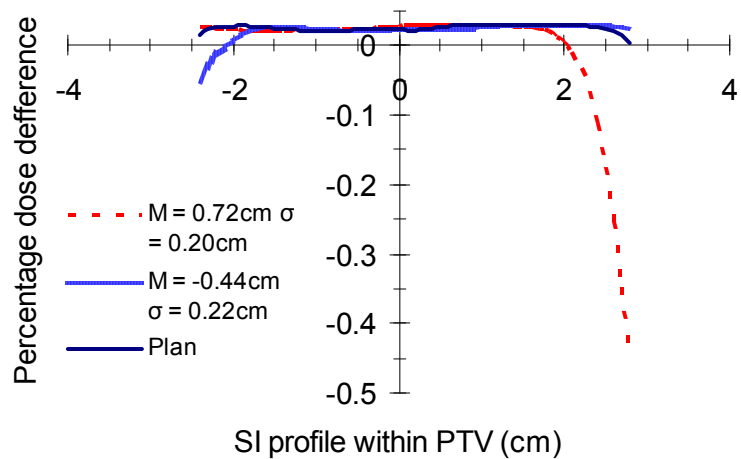
Figure 3. 17: : The dose difference for static 7F IMRT plan with a tight 2mm margin compared to the prescription dose within the PTV in SI direction. Static dose profile and profiles convolved with the PDFs of patient #1 (red) and patient #3 (blue).
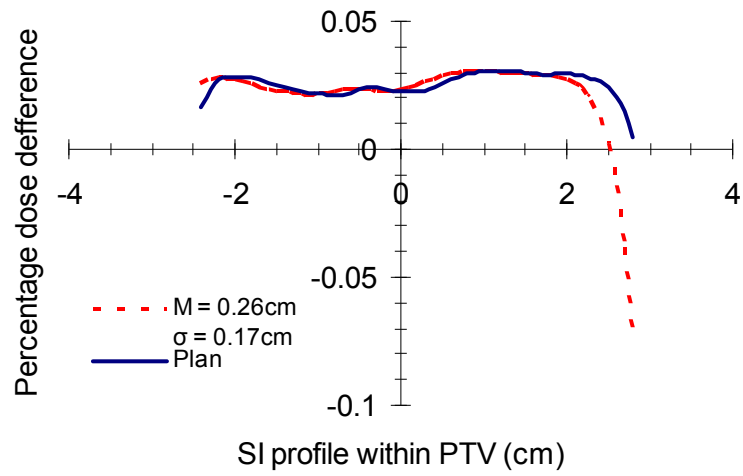
Figure 3. 18: The dose difference for static 7F IMRT plan with a tight 2mm margin compared to the prescription dose within the PTV in SI direction. Static dose profile and profile convolved with the PDF of patient #13.

Table 3. 5: Prostate organ motion for 20 patients in AP, LR and SI directions.

Prostate	AP		LR		SI	
unit: mm	Mean	SD	Mean	SD	Mean	SD
P1(32)	0.22	2.57	1.00	0.70	7.18	2.01
P2(27)	0.88	3.28	-0.30	0.75	1.04	2.41
P3(29)	-0.61	2.77	-1.66	0.85	-4.35	2.16
P4(34)	1.74	2.46	-0.24	0.67	-1.47	1.88
P5(34)	1.46	1.80	-0.21	0.88	-0.52	1.82
P6(33)	-3.15	2.15	-0.72	0.85	-2.36	2.24
P7(37)	2.40	2.67	0.25	1.11	1.24	2.25
P8(33)	0.66	2.46	-0.44	0.76	-1.37	2.29
P9(33)	-0.79	1.42	-0.52	0.41	-1.51	1.26
P10(32)	-0.97	2.44	0.72	1.07	-1.47	1.80
P11(33)	-0.56	1.92	-0.51	0.94	-2.49	1.83
P12(34)	-0.39	2.53	3.40	1.22	-1.71	2.19
P13(31)	1.60	2.21	-0.61	0.94	2.58	1.68
P14(35)	-1.70	1.57	-0.03	0.63	1.17	1.82
P15(35)	-1.61	2.11	0.52	0.83	0.82	1.90
P16(31)	-0.64	2.33	-1.14	0.46	-1.73	1.42
P17(34)	1.47	1.35	0.85	0.85	-0.30	1.20
P18(34)	-0.11	1.41	-0.09	0.60	-0.55	2.20
P19(16)	-0.07	1.20	0.20	1.42	0.34	1.62
P20(34)	0.20	2.45	-0.94	1.46	2.22	2.31

3.3.6　Treatment plan vs. measurement
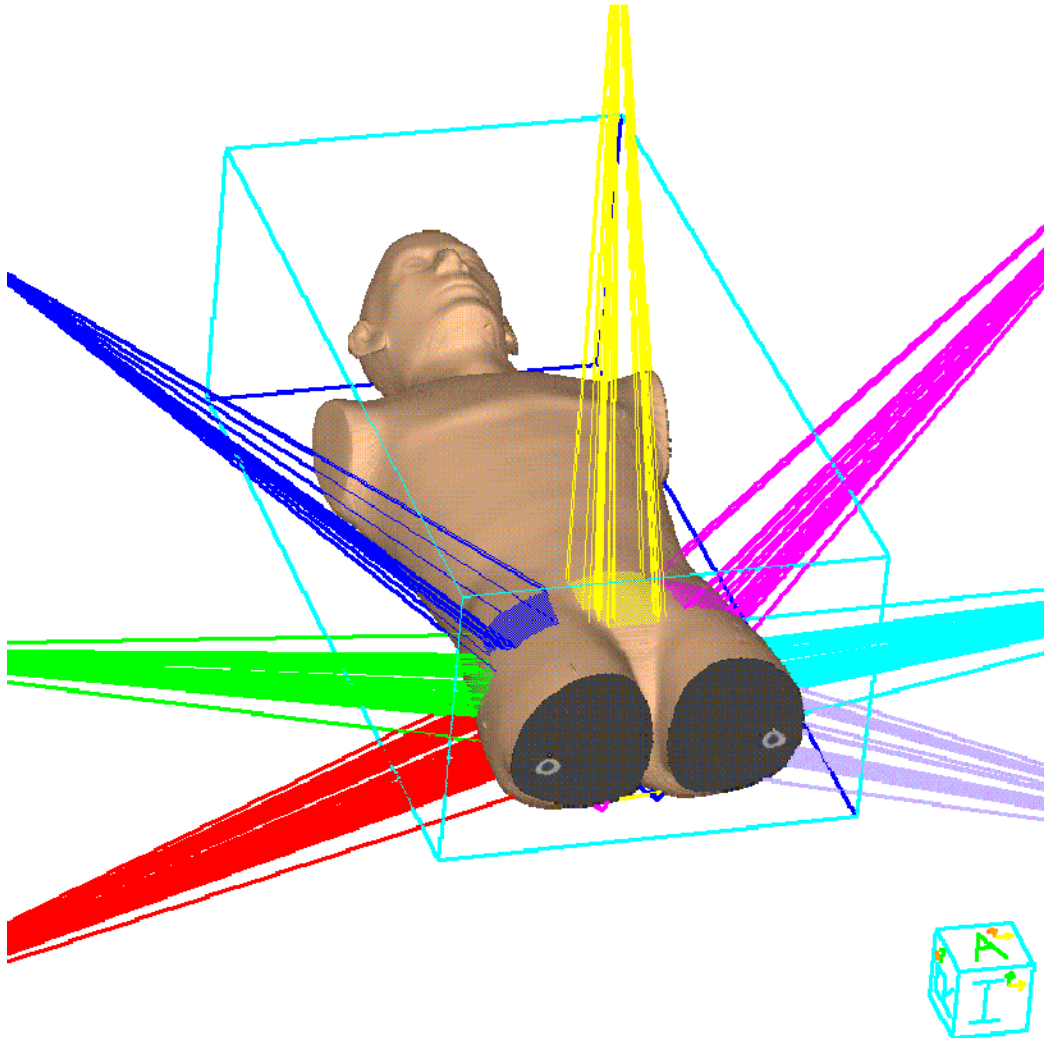
Figure 3. 19: Beam arrangement for seven-field IMRT using Rando phantom.
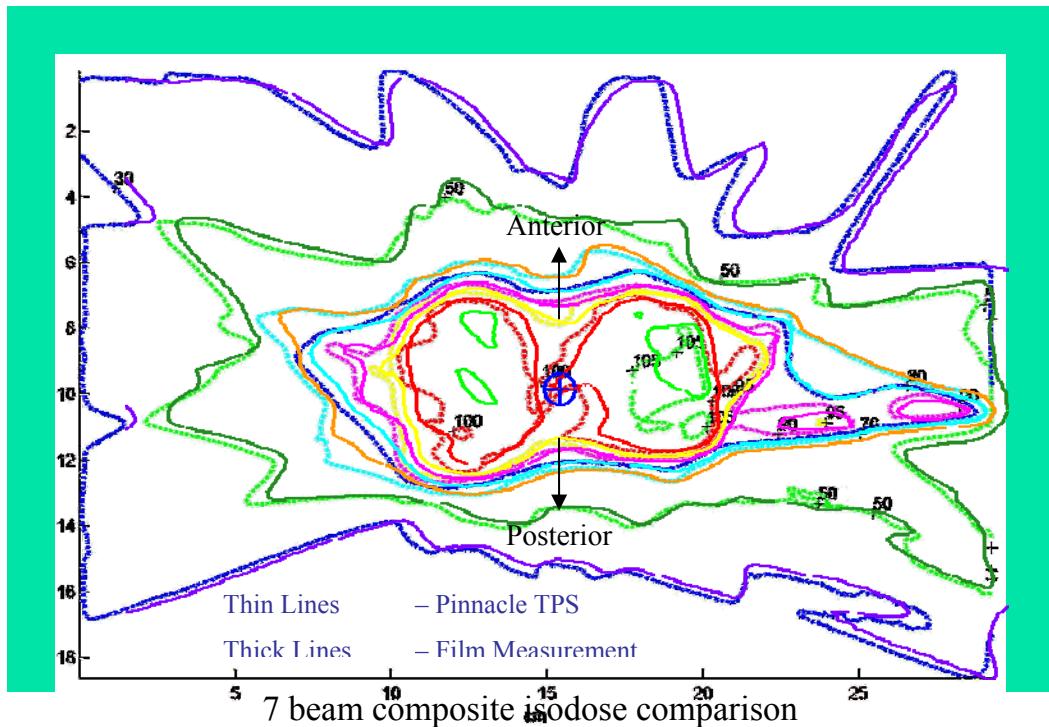
Figure 3. 20: Treatment plan vs. measurement: seven beam IMRT for prostate bed (central plane).

The validity of a treatment planning system-based dose gradient analysis can be tested by comparing planned and measured results. The dose distribution resulting from a seven-field IMRT plan was compared to both film and ion chamber array measurements for the 7 field geometry depicted in Figure 3.19. The isodose line comparison between the treatment plan and film measurement is shown in Figure 3.20. The thin lines are the Pinnacle treatment planning system result; the thick lines are the film measurement result. A similar level of agreement was seen in the coronal ion chamber array measurements. The seven beam composite isodose comparison for prostate bed treatments (double concave "dumbell shaped" target) shows that the treatment planning system is accurate and consistent with measurements, especially in the high dose regions from isocenter to the anterior or the posterior direction. The result shown above is for a single plan vs. measurement comparison. To date, many plans and measurements have been compared with similar levels of agreement. The excellent agreement between the

treatment planning system and measured data validates the treatment plan-based dose gradient analysis method.

3.4 Discussions

The outcome of clinical trials is dependent on dose accuracy; 5% accuracy is desirable and assuming that uncertainties in each procedure are random in nature, then the required accuracy for each step is 2.5% (ICRU50 1993, ICRU62 1999, Van Dyk 1999). In the Tables 3.2 and 3.3, the PMDD with SD of organ motion are listed for all the five plans. The PMDD is within 2.5% in the anterior, posterior, superior, left and right directions, just two plans for small prostate are above 2.5% in the inferior directions when SD equals to 0.5 cm. The PMDD reaches 11% for a small prostate moving along the inferior direction when SD equals to 1 cm.

The standard deviation for prostate and seminal vesicle motion from the studies ranged from 0.7 to 3.2 mm in the LR dimension, 1.5 to 7.3 mm in the AP dimension, and 1.7 to 6.5 mm in the SI dimension (Alasti 2001, althof 1996, Balter1995, crook 1995, Hoekstra 1996, Jiang 2007c, little 2003, Melian 1997, Rudat 1996, van Herk 1995, Vigneault 1997). As reported by Melian *et al* (1997), one SD translations of the prostate was 4.0 mm in AP compared to 3.1 mm in SI. Similar observations were made by Rudat *et al*. (1996) with 6.1 mm in AP, 3.6 mm in LR, 6.5 mm in SI for the combined effect of patient repositioning and prostate motion for prostate patients. Although no major bias for anterior movements was found over posterior movements, a bias was discovered for inferior motion over superior motion (Alasti 2001). This result is consistent with findings by Crook *et al* (1995), who reported 43% of patients as having inferior displacements greater than 5 mm and 11% greater than 10 mm. This predominant motion in the inferior direction was attributed to a reduction in the distension of the rectum during a course of radiation therapy. In our study, the inferior direction has the sharpest dose gradient. When the prostate moves inferiorly, it could move out of the high dose region and cause a much higher dose deficiency. As noted earlier, there is the steepest dose falloff outside of the

PTV in inferior direction. The inferior motion is expected to cause a higher PMDD within the PTV. If SD is less than 5 mm, the PMDD is within 2.5%. But if SD is higher than 5 mm in S-I direction, the PMDD is over 2.5% in inferior direction. Therefore the patient QA checking of treatment plan for prostate patients in inferior directions is essential.

For prostate motion, AP movement is larger than the LR; the preference for AP motion was first explained through the correlation of prostate motion with bladder and rectum fillings by Ten Haken *et al* (1991). The movement is correlated to the bladder and rectal filling (Balter 1995, Beard 1996, Roeske 1995). In the AP direction, the average motion varied from 0.2 mm to 6.4 mm, with SDs ranging from 3.9 mm to 6.7 mm, no major preference for anterior movements was found over posterior movements (Alasti 2001). AP motion would cause complication to the rectum. In our study, the ways to reduce the rectal complication can be realized by either smaller margin or steeper dose gradient. Following the ICRU-62 (1999) recommendations, uncertainties during radiation therapy treatments are generally included in the treatment planning by adding a margin to the CTV to yield the PTV. Large margins result in a high level of confidence that the CTV is adequately covered during treatment. However, PTV overlaps with OAR (ICRU50 1993, ICRU62 1999), which is the case in the prostate patient. The overlap part of rectum and PTV will receive the full prescription dose. Smaller margins and more conformal dose distributions are helpful means to reduce the dose to the rectum, but may compromise the dose coverage of the PTV. However, steep dose gradient between PTV and rectum works well to maintain TCP and reduce NTCP.

In IMRT, the dose distributions are increasingly conformal with an introduction of dose gradients within the PTV in an effort to avoid higher incidences of rectal complications with higher prescribed dose. The shaper dose gradient in posterior direction can be obtained by either different planning techniques or adjusting DVH controls points in IMRT optimization. Dose gradient has relationship with the number of the beams and the selection of beam angles. The rectum has lower complication with the steepest dose gradients between the target volume and critical structures in technique 7B_2, which geometrically avoids the rectum, but still provides excellent coverage of PTV.

The dose gradient is a product of the optimizer, dose objective function and constraints, while specification of controls points is insufficient to set the dose gradient because the dose gradient ∇D also has relation with the beams and beam angles. The results show that the rectum has lower NTCP for 7B_2 (40°, 80°, 110°, 250°, 280°, 310°, 355°) technique with same control points. The dose gradient is a sensitive function of DVH control points of commercial optimization algorithms; the maximum dose gradient should be determined by adjusting DVHs control points for individual patients or by putting an additional shell around PTV to constrain the shell dose with DVH control points. This will be discussed further in next chapter.

3.5   Chapter Summary

Dose gradient and PDF were used to evaluate the effect of internal organ motion for IMRT treatment planning of prostate cancer. The PMDD depended on the dose gradient and PDF. OMDS was defined by the rate of change in PMDD with SD of Gaussian PDF and was found to increase with the maximum dose gradient in anterior, posterior, left and right directions. Due to common inferior and superior field borders of the field segments, the sharpest dose gradient occurred in the inferior or both superior and inferior directions. Thus, prostate motion in the SI direction produced the highest dose difference. The PMDD is within 2.5% when SD is less than 5 mm, but the PMDD is over 2.5% in inferior direction when SD is higher than 5 mm in inferior direction. Verification of organ motion in the inferior directions is essential. Lower rectal NTCP can be achieved by either smaller margin or steeper dose gradient between the PTV and rectum. With the same DVH control points, the rectum had a lower complication in the 7B_2 technique because of the steeper dose gradient between the target volume and rectum. The relationship between dose gradient and rectal complication probability can be used to evaluate the IMRT treatment planning. Dose gradient analysis is a powerful tool to evaluate IMRT treatment plan and can be used for QA checking of treatment plan for prostate patients.

Chapter 4

The Effect of Dose Gradient on

Rectal NTCP

Rectal complication in intensity-modulated radiation therapy (IMRT) prostate treatment planning was evaluated using spatial dose distribution and dose gradient around overlap region of prostate and rectum. Dose distributions were generated from a Pinnacle planning system using five-field (5F) and seven-field (7F) co-planar IMRT techniques with an escalated dose of 82Gy. Local maximum dose gradient (LMDG) were obtained in the transverse and sagittal planes and analyzed to find the relationships between LMDG and organ motion dose sensitivity (OMDS), tumor control probability (TCP) and normal tissue complication probability (NTCP). In the transverse plane, LMDGs exhibited a large variation for a 5F plan and were lowest in posterior direction. However, the variation decreased significantly with increasing beam number. In the sagittal plane, the highest LMDG occurred in the inferior direction or both the superior and inferior directions. The OMDS were much higher in SI direction than LR and AP directions, due to common inferior and superior field borders of the field segments. Thus, prostate motion in the SI direction produced the highest impact on the target dose. Without compromising target dose distribution, LMDG in posterior direction was increased further by adjusting rectal DVH control points. Relative to 5F plans, 7F plans demonstrated a higher LMDG in the posterior direction. The higher LMDG in the posterior direction can be obtained either by modifying the planning technique or adjusting rectal DVH control points. The NTCP was reduced with a higher LMDG

109

between PTV and rectum. LMDG determined from commercial IMRT solutions can be increased further in the posterior direction by manually adjusting DVH control points. By achieving the higher dose gradient in posterior direction, rectal dose and NTCP were improved relative to current RTOG IMRT prostate protocols.

4.1 Introduction

IMRT has developed rapidly in recent years. Despite improving planning technique, delivery skills, the use of sophisticated localization procedures and 4DCT, the irradiated high-dose volume inevitably includes some portions of the bladder and the rectum. Margins are needed around the prostate to account for the uncertainties, such as setup error and prostate motion (Vigneault 1997, Lattanzi 1999, Kitamura 2002, Morr 2002, Nederveen 2002). Dose escalation with IMRT for prostate cancer has been limited by the tolerance of the surrounding normal structures such as the rectum and bladder. The increase in target prescription dose carries a potential risk of inducing chronic toxicity for the normal tissue. The IMRT prostate treatment plan uses specific the dose volume histogram (DVH) control points for the rectum and bladder to determine the treatment dose level (Yan 2000, Martinez 2001). The target dose is prescribed to meet the predetermined rectum and bladder constraints based on different dose-volume limitations of rectum and bladder. A lack of knowledge about safe dose–volume constraints may lead to inappropriate dose delivery with IMRT: an excessively cautious approach to rectum sparing may increase the risk of missing or underdosing the target, whereas the irradiation of large fractions of rectum may result in patients' experiencing moderate/severe bleeding.

A precise understanding of the tolerance of these two organs is essential because it ultimately limits the dose to the target. Despite the large number of prostate cancer patients treated with 3D-CRT, the reported knowledge of bladder and rectum tolerance is still quite unclear and not amenable to being used prospectively (Jackson 2001b, O'Brien 2001). This is due to multiple problems including the lack of standardization of tolerance

scoring or assessment, the lack of detailed and systematic data on individualized dosimetry, and inconsistency in rectal and bladder volume definitions.

Previous studies have shown a close relationship between chronic rectal toxicity and rectal dose volume histogram findings. Several authors have found the relation between chronic rectal toxicity and the volumes of the rectum or rectal wall irradiated to doses ≥50 Gy (Benk 1993, Boersma 1998, Skwarchuk 2000, Jackson 2001a 2001b, Wachter 2001, Fiorino 2002b, Kupelian 2002a). Some reports have clearly indicated a significant dose–volume dependence of late rectal injury (the so-called volume effect) (Cheng 1999, Jackson 2001a, Wachter 2001, Fiorino 2002b, Huang 2002b, Chism 2003). The RTOG toxicity scale is often used to report acute GI and GU toxicity since its publication in 1995 (Zelefsky 1995 2002a, Pollack 1996, Kupelian 2002a, O'Brien 2002, Ruy 2002). IMRT treatment enables us to treat patients without an increase in acute GI toxicity because it provides more degrees of freedom for shaping dose distribution to produce highly conformal dose coverage of PTV and significantly reducing the dose to the rectum. Rectal dose has been considered the most significant factor associated with the risk of Grade 2-4 complications (Zelefsky 1998, Michalsk 2000; Skwarchuk 2000; Storey 2000; Wachter 2001; Pollack 2002). The higher rectal dose we tolerated could be responsible for the difference in acute toxicity.

IMRT is efficacious in permitting safe dose escalation by reducing radiation exposure to dose-limiting normal tissues (Zelefsky 2002a, 2002b). However, in order to keep rectal toxicity at acceptably low levels, knowledge of the dose–volume relationship within a specific patient population must be acquired for a certain treatment setup, so that appropriate treatment constraints may be confidently applied (Lyman 1987, Kutcher 1996). Some studies have been performed to correlate DVH patterns and late rectal toxicity (Boersma 1998, Storey 2000, Fenwick 2001c, Jackson 2001b, Fiorino 2002b). There is a dose–volume relationship for rectal bleeding in the region between 60 and 75 Gy. Boersma *et al* (1998) reported on DVH analysis of a group of 130 patients treated in a 3D-CRT dose escalation protocol (70–78 Gy isocentre dose). None of the DVH parameters was significantly correlated with the actuarial incidence of GI complications grade 2 which was as high as 14% at 2 years. However, for severe rectal bleeding, three

111

dose–volume levels were found, which significantly discriminated between high risk and low risk groups: 65 Gy to 40% of the rectal wall, 70 Gy to 30% and 75 Gy to 5% of the rectal wall. When more than 25% of the rectum received 70 Gy, Storey *et al* (2000) showed evidence for a significant increase in late rectal complications. Furthermore, all grade 3 complications occurred when 30% of the rectum received 70 Gy. An update of the toxicity outcome of this study by Huang *et al* (2002) with a median follow-up of 5 years and more extensive DVH analysis, showed a strong relationship between dose and volume. To reduce the risk of late toxicity they identified the following cut-points: <40% of the defined rectal volume should receive 60 Gy, <25% should receive 70 Gy, <15% should receive 75.6 Gy, and <5% should receive 78 Gy. DVH data from these studies clearly indicate that the percent volume of rectum exposed to doses above 60–70 Gy plays a crucial role in determining radiation-induced rectal morbidity.

The investigations mentioned above have reported relationships between rectal dose–volume data and clinically observed rectal complications. However, few studies specify the spatial dose distribution, such as dose gradient as an indicator of how conformal the dose coverage actually is and its effect to the target and normal tissue (Jiang *et al* 2007a, 2007b). Although DVHs are important planning parameter and are linked to TCP and NTCP, they do not contain spatial dose distribution information and are therefore not as effective as the dose gradient.

The dose profile and dose gradient analysis are carried out to present the dose distribution of a chosen voxel sequence of the 1D interest in this study. The aim of this study is to find dose–volume constraints for IMRT inverse-planning algorithm with an escalated dose of 82 Gy by analyzing the dose profile and dose gradient. The rectum receives higher dose with escalated prescription dose, however the rectal DVH control points were pulled down as much as possible without compromising target dose coverage judged by dose profile and gradient. Although sparing of both the rectum and bladder was considered during treatment planning; only the effects on rectum have been evaluated in detail in this study. Dose gradient analysis is completely general and is independent of optimization algorithm. The analysis of the dose gradient is a useful tool for judging of IMRT treatment plan.

4.2 Methods and Materials

4.2.1 Patients

IMRT Treatment plans are created for fifteen prostate patients, covering a range of prostate target volumes from 17.3 cm^3 to 87.1 cm^3, and different overlap of planning target volume (PTV) with organ at risk (OAR). The prostate, seminal vesicles, bladder, rectum, and femoral heads of the prostate patients were contoured by the therapist using CT data. Two PTVs for each patient are generated: PTV1 includes the prostate and seminal vesicles plus a 10 mm margin; PTV2 includes the prostate only plus 10 mm margin. Table 4.1 shows the volume range and standard deviation of PTVs and OARs determined from Pinnacle[3].

Table 4. 1: Volume range (cm^3) for PTV and OAR.

Prostate	Sem. Vesicles	Rectum	Bladder	PTV2	PTV1	Femur
17.3 to 87.1	5.8 to 24.9	44.9 to 217.6	44.4 to 520.1	78.1 to 254.9	141.1 to 314.1	134.1 to 223.1
45.2±18.3	13.3±5.8	98.25±44.9	232.3±44.4	153.7±43.3	218.4±46.8	172.1±25.1

4.2.2 IMRT treatment planning and objective functions

All cases were planned for supine patient treatment using a 6 MV photon beam from Varian 21EX linear accelerator (Varian Medical Systems, Palo Alto, CA). All were devised for coplanar treatment with the long axis of the patient couch parallel to the axis

of the treatment machine gantry rotation. The prostate IMRT inverse treatment planning was optimized with a coplanar, isocentric five-field (5F: 0°, 72°, 144°, 216°, 288°) and seven-field (7F: 40°, 80°, 110°, 250°, 280°, 310°, 355°) techniques.

Table 4. 2: DVH control points (Gy) from RTOG P-0126.

PTV2	PTV1	Rectum	Bladder	Femur
$D_{2\%} \leq 86$	$D_{95\%} = 56$	$D_{15\%} = 75$	$D_{15\%} = 80$	$D_{2\%} \leq 40$
$D_{95\%} = 82$	$D_{min} = 54$	$D_{25\%} = 70$	$D_{25\%} = 75$	…
$D_{min} = 80$	…	$D_{35\%} = 65$	$D_{35\%} = 70$	…
…	…	$D_{50\%} = 60$	$D_{50\%} = 65$	…

An escalated prescription dose of 82 Gy (2 Gy per fraction) was prescribed for all IMRT plans. The DVH control points for the PTV and OARs were adapted from RTOG 0126 protocol (2004) as shown in Table 4.2. $D_{V\%}$ is the dose (Gy) allowed for percentage volume (%). The minimum and maximum dose to the target and maximum dose to the OARs are parameters in the optimization cost function. The relative weights were adjusted by changing the DVH control points of the PTV and OARs for the IMRT plans. All patients were planned using the same objectives and constraints for PTVs and bladder but different for rectum in plan1 and plan2 as shown in Table 4.3, rectal DVH control points were lowered down as much as possible in plan2 without compromising PTV coverage. For each PTV, 3D uniform margins of 10 mm were used in plan1 and plan2; non-uniform margins of 5mm in posterior direction and 10mm margins in other directions were used in plan3. While rectal DVH control points in plan 2 and plan3 are same but plan2 with uniform margin and plan3 with non-uniform margin (5 mm in posterior direction and 10 mm in other directions). A 3D dose distribution was calculated using the Pinnacle inverse treatment planning system.

Table 4. 3: DVH control points (Gy) of rectum and bladder for different plans.

Plans	PTV	DVH Ctrl Points	$D_{15\%}$	$D_{25\%}$	$D_{35\%}$	$D_{50\%}$
Plan1	$PTV_{1,2}$=CTV+1cm	Rectum	75	70	65	60
		Bladder	78	70	65	45
Plan2	$PTV_{1,2}$=CTV+1cm	Rectum	70	60	50	45
Plan3	$PTV_{1,2}$=CTV+0.5~1cm	Bladder	78	70	65	45

4.2.3   Dose profile and LMDG

Doses at points along the specific line from the isocenter to different direction were used to define the dose profile in that direction for each patient. The dose gradient gives the slope of the dose fall in that direction and can be derived from dose profile. The dose gradient used in this study is the absolute value of dose gradient. The dose profiles are determined from the isocenter to a specific direction in the transversal plane and sagittal plane in vicinity of posterior directions. The magnitude of the dose gradient will tell how fast the dose falls in the specific direction. The LMDG is the steepest slope of the dose profile outside of PTV.

4.3 Results

4.3.1 LMDG in transverse and sagittal planes

Figure 4.1 shows the LMDG in the transverse and sagittal planes for two randomly selected patients. In the transverse plane for a 5F plan, there is a large variance in the LMDG with the lowest value in the posterior direction. By increasing the number of IMRT beams to seven, however, there is a significantly lower variance along with a higher LMDG in the posterior direction and lower LMDG in lateral direction in Figure 4.1 (a). In the sagittal plane, the largest LMDG appears in the inferior direction for both 5F and 7F plans, and there is higher LMDG in superior direction as shown in Figure 4.1 (b). The organ motion had the most effect on the target dose in the inferior direction or both superior and inferior penumbrae (Jiang *et al* 2007a). The LMDG in sagittal plane in Figure 4.1 (b) shows the same result that lowest LMDG appeared in posterior direction for 5F plan.
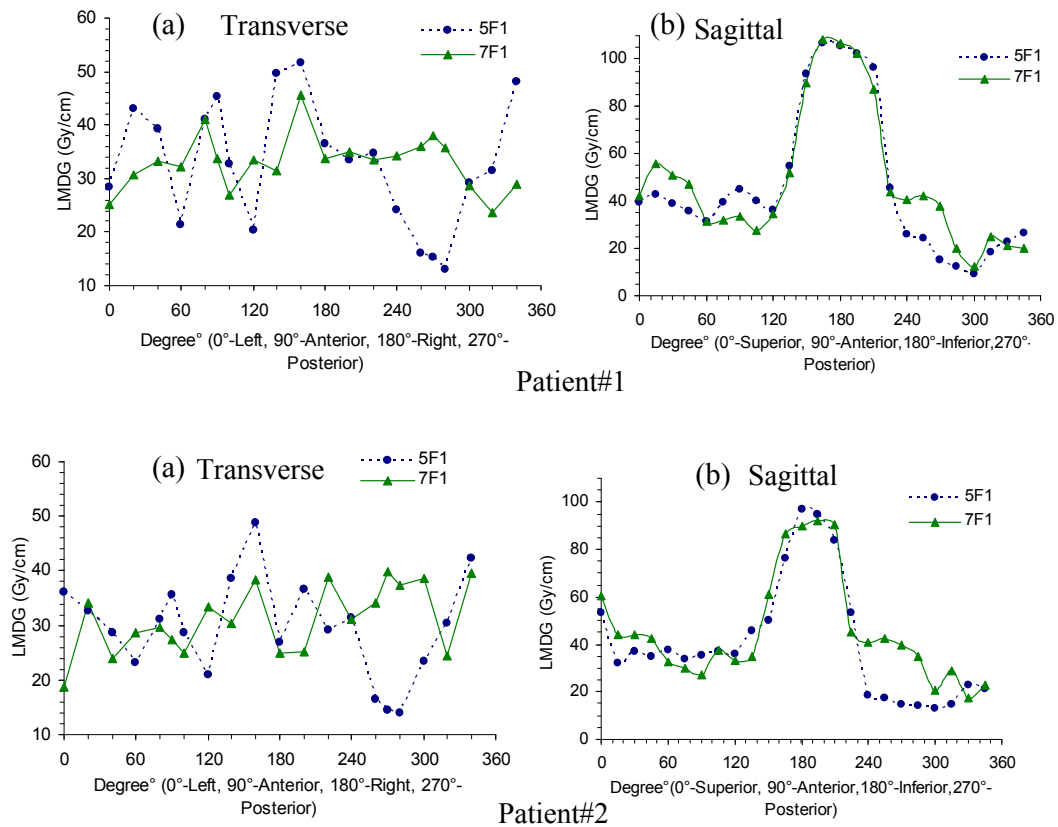
Figure 4. 1: LMDG for two randomly selected patients in (a) transverse plane and (b) sagittal plane.

4.3.2 Dose profiles and LMDG in sagittal plane

The profiles from isocenter in directions where the PTV and rectum overlap in Figure 4.2 were used to analyze the effect of LMDG on rectum. The profiles show that 7F plan have much lower dose in the dose region from 40Gy-70Gy than that of 5F plan in Figure 4.2. The dose profile for 5F1 is the highest one for all the profiles in vicinity of the posterior direction, and there is plateau around 50 to 60Gy. The beam number and beam direction affect the dose profiles in the area where the PTV and rectum overlaps. The profiles in plan2 have lower dose than that in plan1 for both 5F and 7F plans because rectal DVH

control points in plan2 pull down the profile in vicinity of the posterior direction. With non-uniform margin in plan3, dose profile drops down compare with uniform margin in plan2 for both 5F and 7F plans.
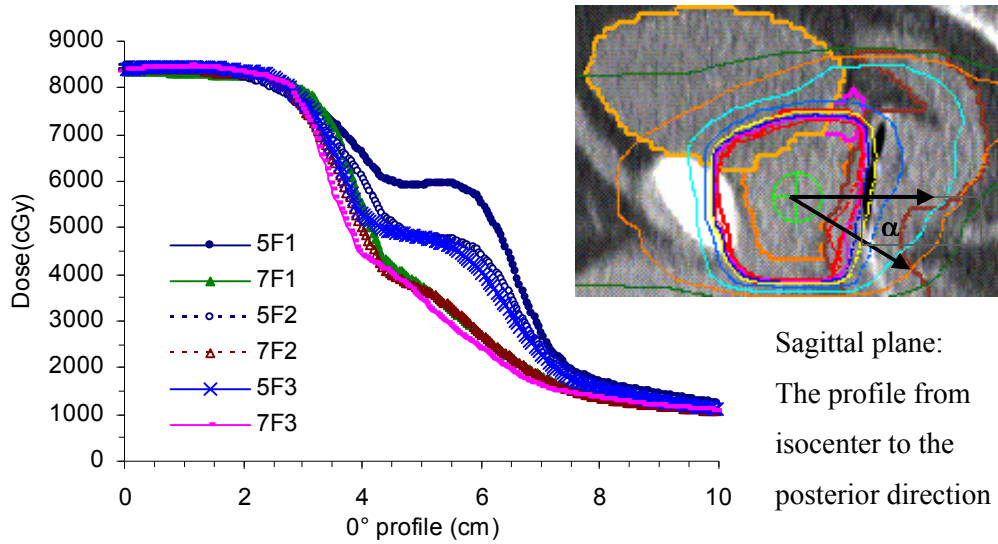
Figure 4. 2: Dose Profiles in sagittal plane from isocenter to posterior direction ($\alpha=0^{\circ}$).

The LMDG is obtained every five degrees between 0° to 15° in vicinity of the posterior directions in the sagittal plane for different IMRT techniques. The LMDG distance from isocenter is the distance from the isocenter to the position where the dose gradient reaches maximum, as shown in Figure 4.3. LMDG in vicinity of the posterior direction, LMDG distance from isocenter and rectal NTCP for one patient are shown in Figure 4.4 (a), (b) and (c), respectively. LMDG increases from plan1 to plan2 because of lower rectal DVH control points, and LMDG increases from plan2 to plan3 because of the non-uniform margin for plan3 in Figure 4.4 (a) for both 5F and 7F plans. The distance of LMDG position from isocenter is shorter from plan3 to plan2 and from plan2 to plan1 in Figure 4.4 (b), the corresponding dose outside of edge of PTV decreases quickly with higher LMDG and shorter LMDG distance from isocenter which cause lower NTCP in

Figure 4.4(c). The LMDG in vicinity of the posterior direction should be higher enough to ensure the dose fall off quickly to avoid the rectal complication.
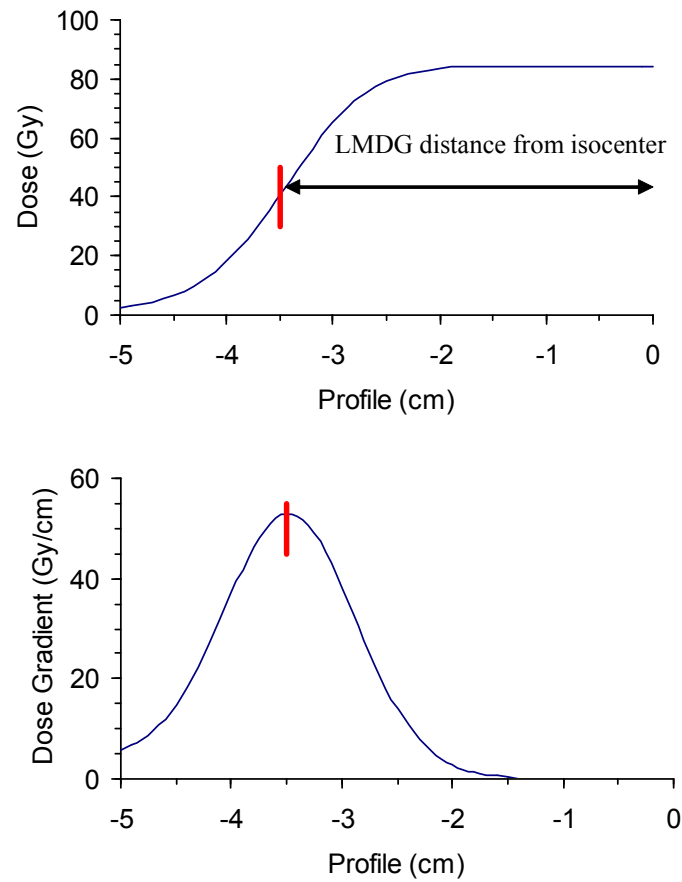
Figure 4. 3: LMDG distance from isocenter.
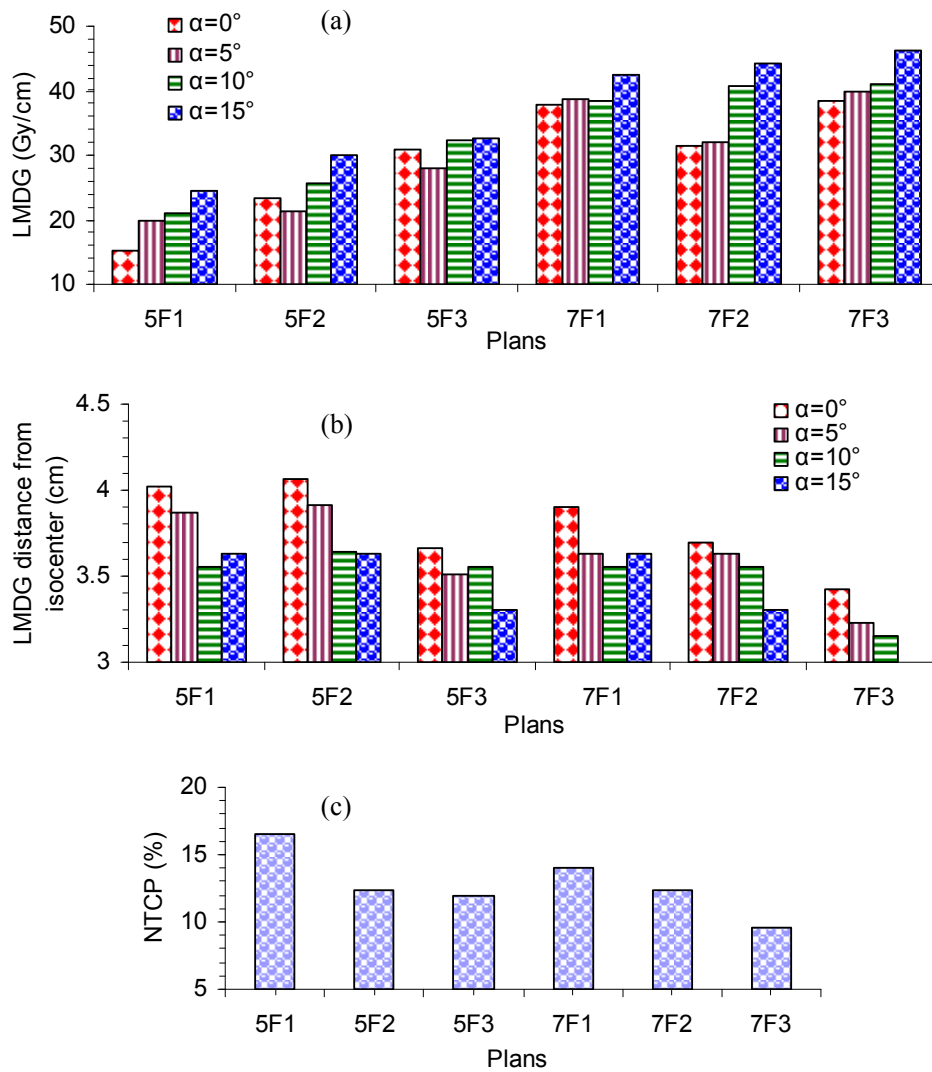
Figure 4. 4: (a) LMDG in vicinity of posterior direction, (b) LMDG distance from isocenter, (c) rectal NTCP for one patient.

4.3.3   Rectal dose at different percentage volume

For prostate cancer, the treatment dose is prescribed based on different dose-volume limitations of bladder and rectum defined as the pretreatment reference. The dose is prescribed so as to meet the predetermined PTV, rectum and bladder DVH constraints and objective functions. The rectum DVH control points were established from the RTOG P-0126 protocol (2004) for treatment planning. IMRT can permit safe dose escalation by reducing radiation exposure to dose-limiting normal tissues. The need for finding reliable dose-constraints is vital in order to keep rectal toxicity at acceptably low levels without compromising PTV. The percentage of rectal volume exposed to 45, 50, 60, and 70 Gy were limited to 50, 35, 25, and 15%, respectively in plan2. Table 4.4 shows $D_{V\%}$ for 5F and 7F plans with different DVH control points for randomly selected three patients include different rectum and bladder volume combination due to limited space. The average $D_{V\%}$ decreases from plan1 to plan2 for both 5F and 7F plan. 5F1 has obvious higher dose covering large portion of rectum. The DVH control points in 5F2 lowered the rectal DVH down to reduce the rectal dose, similar to 7F plan; however, the rectal dose $D_{V\%}$ (Gy) at different rectal percentage volume (V%) value in 7F1 is lower than 5F1 in Table 4.4.

4.3.4   Rectal percentage volume at different dose level

Table 4.5 shows the rectal percentage volumes at dose level 50Gy, 60Gy and 70Gy; mean dose, NTCP and average LMDG for 5F and 7F plans with different DVH control points. 5F1 has highest rectal percentage volume for all the patients.

Table 4. 4: Rectal dose (Gy) at different rectal percentage volume ($D_{V\%}$) for three randomly selected patients.

Patients	Plans	$D_{15\%}$	$D_{25\%}$	$D_{35\%}$	$D_{50\%}$
Patient #1					
Prostate:	5F1	78.4	72.3	66.2	59.1
51.58cm^3	5F2	75.8	66.8	57.1	47.2
Rectum:	5F3	74.9	64.3	55.2	46.8
82.87cm^3	7F1	78.2	68.4	58.0	44.9
Bladder:	7F2	76.0	64.9	55.4	43.5
274.78cm^3	7F3	72.1	61.2	49.6	38.6
Patient #2					
Prostate:	5F1	78.2	71.0	65.7	59.4
56.03cm^3	5F2	75.0	64.4	56.8	49.1
Rectum:	5F3	72.1	62.2	55.6	48.2
217.57cm^3	7F1	73.8	61.4	54.6	42.4
Bladder:	7F2	72.2	60.0	53.8	42.0
270.96cm^3	7F3	70.1	59.5	53.4	41.3
Patient #3					
Prostate:	5F1	78.8	73.4	68.3	61.9
87.08cm^3	5F2	76.5	70.0	62.4	51.8
Rectum:	5F3	76.2	67.2	58.2	49.7
76.65cm^3	7F1	79.2	71.7	64.1	56.2
Bladder:	7F2	77.8	68.7	58.2	49.1
290.68cm^3	7F3	74.7	63.8	55.3	48.7

Table 4. 5: Rectal percentage volume (%) at different dose level (V_{DGy}) for three randomly selected patients.

Patients	Plans	V_{50Gy}	V_{60Gy}	V_{70Gy}	MD (Gy)	NTCP (%)	LMDG (Gy/cm)
Patient #1							
Prostate:	5F1	70.3	46.6	27.6	57.1	16.5	21.4
51.58cm³	5F2	43.3	31.3	21.0	50.2	12.3	25.8
Rectum:	5F3	41.5	29.1	18.6	48.6	12.9	34.1
82.87cm³	7F1	42.6	32.5	22.6	47.2	14.0	35.8
Bladder:	7F2	40.5	29.7	19.7	46.1	12.4	34.0
274.78cm³	7F3	33.8	25.4	15.9	42.1	11.6	37.3
Patient #2							
Prostate:	5F1	69.6	47.3	26.0	54.7	16.7	20.2
56.03cm³	5F2	47.4	29.3	18.8	48.4	12.0	24.1
Rectum:	5F3	45.4	26.9	16.2	46.9	9.9	24.2
217.57cm³	7F1	40.3	25.7	17.0	43.6	11.1	48.9
Bladder:	7F2	39.6	24.2	15.7	43.1	10.6	47.7
270.96cm³	7F3	38.5	23.6	14.4	42.0	8.6	42.3
Patient #3							
Prostate:	5F1	86.1	54.3	31.0	61.8	19.0	15.0
87.08cm³	5F2	53.2	37.7	24.5	54.5	14.0	17.6
Rectum:	5F3	48.7	32.4	21.6	52.5	12.9	26.2
76.65cm³	7F1	63.7	41.2	26.4	55.8	17.0	40.8
Bladder:	7F2	46.9	32.3	22.8	52.2	15.5	34.9
290.68cm³	7F3	45.9	27.8	18.8	49.0	11.6	45.1

4.3.5 Average results for all patients
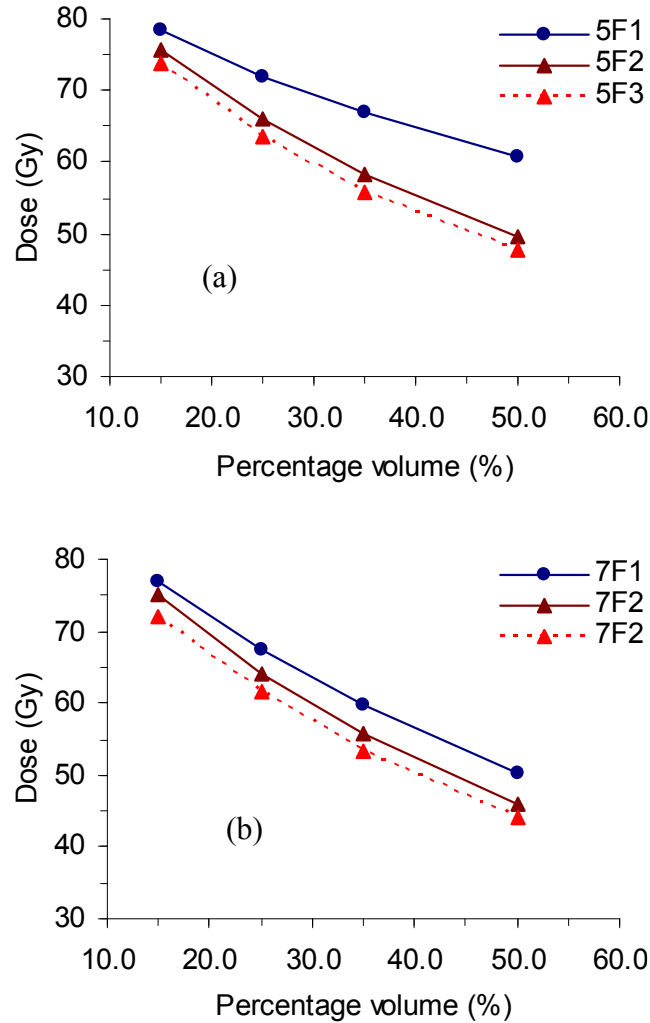
Figure 4. 5: Average rectal dose (Gy) at different percentage volume for different techniques (a) 5F, (b) 7F for all patients.

The sharper dose profiles in posterior direction, the lower dose at rectal percentage volume as shown in Figure 4.5. With the 7F plan, there is a natural reduction in the rectal dose at specific percentage volumes; also it is possible to lower the rectal DVH control

points further to obtain a better dose gradient without sacrificing or impacting on other constraints for the IMRT plans. $D_{15\%}$, $D_{25\%}$, $D_{35\%}$ and $D_{50\%}$ decrease 4%, 8%, 13% and 18% respectively from 5F1 to 5F2, while for 7F plan, the rectal dose decreasing from 7F1 to 7F2 is 3%, 5%, 7% and 8%, respectively. The 5F1 has highest dose at different rectal percentage volume; $D_{15\%}$ in plan2 is lower than 75Gy for 5F plan and 7F plan. For non-uniform margin, $D_{15\%}$ decreases 2% from 5F2 to 5F3, while decreases 4% from 7F2 to 7F3.
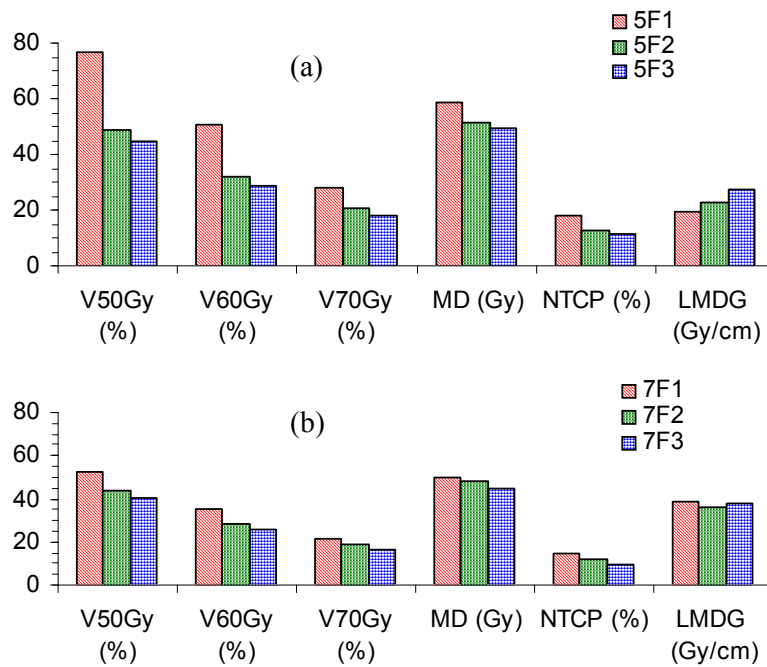
Figure 4. 6: Average rectal percentage volume, mean dose (MD), NTCP and LMDG for (a) 5F and (b) 7F plans for all patients.

Relative to a 5F plan, the 5F plan demonstrates a higher LMDG in the posterior direction causing lower rectal complications. In Figure 4.6, the average rectal percentage volume V_{50Gy}, V_{60Gy} and V_{70Gy} decreased 37%, 38% and 26% respectively from 5F1 to 5F2, while for 7F plan, the rectal percentage volume decreasing from 7F1 to 7F2 is 16%, 19% and 13% respectively. The average mean dose and NTCP decreasing are 13% and 29% from

5F1 to 5F2, and 5% and 13% from 7F1 to 7F2. For non-uniform margin, the NTCP decrease 10% for 5F plan and 17% for 7F plan. To achieve the high LMDG, V_{70Gy}, V_{60Gy} and V_{50Gy} of the rectal DVH are below 21%, 32% and 48%, respectively. These values are lower than RTOG guideline (25%, 35% and 55%, respectively) and do not compromise the dose distribution elsewhere.

4.4   Discussions

4.4.1   Dose profile and LMDG

The increase in prescription dose for the target carries a potential risk of higher rates of rectal chronic toxicity. The importance of reliable dose–volume constraints in treatment planning is becoming more apparent with IMRT. Few studies have previously focused on dose profile and dose gradient as end points of commercial optimization algorithms (Jiang *et al* 2007a). The DVH data clearly indicate that the percent volumes of rectum were lowered with lower rectal DVH control points either for the 5F plan or 7F plan; With the same DVH control points and different beams and beam angles, the rectum has lower complication in 7F plan, which has the sharper dose profile and higher LMDG in the posterior direction between the target volume and critical structures as shown in Figure 4.4. The study shows that 7F plan has sharper dose profile in posterior direction causing lower rectum complications. The results revealed that IMRT technique has the ability to redistribute the dose to achieve high LMDG in a particular region with some loss of dose gradient elsewhere.

The sharper dose profile and higher LMDG in the posterior direction can be obtained by either different planning technique (5F to 7F) or adjusting DVH controls points (plan1 comparing to plan2) in IMRT optimization. The rectum has lower complication with the steeper dose profile and higher LMDG between the target volume and rectum, which

geometrically avoids the rectum with adjusted DVH control points, but still provides excellent coverage of PTV.

In IMRT, the dose distributions are increasingly conformal with an introduction of high LMDG on the edge of the PTV in an effort to avoid higher incidences of rectal complications with higher prescribed dose. LMDG is a function of DVH control points, also a product of optimizer, dose objective function and optimization constraints. The sharper dose profile and higher LMDG in posterior direction can be obtained by either different planning techniques or adjusting DVH controls points in IMRT optimization. The LMDG around posterior direction should be higher enough to ensure the dose fall quickly to avoid the rectal complication.

4.4.2 DVH comparison for patients with and without bleeding

Several investigations have reported relationships between rectal dose–volume data and clinically observed rectal complications. Storey (2000) *et al* reported a correlation between rectal toxicity and V_{70Gy} in 91 patients treated with 3D-CRT at 78 Gy: the late Grade 2–3 rectal bleeding was 12% and 28%, respectively, for patients with V_{D70} lower or higher than 25%; Jackson (2001b) *et al* suggested that the irradiation of large fractions of the rectum at intermediate dose around the portion of rectum irradiated at high dose may result in a loss of repair capacity of the mucosa cells, which may lead to bleeding. Fiorino (2002) *et al* found several DVH constraints to be significant in a population of 229 patients treated at 70–76 Gy (ICRU dose) in three of the four institutions. In the article by Huang (2002) *et al*, the fraction of rectal volume receiving more than 60, 70, 75.6, and 78 Gy was found to be predictive of late moderate/severe rectal toxicity. Optimal cutoff values were suggested to be 40.6%, 26.2%, 15.8%, and 5.1% for V_{60Gy}, V_{70Gy}, $V_{75.6Gy}$, and V_{78}, respectively. Based on Fiorino (2003) *et al.*'s results, optimal dose–volume constraints for 3D-CRT and IMRT planning optimization: V_{50Gy} below 60–

65%, V_{60Gy} below 45–50%, and V_{70Gy} below 25–30% should keep the rate of late bleeding (Grade 2–3) below 5–10% for an ICRU dose between 70 and 78 Gy. Our results in Figure 4.5 show: V_{70Gy} below 25%, V_{60Gy} below 35% and V_{50Gy} below 55% for plans 5F2, 5F3, 7F1, 7F2 and 7F3, respectively.

The rectal dose value of $D_{15\%}$, $D_{25\%}$, $D_{35\%}$ and $D_{50\%}$ should be below 75Gy, 70Gy, 65Gy and 60Gy, respectively for RTOG 0126 (2004) treatment planning guideline. Figure 4.4 shows the rectum $D_{15\%}$, $D_{25\%}$, $D_{35\%}$ and $D_{50\%}$ are below 75Gy, 70Gy, 65Gy and 60Gy, respectively, for 5F2, 5F3, 7F2 and 7F3 with prescription dose 82 Gy. The constraints in treatment plan2 fulfill the guideline with escalation dose 82Gy.

4.4.3   Mean dose and NTCP

If the value of mean dose of the rectum was used as a cutoff value for predicting late rectal bleeding, Tucker (2004) *et al* predicted rectal bleeding for patients with rectal mean dose (MD) >56.3 Gy and no bleeding for patients with MD < 56.3 Gy. The average mean dose in our research shows the mean dose is lower than 51 Gy for all the plans except 5F1, which is 58.5 Gy. The mean dose decreases 4% and 6% for 5F plan and 7F plan respectively with non-uniform smaller margin at the prostate–rectum interface in plan3. PTV overlaps with OAR (ICRU50 1993, ICRU62 1999), which is the case in the prostate patient. The ways to reduce the rectal complication can be realized by either non-uniform margin or steeper dose profile and higher LMDG between the PTV and rectum. The overlap part of rectum and PTV will receive the full prescription dose, the more conformal dose distributions are helpful reduce the dose to the rectum, but may compromise the dose coverage of the PTV. However, steep dose profile and higher LMDG between PTV and rectum works well to maintain TCP and reduce NTCP.

Rectal volume changing during the treatment course may significantly affect the actual dose distributions, thus influencing the reliability of DVHs derived from the initial CT scan (Lebesque 1995; Roeske 1995; Tinger 1998; Wu 2001). The initial DVH from the

simulation CT must be regarded as a rough approximation. Nevertheless, the results of the current analysis do show a correlation between the dose profile of rectum and late rectal morbidity, even if the effects of treatment uncertainties are not accounted for. The research for rectal motion is further discussed in another paper.

4.5   Chapter Summary

Rectal complication probability in IMRT prostate treatment planning was evaluated using spatial dose distribution and LMDG to find the reliable dose–volume constraints for IMRT inverse-planning with an escalated dose of 82Gy. The LMDG is dependent upon the IMRT treatment technique, and DVH control points, also it is a product of the optimization routine. The sharper dose profile and higher LMDG in posterior direction can be obtained by either different planning technique or adjusting rectal DVH controls points in prostate IMRT optimization. 7F plans have higher LMDG than 5F plans. The profiles from isocenter to the directions where the PTV and rectum overlaps show the 7F plans have much lower dose in the dose region from 40Gy-70Gy than that of 5F plans. Steeper dose profiles and higher LMDGs between the PTV and rectum work well to maintain TCP and reduce NTCP. The LMDG in the posterior direction should be high enough to ensure the dose fall off quickly to avoid high rectal complication probability. The results show that 7F plans have sharper dose profile around posterior direction and resulting in lower rectum complication probability. V_{70Gy} V_{60Gy} and V_{50Gy} are below 25%, 35% and 55% respectively for 5F2, 5F3, 7F1, 7F2 and 7F3 for all the patients. The adjusted DVH control points fulfill the RTOG guideline with dose escalation to 82Gy. LMDG analysis is a powerful tool for judging the quality of IMRT treatment plans and can be used for QA of treatment plans for prostate patients.

Chapter 5

The Cumulative Rectal Dose
Incorporating Rectal Movement

5.1   Introduction

Incorporating organ motion in the treatment planning process is a challenging problem in the multi-fractional radiation treatment. In conventional treatment, the positional uncertainty of the CTV is handled by irradiating a larger volume to ensure the desired tumor dose coverage. This approach generally leads to increased normal tissue complications. The choice of the margin represents an empirical tradeoff strategy in radiation treatment. Rectal toxicity is one of the major limiting factors for dose escalation in external beam treatment of prostate cancer. The DVH of the rectum in the CT scan is commonly used as a predictive tool to estimate rectum complications and optimize treatment planning for prostate cancer. The dose volume constraints are predictors of rectal toxicity (Fiorino 2002, Foppiano, 2003, Mirabell 2003, Pollack 2002). Other parameters can be derived from DVH, such as the equivalent uniform dose (EUD) (Niemierko 1997, Wu 2002, Schwarz 2004) or the normal tissue complication probability (NTCP) (Lyman 1985), volume points at certain dose levels or the average dose (Boersma 1998, Jackson 2001, Skwarchuk 2000). However, both EUD and NTCP calculation need rectal DVH as input. While rectal DVH is affected by a number of uncertainties and limitations; for example, the dose distribution delivered to the rectum for prostate patient over the course of treatment is different fraction-to-fraction because

of the uncertainties such as patient setup error, rectal movement with respect to the bony anatomy, the delineation of the rectum, and the filling of rectum etc (Urie 1991, Webb 1997, Fiorino 2002, Stasi 2006) and it is necessary to study the impact of organ motion on the rectal cumulative dose.

Rectal movement causes considerable dose uncertainty over the course of treatment and leads to the differences between planned dose distribution and the dose distribution that is actually delivered to the rectum. The most important limitation of analyzing dose to the rectum lies in the fact that the rectum moves during the course of treatment, both by distorting and by moving bodily (eg, in the anterior-posterior direction).

Studies of patients with multiple CT scans taken during treatment for prostate cancer (Balter 1995, Mageras 1996, Melian 1997, Lebesque 1995, Roeske 1995, van Herk 1995) showed that the rectum can move 1 cm in the anterior-posterior direction with respect to the bony anatomy. The calculation of dose is typically based on a rigid-body model of localization uncertainty involving translations (Killoran *et al* 1997) of the entire patient relative to a fixed dose distribution. Although the rectal movement is obvious for the rectum during a course of treatment for prostate cancer, it is not clear what kind of influences these variations might have on the predictive value of NTCP for the course of treatment. Few study reported the dosimetric consequences of the rectal movement. In this study, the rigid body model and serial portal imaging data were used to reproduce the cumulative dose distribution to the rectum considering internal organ motion using EUD per fraction method for prostate patients.

The uncertainties of the internal organ motion result in variation of the delivered dose and can be evaluated fraction-to-fraction using EUD. The EUD in each fraction is called fractional equivalent uniform dose (EUD_f) (Jiang *et al* 2006b). The rectal positional variations can be measured from portal imaging with gold seeds for prostate patients and rectal dose change per fraction can be expressed as EUD_f deviation. This evaluation is performed by comparison of the fractional dose-volume-histogram, the rectal EUD_f considering organ motion, and NTCP, with and without considering the internal organ motion.

5.2   Methods and Materials

5.2.1   Patients and IMRT planning

IMRT plans for prostate patients were made with prescribed dose D = 78 Gy (2 Gy per fraction). The DVH control points of the PTV and OAR were used according to the RTOG 0126 protocols (Michalski 2004). PTV includes the prostate plus a 10 mm margin in the anterior, left-right, superior-inferior directions, and 7mm in posterior direction. A 3D dose distribution of one fraction planning was calculated using the Pinnacle[3] treatment planning system for five-field (5F: 0°, 72°, 144°, 216°, 288°) and seven-field (7F: 40°, 80°, 110°, 250°, 280°, 310°, 355°) IMRT using 15 MV X-rays. Repeated portal images and good seeds dada have been used to characterize daily patient organ motion for 20 prostate patients. The patients were asked to have full bladder and empty rectum in treatment CT scanning. The geometric uncertainties of prostate and rectum were assumed to be rigid body; the calculation of rectal dose is based on a rigid-body model of localization uncertainty involving translations of the prostate and rectum relative to a fixed dose distribution. The rectum was shifted in AP direction according to the prostate AP motion. The prostate motion was covered by the PTV. The EUD_f , cumulative dose to rectum and NTCP of the rectum were calculated for the course of the treatment.

5.2.2 EUD_f (EUD per fraction)

The survival fraction for a fractionated regimen of interest was obtained using the Linear-Quadratic (LQ) model (Fowler 1989):

$$SF = \left[e^{-(\alpha d + \beta d^2)} \right]^{fx}$$

(5.1)

Where d = dose/fraction; fx = number of fractions, integer. If the organ motion uncertainties were considered, the survival fraction can be expressed as:

$$SF = SF_1 \cdot SF_2 \cdot SF_j \cdots SF_{fx}$$

(5.2)

Where j = 1, 2…39 are fraction number. For inhomogeneous dose distribution, d_i is the dose point in one fraction treatment planning, the survival fraction for one fraction was:

$$SF_j(d_i) = \frac{1}{N} \sum_{i=1}^{N} (SF_{2Gy})^{\frac{d_i}{2Gy}}$$

(5.3)

Where SF_{2Gy} is the survival fraction at 2 Gy, N is number of dose calculation points within the target volume. The expend abbreviation EUD for a fractionated regimen was therefore obtained:

$$EUD = \frac{2Gy}{\ln(SF_{2Gy})} \ln(SF) = \frac{2Gy}{\ln(SF_{2Gy})} \ln(SF_1 \cdot SF_2 \cdots SF_j \cdots SF_{fx})$$

$$= EUD_1 + EUD_2 + \cdots EUD_j + \cdots EUD_{fx} = \sum_{f=1}^{fx} EUD_f$$

(5.4)

5.2.3 The Lyman-EUD model

When considering non-uniform dose distributions, the DVH is converted to an effective homogeneous dose to total volume (D = EUD, v = 1). The EUD algorithm uses the power-law relationship (Niemierko 1997):

$$EUD = \left(\sum_i v_i D_i^{\,a} \right)^{\frac{1}{a}}$$

(5.5)

where a = 1/n, n is a parameter that describes the volumetric dependence of the dose-response relationship. EUD_f for the rectum was calculated for each fraction according to the rectal AP movement over the course of treatment and was used to calculate the NTCP for the rectum.

The NTCP model was proposed by John Lyman (Lyman 1985) and is defined by the equations:

$$NTCP = \frac{1}{2} + \frac{1}{2} erf\left(\frac{EUD - TD_{50}}{m\sqrt{2}TD_{50}}\right)$$

(5.6)

where TD_{50} is the dose that causes 50% probability of injury, and m is the slope of the response curve at TD_{50}, the steepest part of the curve. TD_{50} of 80 Gy, n of 0.12, and m of 0.15 were use for rectum.

5.2.4 Compare the effect of the rectal position and volume changes on NTCP using Rando phantom
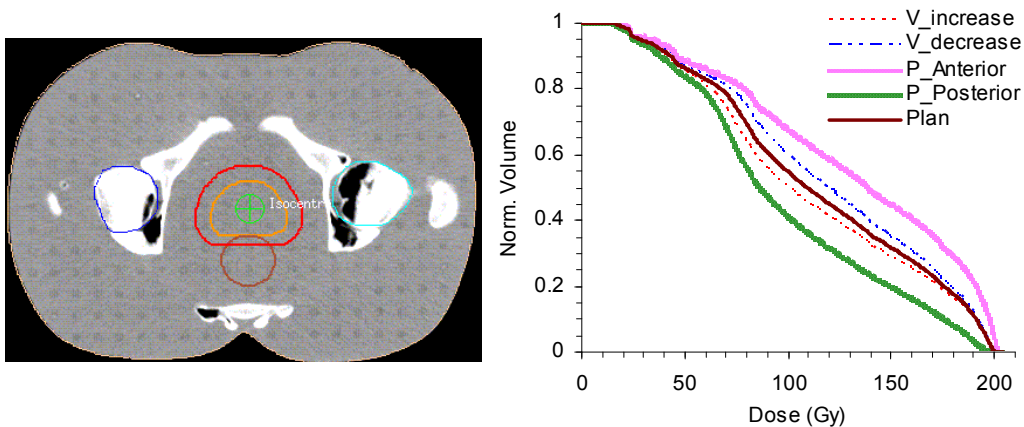
Figure 5. 1: Rectal DVH versus position (P) and volume ((V) effects with reference to Random Phantom (1) P_Anterior: rectum moves 5mm in anterior direction (2) P_Posterior: rectum moves 5mm in posterior direction (3) V_increase: rectal volume increase 30% (4) V_decrease: rectal volume decrease (26%).

Rectal DVH of Rando Phantom for the 7F IMRT plan result is shown in Figure 5.1. In order to quantify the different effect of rectal volume and position changes on the rectal dose during the course of the treatment, the volume and position changes are considered separately: Only rectal position change 5mm in anterior direction (P_Anterior) and 5mm in posterior direction (P_Posterior); and only rectal volume increase 30% (V_increase) and decrease (26%) (V_decrease). Rectal volume increasing 30% resulted in the NTCP decreases from 7.59% to 6.88%, Rectal volume decreasing 26% resulted in the NTCP increases from 7.59% to 8.36%. Rectal position change resulted in NTCP change significantly compared to rectal volume changes, from 7.59% to 13.36% when rectum moves 5mm in anterior direction, and from 7.59% to 3.18% when rectum moves 5mm in posterior direction.

Roeske *et al* (1995) reported rectum varied +/- 30% using CT scan for 10 prostate patients. The CT-based volumes' study from Stasi *et al* (2006) showed a slight systematic variation of the rectal volume between planning and treatment with an average rectal volume increase of around 8 cm^3 (range: 2–20 cm^3) for 10 prostate patients. In our study, the volume increase from 77 cm^3 to 100 cm^3 (23 cm^3 or 30% increase in volume) and decrease from 77 cm^3 to 57 cm^3 (20 cm^3 or 26% decrease in volume) for Rando phantom revealed the possible range of rectal volume change simulated during treatment compared with Roeske and Stasi's results. The increasing of rectal volume caused the NTCP decrease slightly, and the change is smaller comparing to the rectal position change. For the limitation of the data, only rectal position change was considered to evaluate the impact of rectal anterior-posterior movement on the cumulative rectal dose, EUD$_f$ and NTCP for 20 prostate patients in this study, and the results can be considered a surrogate for the cumulative rectal dose for a full treatment course.

5.2.5 Rectal anterior-posterior movements for 20 patients

The range of prostate motion varied significantly and the comparisons among studies are complicated due to different procedures and methods used by researchers. Organ motion was reported to be the result of pressure from bowel gas, feces, and urine in the urinary bladder (Lebesque 1995, van Herk 1995, Roeske 1995, Melian 1997, Padhani 1999, Stroom 2000). Additionally, high variability was noted in many of the studies due to different patient population sizes, different rectum and bladder states (full vs. empty), and differences in the number of measurements taken, methods of measurement collected, and time between measurements (Alasti 2001, Wu 2001, Huang 2002, Litzenberg 2002, Nederveen 2002, Deurloo 2005, Wong 2005). Motion of the prostate in the anterior-posterior and inferior-superior directions was significantly larger than motion in the left-right direction (Tinger 1998, Zelefsky 1999, Alasti 2001). The same result was revealed in our study using gold seeds and every day portal imaging for 20 prostate patients as shown in the Figure 5.2. In this 20 patients group, for patient #6, most of the prostate AP motions are in the anterior direction with mean = - 3.15 mm (anterior direction) and SD = 2.15 mm (P6: Prostate: 83.6 cm^3; Rectum: 61.77 cm^3; Bladder: 578.16 cm^3). While for patient #7, most of the prostate AP motions are in the posterior direction with mean = 2.40 mm (posterior direction) and SD = 2.67 mm (P7: Prostate: 79.2 cm^3; Rectum: 83.44 cm^3; Bladder: 278.88 cm^3). These two patients' results are shown as representatives for evaluating rectal dose fraction-to-fraction and all the patients' results for the dose gradient, NTCP, and cumulative dose to the rectum considering organ motion are also listed and discussed.
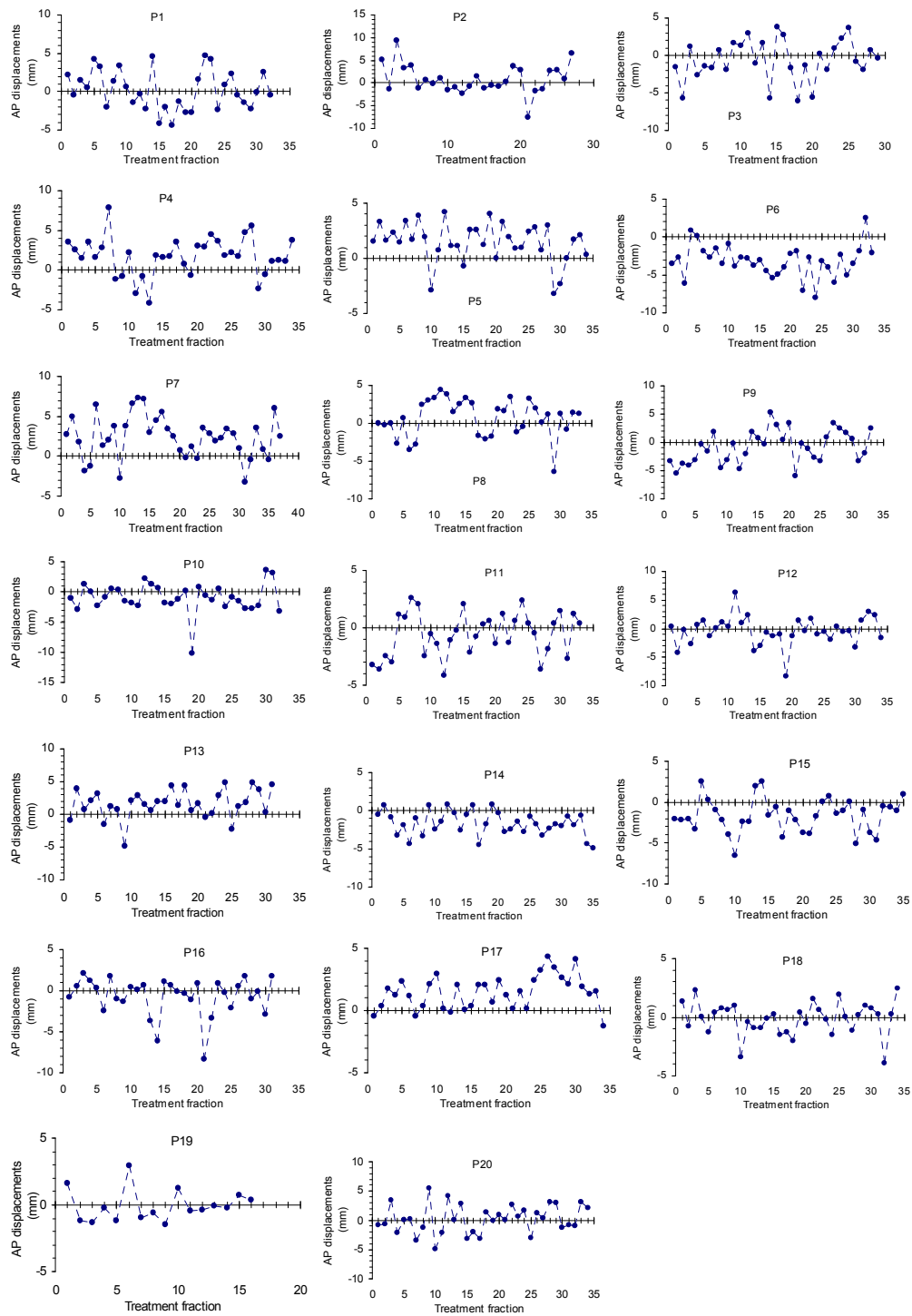
Figure 5. 2: Prostate anterior-posterior motion relative to bony anatomy for 20 patients

137

5.2.6 Rectal EUD$_f$ including rectal movement
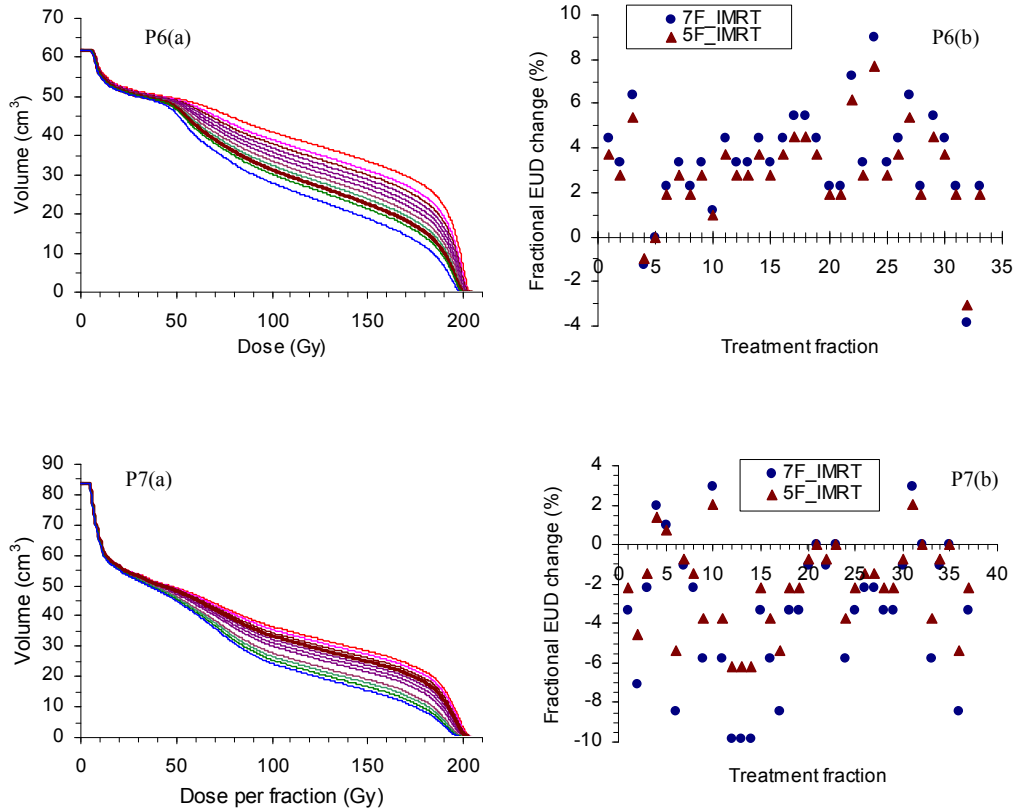
Figure 5. 3: Data for patient 6 and 7 (a) Simulated rectal DVHs including rectal motion (planning DVH in bold) for 7F_IMRT; and (b) rectal fractional EUD change (%) for the course of treatment for 5F and 7F IMRT plans

The rectal DVHs per fraction considering rectal movement for 7F plan are shown in the Figure 5.3(a). The fractional EUD$_f$ was calculated from rectal DVHs and EUD$_f$ changes relative to planning EUD are shown in Figure 5.3(b) for 5F and 7F plans. Because most of the rectum movements are in the anterior direction for patient 6, the most rectal fractional EUD$_f$ changes are positive (EUD$_f$ increased) for both 5F and 7F IMRT plans in Figure 5.3 P6(b). The fractional EUD$_f$ change for 7F plan is higher than that of 5F

plan. While for patient 7, the most rectal fractional EUD_f changes are negative (EUD decrease) for both 5F and 7F IMRT plans in Figure 5.3 P7(b) because most of the motions are in the posterior direction, also the fractional EUD_f change for 7F plan is much lower compared to 5F plan.

The rectal DVHs for 5F and 7F are compared and shown in Figure 5.4(a) for both patient 6 and 7. The rectal DVH is lower for 7F plan compared with 5F plan. For patient 6 in Figure 5.4 P6(b), NTCP increases for both 5F and 7F IMRT plans considering rectal movement due to most of the rectal movements are in the anterior direction, while for patient 7 in Figure 5.4 P7(b), NTCP decreases for both 5F and 7F IMRT plans considering rectal movement because most of the rectal movements are in the posterior direction for patient 7.
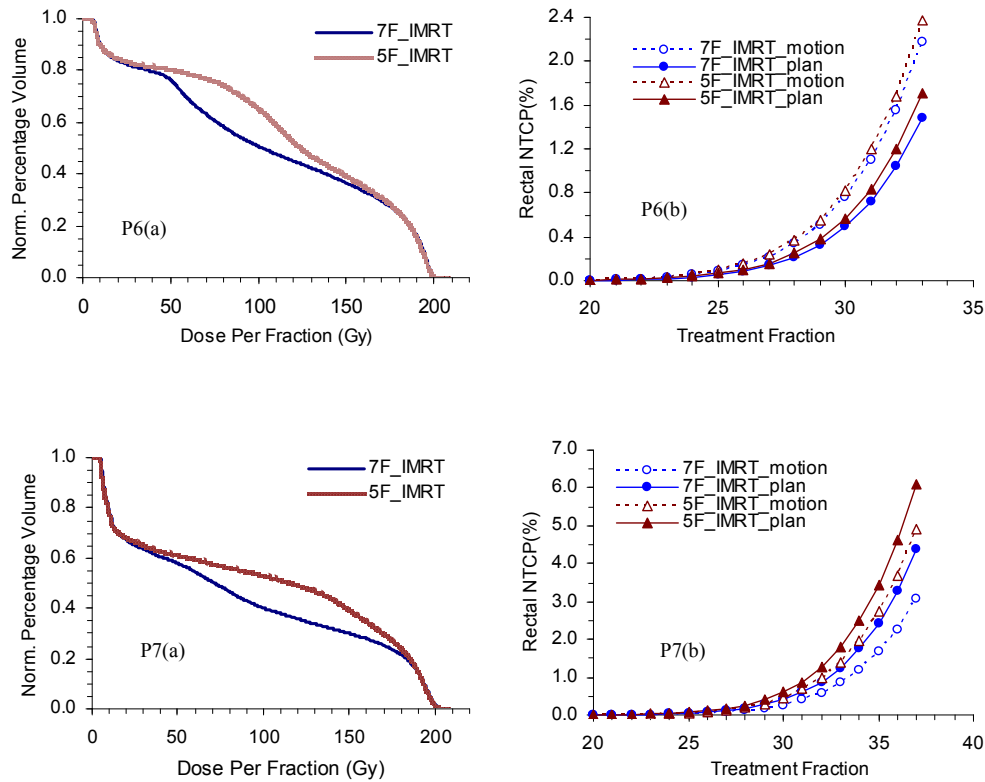
Figure 5. 4: Data for patient 6 and 7 (a) rectal fractional DVHs for 5F and 7F IMRT plans (b) Rectal NTCP changes with treatment fraction.

5.2.7 Dose Gradient and rectal NTCP for 20 patients

The profiles in AP direction (a) and the direction 15° from AP direction (b) show that 7F plan have much lower dose in the dose region from 40 Gy – 60 Gy than that of 5F plan as shown in Figure 5.5. There is plateau around 50 Gy for 5F plan in the posterior direction and the dose profile for 5F plan is the higher around the posterior direction. The dose gradient is defined as the derivation of dose along specific direction and denoted by the term $G(Gy/cm) = \partial D / \partial \vec{r}$, where $\vec{r}$ is the vector. The dose gradient used in this study is the absolute dose gradient and can be derived from dose profile to indicate the slope of

the dose fall in that direction. The magnitude of the dose gradient will tell how fast the dose falls in the specific direction. The local maximum dose gradient is the steepest slope of dose profile outside of planning target volume. But for 5F plan, the plateau divided the posterior profile into two parts, the two parts were analyzed and the average maximum dose gradient was used. The local maximum dose gradient from profile (a) and (b) were calculated and averaged for both 5F and 7F plans.

Maximum dose gradient for 7F IMRT plan is higher than 5F IMRT planning for all the 20 patients. In Figure 5.6, the larger gradient difference for 7F and 5F IMRT planning occurs in patients #2, #8, #11, #17 and #19, in which the patients #2, #8, #11 and #17 have rectal volume over 100 cm^3. The planning rectal NTCP is lower for these patients, especially for 7F IMRT planning as shown in Figure 5.7.

Rectal NTCP for 5F and 7F IMRT planning is shown in Figure 5.7. The mean NTCP is 6.8±1.7 % for 7F planning, and 9.2±1.7 % for 5F planning. NTCP calculation is based on relative volume, the patient with higher rectal volume had lower NTCP, such as patient #2, #8, #11 and #17, also the rectal DVH control points have the potential to be lowered further without compromising PTV to obtain higher dose gradient and lower NTCP.

The relationship of rectal NTCP and maximum dose gradient for all the 20 patients are shown in Figure 5.8. The NTCP decreased with the increasing of dose gradient for 5F and 7F IMRT plans. The correlation coefficient for the rectal NTCP and the dose gradient is - 0.71.
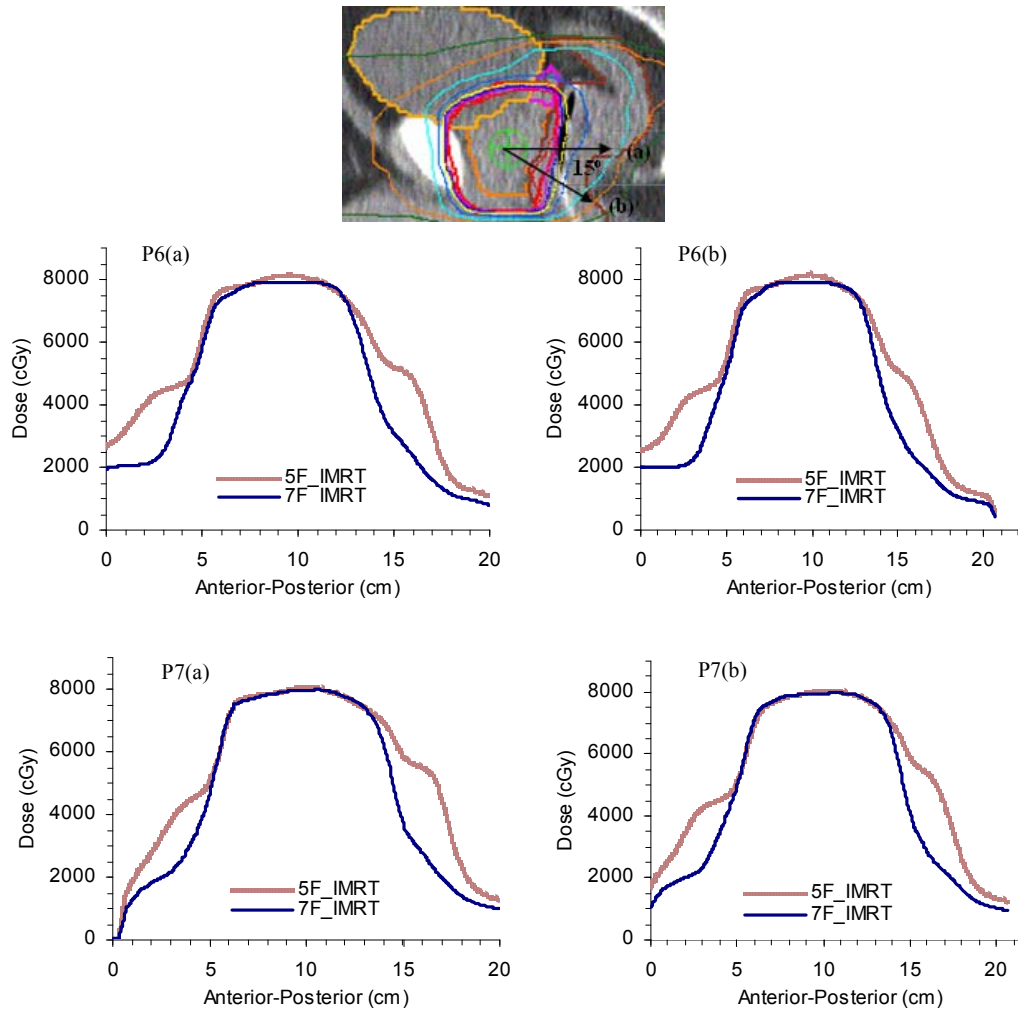
Figure 5. 5: Dose profile close to posterior direction where the PTV and rectum overlap (a) 0°, and (b) 15° for patients 6 and 7.
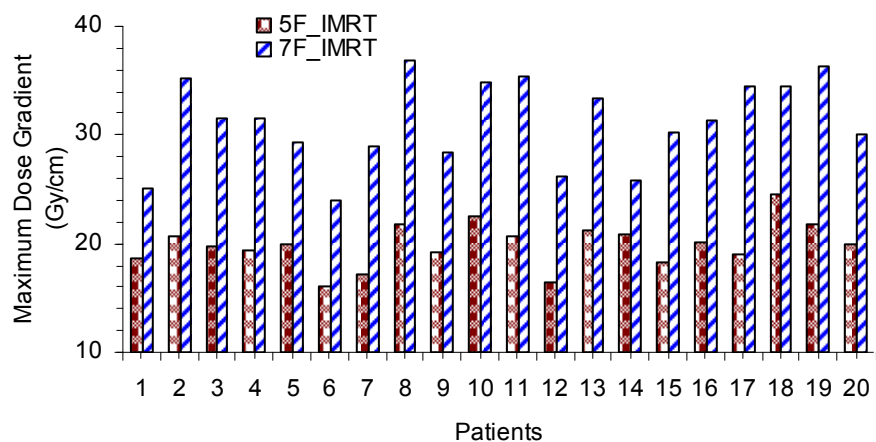
Figure 5. 6: Average LMDG in vicinity of posterior direction for 5F and 7F IMRT plans.
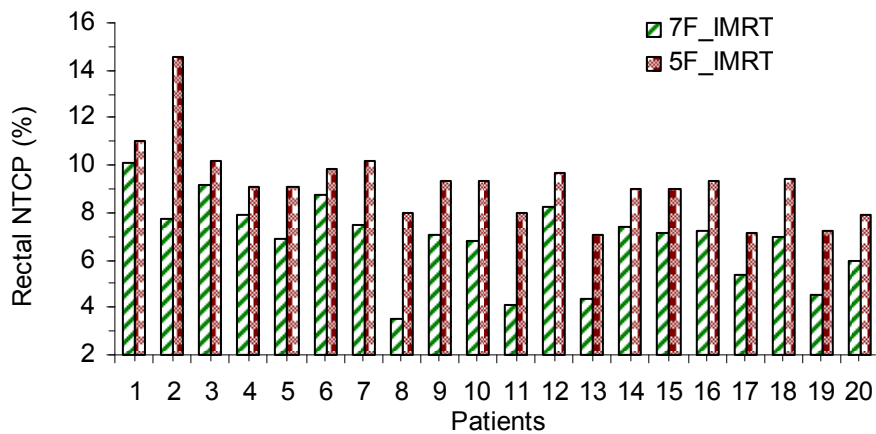
Figure 5. 7: Rectal NTCP for 5F and 7F IMRT treatment planning.

143
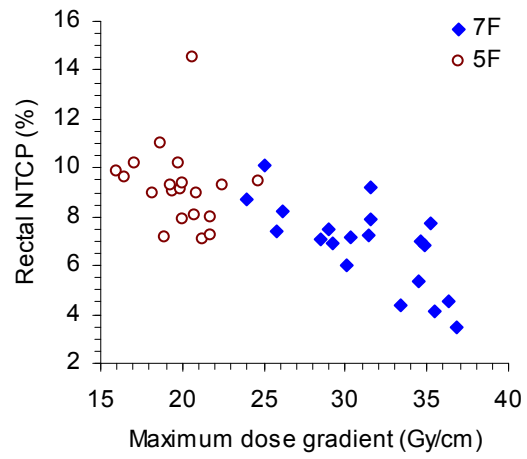
Figure 5. 8: The relationship of rectal NTCP and maximum dose gradient for 5F and 7F IMRT plans.

5.2.8 Dose Gradient and rectal NTCP considering rectal movement
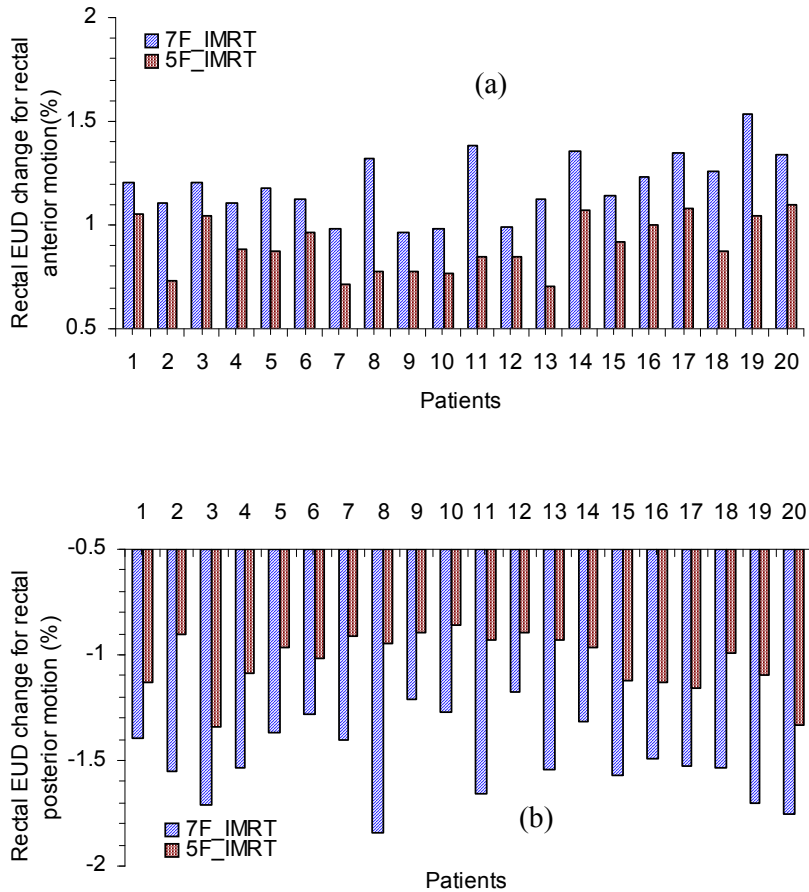
Figure 5. 9: EUD change versus rectal motion in mm steps (a) anterior and (b) posterior directions.

In Figure 5.9, when rectum moves into the high dose region (anterior direction), EUD increased for both 5F and 7F IMRT plans comparing with the respective planning EUD, while when rectum moves out of the high dose region (posterior direction), the EUD decreased for both 5F and 7F plans comparing with the respective planning EUD. The

average EUD increase are 1.2% and 0.9% for 7F and 5F IMRT plans respectively when rectum moves anterior direction every millimeter, while the EUD decrease are 1.5% and 1.0% for 7F and 5F IMRT plans respectively when rectum moves posterior direction every millimeter. The EUD change is higher for 7F IMRT plan comparing with 5F plan because of the higher dose gradient for 7F plan.
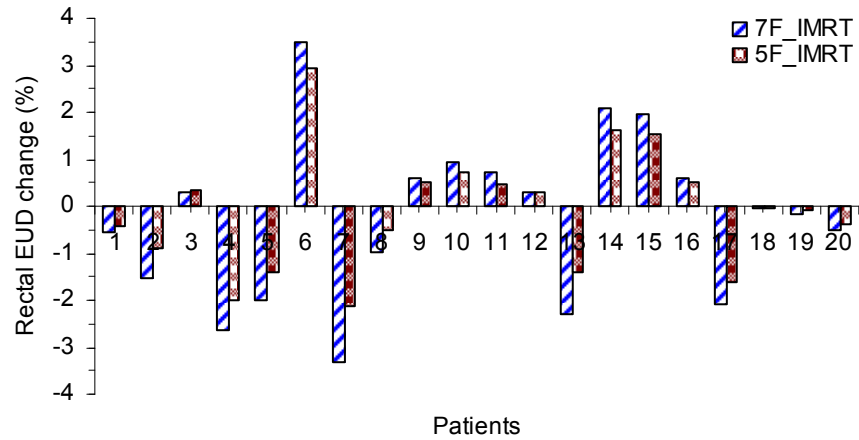
Figure 5. 10: The rectal EUD change for the whole course of treatment considering rectal motion for 20 patients.

The total rectal EUD changed comparing with the planning rectal EUD for the course of treatment because of rectal anterior-posterior motion. For the 20 patients group in Figure 5.10, 45% of patients EUD increased, in which 5% of patients increased more than 2.5%, while 55% of patients EUD decreased, in which 10% of patients decreased 10%. The EUD increase and decrease are higher for 7F plan comparing with 5F plan because of higher dose gradient for 7F plan. For patient #6, most of the rectal motions are in the anterior direction (- 3.15 ± 2.15 mm) for the course of treatment. EUD increased most for patient #6 in these patients group. However for patient #7, most of the rectal motions are in the posterior direction (2.40±2.67 mm) for the course of treatment. EUD decreased most for patient #7 in these patients group. But the EUD increase and decrease are relative to the respective planning EUD. The planning EUD for 7F plan is lower than 5F plan. The final rectal NTCP are shown in Figure 5.11 for planning NTCP and NTCP

146

considering rectal motion. The cumulative rectal EUD increase or decrease for the course of treatment depends on the motion amplitude and frequency in anterior or posterior directions. However, the amplitude of increase or decrease of rectal EUD depends on the dose gradient in posterior direction. Higher dose gradient leads to higher EUD change for both increasing and decreasing.
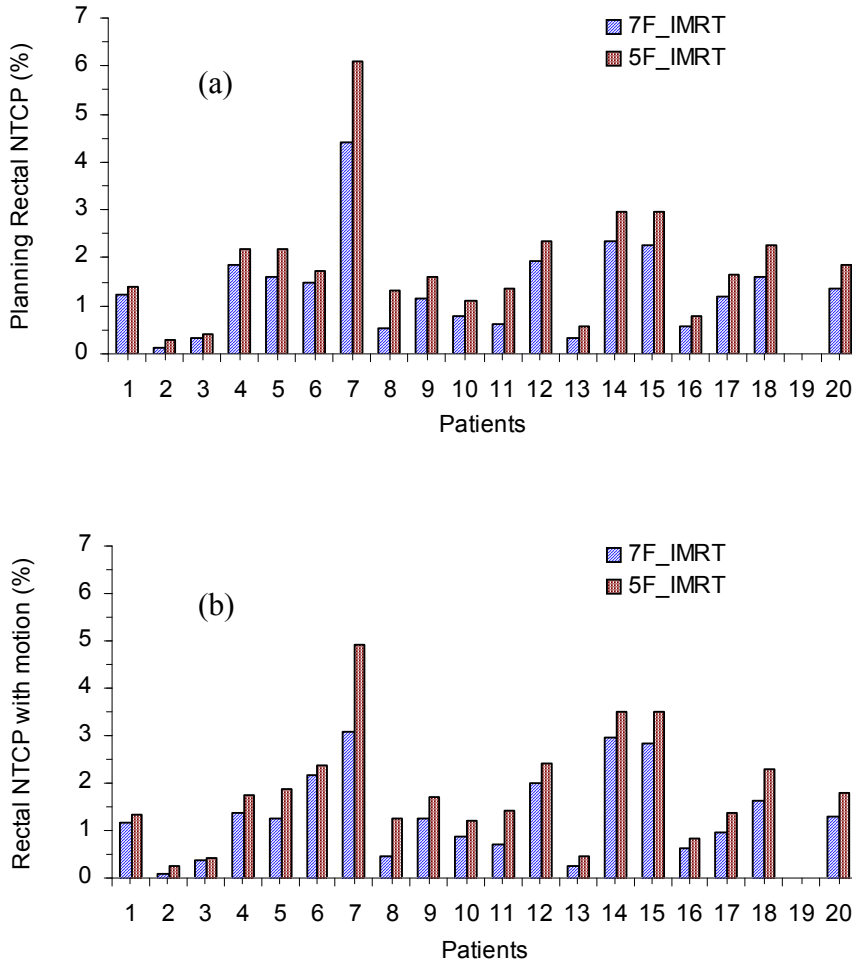
Figure 5. 11: The rectal NTCP of 5F and 7F IMRT plans for (a) static planning and (b) including rectal motion.

The planning rectal NTCP for 5F and 7F plans are shown in the Figure 5.11 (a). Because the fraction numbers are different for different patients, the NTCP changed from patient to patient, but comparing 5F and 7F plans for the same patient, NTCP is lower for 7F plan compared with 5F plan. When considering rectal movement, although the EUD changed more for 7F plan compared with 5F plan no matter rectum moves in anterior or posterior directions, the final rectal NTCP in Figure 5.11(b) shows that rectal NTCP for 7F plan is lower than 5F plan.

Comparing rectal NTCP of planning results and considering rectal motion results for (a) 7F and (b) 5F IMRT plans in Figure 5.12 for 20 patients, the results shows the rectal NTCP decreases for half of the patients and increases for the other for both 5F and 7F plans in the patient group. For patient #6, NTCP increased from 1.48% to 2.18% for 7F plan and from 1.71% to 2.36% for 5F plan for the total 33 fractions. For patient #7, NTCP decreased from 4.39% to 3.07% for 7F plan and from 6.11% to 4.90% for 5F plan for the total 37 fractions.

Previous studies on late rectal toxicity after radiation treatment for prostate cancer are based on dose distribution established at treatment planning and fitted to clinical normal tissue tolerance using NTCP models as described by Lyman (1985), Kutcher (1991) and Burman *et al* (1991). Lebesque *et al.* (1995) , in a study of 11 prostate cancer patients with serial CT scans, observed that the variation of the high-dose rectal volume was relatively small and that the NTCP variation did not correlate with rectal filling. Hence, they concluded that NTCPs as estimated from the initial scan are representative for the whole treatment. Fenwick (2001a, 2001b) stated that dose distribution uncertainties within the rectum during a treatment course (e.g., owing to rectal volumetric changes) have only a marginal impact on fitting a NTCP mode for late rectal bleeding. However, few studies gave the cumulative dose to the rectum in multi-fraction treatment. In this study, rectal cumulative dose and NTCP changing with treatment fractions were reported and compared for 5F and 7F IMRT plans for 20 patients.
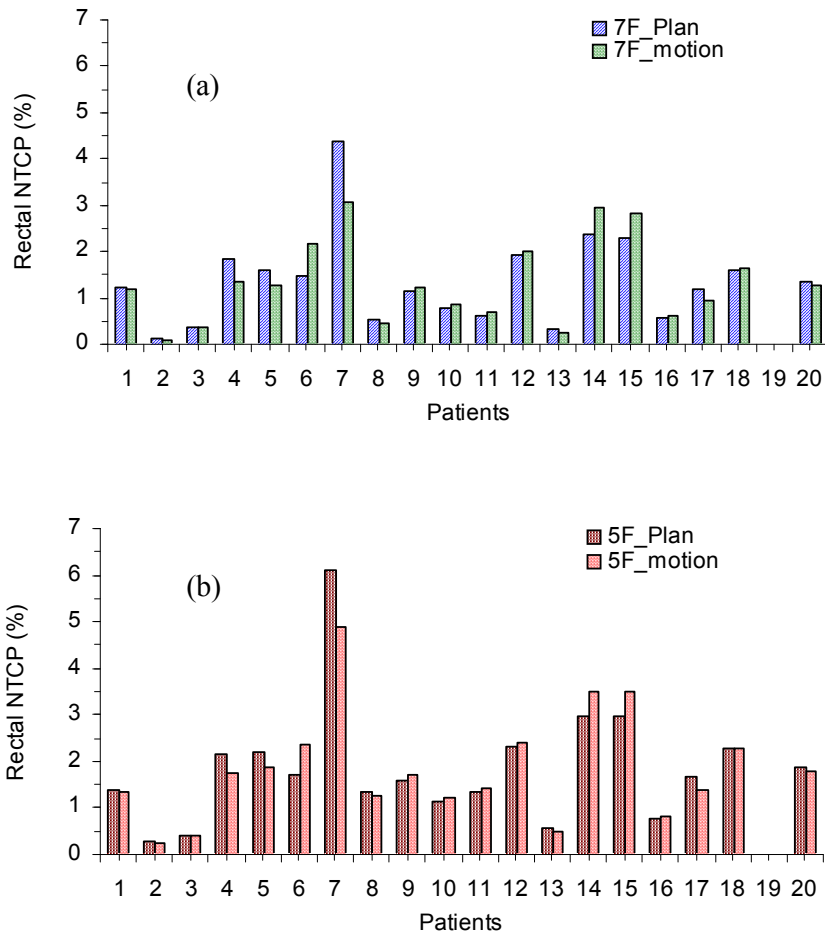
Figure 5. 12: Comparing rectal NTCP for static planning and planning including rectal motion for 20 patients (a) 7F and (b) 5F.

Severe rectal late effects are mostly dose dependent, and influenced more strongly by rectal movement. The rectal fractional EUD_f, defined by the present study, can be considered a surrogate for the rectal dose for each patient during a full treatment course. However, daily changes in rectal volume and the respective DVH during a treatment course are potentially clinically relevant and merit further evaluation.

5.3   Chapter Summary

The EUD_f model evaluates the rectal dose fraction-to-fraction. Rectal movement includes motion into and out of the high dose region of the PTV. EUD_f increases when rectum moves in the anterior direction and decreases when rectum moves in the posterior direction. The amplitudes of EUD_f increase and decrease are correlated with the dose gradient. Higher dose gradients lead to higher rectal EUD_f change. 7F IMRT plans have higher dose gradients compared with 5F IMRT plans in the posterior direction and lead to higher EUD_f change, including both EUD_f increases and decreases. The increase or decrease of the cumulative rectal dose for the whole course of treatment depends on the motion amplitude and frequency in anterior or posterior directions.

Rectal NTCP is lower for 7F IMRT plans compared with 5F IMRT plans. When considering rectal movement, including motion amplitude and frequency, for the whole course of treatment, the rectal NTCP decreases for half of the patients and increases for the other half for both 5F and 7F plans in the 20 patient group. The work in the thesis focuses on rectum; rectal wall will show a greater sensitivity to motion than rectum. This method provides a simple way to estimate the normal tissue complication probability dynamically by considering internal organ motion throughout the whole treatment course.

Chapter 6

Summary and Conclusions

6.1 Summary

IMRT results in a steep decrease in dose outside the target and causes sensitivity to geometric uncertainties. The dominant uncertainties in conformal treatment are setup error and internal organ motion. Both can be reduced significantly by use of online image guidance. Geometric uncertainties and day-to-day variability in target position emphasize the need for image-guidance radiation therapy. Frequent imaging with patient repositioning during the course of treatment has become standard practice in radiation oncology.

In this study daily EPI for localization of implanted fiducial markers (gold seeds) provided data for analysis of setup error and organ motion for 118 patients. The simultaneous time-course trends of prostate motion and setup error showed that prostate motion occurred independently from bony anatomy displacement during treatment. Additional analysis revealed that the prostate motion correlates with bladder and rectum filling and setup error correlates with body size. A margin around the PTV is needed to account for internal organ motion after correcting for setup error using bony landmarks. The margin was determined according to the specific setup technique. For a conventional beam setup without image guidance, both setup error and organ motion should be considered. For correction of daily bony setup error by EPID without fiducial markers, a

margin should be considered to account for internal organ motion. Although the use of fiducial markers for positioning correction is reliable, a margin should be included to account for intra-fraction organ motion during treatment and other uncertainties. The margin also depended on treatment technique. For a four-beam box, 95% coverage is required according to the report ICRU-62 (ICRU 1999). For IMRT with correction of inter-fraction tumor motion, a 4mm margin should be used for intra-fraction motion and other uncertainties. Daily electronic portal images with implanted gold seed fiducials provided an effective way to verify and correct the position of the target immediately prior to radiation delivery for prostate radiation therapy. Significant reduction in both setup error and organ motion was achieved with this system.

IMRT generates high dose gradients between the PTV and OARs. Treatment accuracy depends on both setup errors and organ motion that need to be precisely evaluated for individual patients. The dose gradients and motion PDF were used to evaluate the effect of internal organ motion for IMRT treatment planning of prostate cancer. The dose distribution including geometric uncertainties depended on the static IMRT dose gradient and motion PDF. The blurred dose gradient was calculated from the static dose gradient convolved with the PDF. The dose including geometric uncertainties was obtained by integration of blurred dose gradient along specific directions. For the section of the dose profile where the dose gradient is near zero inside the PTV, there was minimal impact on the blurred dose for the internal organ motion, while for the section of the profile at outside edge of the PTV where the dose gradient is the steepest, there was maximal impact for internal organ motion. The dose including geometric uncertainties can also be determined from integration of the static dose convolved with the derivative of the PDF. This method was not investigated in this thesis because the primary objective was to provide a more fundamental understanding of the inclusion of geometric uncertainties using dose gradient.

The blurred dose gradient was maximized by manually optimizing the dose objective function using DVH control points, or by reducing geometric uncertainty with corrective verification imaging. A parameter defined as the PMDD was introduced to characterize

the relationship of mean dose deviation and dose gradient. The PMDD depended on the dose gradient and motion PDF. OMDS was defined as the rate of change in PMDD with SD of Gaussian PDF and was found to increase with the LMDG in anterior, posterior, left and right directions. Due to common inferior and superior field borders of the field segments, the sharpest dose gradient occurred in the inferior region or both the superior and inferior regions of the perimeter of the target volume. Thus, prostate motion in the superior-inferior direction produced the highest dose difference. Verification of organ motion in the inferior direction is essential.

Lower rectal NTCP was achieved by either selecting smaller margin or creating steeper dose gradient between PTV and rectum. Rectal complication probability was evaluated using spatial dose distributions and a dose gradient analysis. In the transverse plane, LMDGs exhibited a large variation for five-field plans and were lowest in the posterior direction. Dose objective function used for IMRT optimization did not necessarily produce higher dose gradient in all directions and could result in considerable variability depending on beam numbers and beam directions. The numbers of beams, beam direction, DVH control points, and the choice of optimizer had important effects on the dose gradients. In general, the dose objective function including desirable dose constraints should be satisfied. However, the conformality index and the magnitude variability in the dose gradient between the PTV and OAR depended on the number of beams, beam directions in the plan and on the performance characteristic of the DMLC. The LMDG was determined from reliable rectal dose–volume constraints for IMRT inverse-planning in vicinity of the posterior direction in the sagittal plane. Relative to the five-field plans, the seven-field plans demonstrated a higher LMDG in the posterior direction and also lower NTCP. The main advantage of IMRT is creating high dose gradients in more optimal locations with respect to normal tissues and targets. LMDG were achieved either by modifying the planning technique or adjusting rectal DVH control points. With lower rectal DVH control points, a higher LMDG in the posterior direction was obtained for both five-field and seven-field plans. A steeper dose profile and higher LMDG between PTV and rectum worked well to maintain TCP and reduce NTCP. The LMDG in vicinity of the posterior direction should be high enough to ensure that the dose falls off quickly to avoid high rectal dose. Relative to a five-field plan, the

seven-field plan demonstrated a higher LMDG in the posterior direction and resulted in lower rectal NTCP. To achieve the higher LMDG, V_{70Gy}, V_{60Gy} and V_{50Gy} of the rectal DVH are below 21%, 32% and 48%, respectively. These values were lower than RTOG guidelines (25%, 35% and 55%, respectively) and did not compromise the dose distribution elsewhere.

Cumulative rectal dose was analyzed in an effort to identify features associated with an increased rectal complication probability. Rigid body rectal motion was evaluated fraction-to-fraction using equivalent uniform dose per fraction. Positional variations of the rectum were measured from portal imaging using gold seeds for 20 prostate patients and the rectal dose deviation was expressed as EUD_f deviation. Rectal movement included movement in and out of the high dose region of PTV. The amplitudes of EUD_f increase and decrease were correlated with the dose gradient. A higher dose gradient led to higher rectal EUD_f change. Seven-field IMRT plans had higher LMDG compared to five-field IMRT plans in the posterior direction and led to higher EUD_f change, including both EUD_f increase and decrease. The increase or decrease of the cumulative rectal dose for the course of treatment depended on the dose gradient in vicinity of posterior direction, motion amplitude and frequency in anterior or posterior directions. Rectal NTCP was lower for seven-field IMRT plans compared with five-field IMRT plans. When considering rectal movement for the whole course of treatment, the rectal NTCP decreased for half of the patients and increased for the other half when compared to the NTCP from the static plan for both techniques (as calculated from the motion amplitude and frequency in anterior or posterior direction). This method provided a simple way to estimate the NTCP by considering internal organ motion throughout the whole treatment course.

6.2 Conclusions

A Gaussian PDF is reasonable for modeling geometric uncertainties as indicated by the clinical IGRT patient study in Chapter 2. The PDF is patient specific and group SD should not be used for accurate treatment planning for individual patients. In addition, individual SD should not be determined or predicted from small imaging samples because of random nature of the fluctuations. Frequent verification imaging should be employed in situations where geometric uncertainties were expected and cumulative PDF data could be used for re-planning to assess accuracy of delivered dose. Group statistical data is useful for determining worst case discrepancy between planned and delivered dose. The margins for the PTV should ideally represent true geometric uncertainties. The measured geometric uncertainties were used in this thesis to assess PTV coverage, dose to OAR, EUD_f and NTCP.

The dose distribution including geometric uncertainties was determined from the integral of the blurred dose gradient along a specific direction relative to the motion. In general, the directions are arbitrary, but for prostate motion, it was convenient to use conventional orthogonal directions. The blurred dose gradient was obtained from the convolution of the static dose gradient with the PDF. The effect of organ motion on the dose gradient showed that geometric uncertainties reduce the planned dose gradient and cause a blurred dose gradient (Chapter 3). The blurring of dose gradient was minimized by improving individual LMDGs in the static plan or by reducing geometric uncertainty with corrective verification imaging. The LMDG was initially determined via optimization of the dose objective function, and was improved by manually adjusting rectal DVH constraints or by modifying beam angle and number (Chapter 4). Static dose was insufficient to assess PTV coverage and the dose to OAR. The inclusion of geometric uncertainties was required for close agreement between planned and delivered dose. Minimum SD is used when geometric uncertainty was corrected with verification imaging. Maximum SD was used when the geometric uncertainty was known to be large and difficult to manage. The maximum SD was 4.38 mm in AP direction, 2.70 mm in LR direction and 4.35 mm in SI

direction. The minimum SD was 1.1 mm in all three directions if less than 2 mm threshold was applied for uncorrected fractions in every direction.

EUD_f is a useful QA parameter for interpreting the biological impact of geometric uncertainties on the static dose distribution. EUD_f has been used as the basis for the NTCP evaluation in the thesis (Chapter 5). Relative NTCP values were useful for comparative QA checking by normalizing known complications (e.g. reported in the RTOG guidelines) to specific DVH control points. The increase or decrease of the cumulative rectal dose for the course of treatment depended on the dose gradient in vicinity of the posterior direction, motion amplitude and frequency in anterior or posterior directions. For prostate cancer patient, rectal complication was evaluated from RTOG clinical trials, and detailed evaluation of the treatment techniques (e.g. dose prescription, DVH, number of beams, beam angles). Treatment plans that did not meet DVH constraints represented additional complication risk. Geometric uncertainties improved or worsened rectal NTCP depending on individual internal organ motion within patient.

6.3 Recommendations for future Work

The inclusion of geometric uncertainties in treatment planning and delivery as described in the thesis is based on the determination of LMDG and motion PDF. New imaging technologies, e.g. CBCT, will likely provide improvement in the determination of PDF. In addition, by including the dose gradient explicitly in the dose objective function, it will likely be possible to obtain high LMDG without additional adjustment of the DVH control points. These concepts are described briefly in the following sections.

6.3.1 CBCT and other emerging verification imaging technologies

Advancements in linear accelerator design, especially the introduction of kilovoltage X-ray tubes and flat detectors have made CBCT available. This has recently been installed at GRRCC. CBCT offers opportunities for IGRT data collection and deformable model research for both target and OAR. CBCT and other emerging verification imaging technologies can be used to better characterize motion PDF for tumor and OAR.

Unlike the relatively rigid body motion of human bony anatomy, physiological actions can cause non-rigid motion or deformation of human tissues. A common restriction of organ motion study is the absence of a full 3D description of the organ deformation because this deformation is often expressed in a variation of volume only. To incorporate internal organ motion into the treatment planning for treatment evaluation and optimization, the reconstruction of a cumulative dose distribution in a deforming organ should be solved. For IGRT, it is essential to know the relative magnitude of translations, rotations, and shape variation such that the most appropriate correction strategy can be chosen. The most critical step in solving the problem is to track the displacement of each volume element in the organ between moments of dose delivery. Tracking individual elements in a deformable organ requires basic information of organ shape before and after organ motion. To predict the distribution of patient-specific organ motion, the organ volume in the daily CBCT scans acquired during the treatment process can be used. Due to the non-rigid nature of organ motion, the volume elements in the organ should be registered between any pair of organ volumes before, during, and after motion.

6.3.2 4D CT and respiratory motion

One potential application of image-guided radiotherapy is to track the target motion in real time and then deliver adaptive treatment to a dynamic target by DMLC tracking or respiratory gating. For successful implementation of real-time beam tracking or beam gating, the precise location of a moving tumor or organ must be determined reliably from separate imaging system. Stereoscopic diagnostic x-ray imaging systems can provide precise 3D location information for a moving tumor through real-time x-ray imaging of fiducial markers during the treatment. Such systems provide a direct way for internal tumor and organ motion assessment and correction. The Cyberknife (Accuray Inc., Sunnyvale, CA) system uses orthogonal x-ray imaging to update their internal/external correlation for tumor tracking. Advanced radiation treatment tools, such as beam tracking, respiratory gating and DMLC, promise to improve the accuracy of radiation delivery to moving tumors.

The breathing motion for lung patients can be considered using dose gradient analysis by determining the correlation between the respiratory motion kernel and dose gradient. The effect of respiratory motion on LMDG is a topic for further research. IGRT data collection and current methodology can be used as input for respiratory registration for both target and organs at risk. The framework for using LMDG and respiratory motion PDF remains useful for 4D CT or any other imaging technologies that can characterize the motion PDF. The method developed in this thesis can be extended to multi-dimensional motion analysis by combining with data from other imaging modalities, such as 4D CT data. First, the motion parameters and motion patterns can be discovered to estimate a complete motion representation, and then the motion kernel results can be integrated into dose gradient analysis for tumor motion and predicting the effectiveness of IGRT.

6.3.3   Determining optimum LMDG between the PTV and OAR for other tumor sites

The framework for using LMDG and PDF remains useful for CBCT or any other imaging technologies that can better characterize a GPDF or a non-GPDF. Even with Cyberknife technology, which ideally allows a beam to "track" target motion, there will always be an impact of target motion on the static plan – and the impact can be modeled with the framework presented in the thesis.

IMRT is often used in conjunction with dose escalation. For the same cost functions, by analyzing the dose gradients versus plan type, and number and direction of beams, IMRT dose distributions determined from commercial planning system do not have steep (local maximum) dose gradient in every direction. However, IMRT can redistribute dose to achieve locally higher dose gradients in a particularly region, with potential loss of high dose gradient elsewhere. One advantage of IMRT is the ability to place dose gradients in more optimal locations with respect to normal tissues and/or targets, rather than explicitly achieving higher dose gradients all around the target. What is the optimal LMDG between the PTV and OAR for other tumor sites, such as head and neck, breast etc? The treatment strategies in these tumor sites using dose gradient analysis need to be assessed individually: (1) Qualify extension to other sites, spatial invariance of convolution kernel at surface; (2) PDF characterization separately for each treatment site.

6.3.4   Inclusion of dose gradient and motion PDF into commercial IMRT optimization software

The incorporation of the dose gradient and organ motion PDF into commercial IMRT optimization software is another potential research avenue for improving IMRT optimization. The optimization functions currently employed in IMRT are somewhat

insensitive to the creation of optimum LMDG between the PTV and OAR. Explicit parametric inclusion of the dose gradient between the PTV and OAR should help the optimizer find optimum LMDG and optimum DVH for a given plan. The feasibility and potential utility of IMRT scoring functions based on the optimal LMDG in vicinity of PTV and OAR will improve inadequacies of DVH-based evaluation of IMRT target coverage and dose to OAR. The dose gradient method used in this thesis is of value for overcoming the known limitation of DVH (i.e., lack of spatial and functional information).

A higher dose gradient can also be achieved by adding a "shell" around PTV overlapping slightly with OAR. The dose can be constrained with the shell either by absolute or percentage dose value via a DVH. The "shell" can be added uniformly or non-uniformly around the PTV and the dose objective functions can be specified. Multiple shells can also be added to obtain the optimal dose gradient between PTV and OAR. The identification of a shell helps to define a region where the magnitude of dose gradient can be specified.

6.3.5 Radiobiological considerations in IMRT optimization

Niemierko (1997) introduced the concept of EUD in an attempt to establish a reliable scalar for reporting non-uniform dose results. To consider volume effects in a physical dose-constrained optimization, the planner can define additional DVH control points - EUD. The EUD is the homogeneous dose inside an organ that has the same biological effect as a given, heterogeneous dose distribution. For targets, the EUD is mostly determined by the lowest dose values. For OARs structured in parallel functional cells, the EUD is near the mean dose, whereas for OARs structured in serial cells, the EUD is more dominated by the maximum dose values. EUD was used for inverse treatment planning as a parameter in a sigmoid dose-effect curve that resembles the basic shape of

TCP/NTCP models. Because the EUD for OAR is an empirical model, the clinical relevance of EUD directly corresponds to the quality of the clinical data available. Planning based on TCP/NTCP models is still not widely used in clinical practice. The EUD is an intermediate concept between physical doses and TCP/NTCP models. The comparison of plans with varying PTV dose homogeneity is not reliable using mean dose alone, but the use of EUD has the potential to overcome this problem as it considers the contributing effect of each part of the PTV dose distribution. For fractionated treatments where the mean dose to the PTV per fraction is varying due to geometric uncertainties, both EUD and TCP showed little variation with the degree of dose non-uniformity. For other time dependent factors, such as fractionation rate and cell repopulation times, TCP again showed significant variation relative to EUD. The relative insensitivity of EUD implies that this index will be useful for dose evaluation when biological parameters are not known with accuracy, for the study of the radiobiological based optimization objective and dose gradient. Biological IMRT plans optimization should be evaluated using the dose gradient to determine the level of sensitivity of EUD to model parameters including TCP and NTCP.

Bibliography

Alasti H, Petri M P, Catton C N and Warde P R, Portal imaging for evaluation of daily on-line setup errora and off-line organ motion during conformal irradiation of carcinoma of the prostate, *Int. J. Radiat. Oncol. Biol., Phys.* **49:** 869-884 (2001)

Althof V G, Hoekstra C J, and te Loo H J, Variation in prostate position relative to adjacent bony anatomy, *Int. J. Radiat. Oncol. Biol., Phys.* **34:** 709-715 (1996)

Amer A.A., Mackay R.I., Roberts S.A., et al., The required number of treatment imaging days for an effective off-line correction of systematic errors in conformal radiotherapy of prostate cancer: A radiobiological analysis, *Radiother Oncol* **61**: 143-150 (2001)

Antolak J. A., I. I. Rosen, C. H. Childress, G. K. Zagars, and A. Pollack, 'Prostate target volume variations during a course of radiotherapy,' *Int. J. Radiat. Oncol. Biol. Phys.* **42:** 661–672 (1998)

Arfken G B and Weber H J, Mathematical Methods for Physicists *Acadmic Press, San Diego* (1995)

Aubin M, Pouliot J, Milender L, Shinohara K, Pickett B, Anezinos C, Verhey L and Roach M, Daily prostate targeting with implanted gold markers and an a-Si flat panel EPID at UCSF: A five year clinical experience, *Suppl Int J Radiat Oncol Biol Phys* **60:** 266-267 (2004)

Balter J M, Sandler H M, Lam K, Bree R L, Lichter A S and ten Haken R K, Measurement of prostate movement over the course of routine radiotherapy using implanted markers, *Int. J. Radiat. Oncol. Biol. Phys.* **31:** 113–118 (1995a)

Balter, J.M.; Lam, K.L.; Sandler, H.M., Automated localization of the prostate at the time of treatment using implanted radiopaque markers; Technical feasibility, *Int J Radiat Oncol Biol Phys* **33:** 1281-1286 (1995b)

Balter JM, Lam KL, McGinn CJ, et al, Improvement of CT-based treatment-planning models of abdominal targets using static exhale imaging, *Int J Radiat Oncol Biol Phys* **41**:939-943 (1998)

Balter J M, Litzenberg D W, Brock K K, Sanda M, Sullivan M, Sandler H M and Dawson L A, Ventilatory movement of the prostate during radiotherapy, Proc. 42nd Annual ASTRO Meeting, *Int. J. Radiat. Oncol. Biol. Phys.* **48**: 167 (2000)

Beard C J, Kijewski P, Bussiere M, Gelman R, Gladstone D, Shaffer K, Plunkett M, Castello P and Coleman C N, Analysis of prostate and seminal vesicle motion: implications for treatment planning, *Int. J. Radiat. Oncol.Biol. Phys.* **34:** 451–8 (1996)

Bel A., Vos P.H., Rodrigus P.T., et al., High-precision prostate cancer irradiation by clinical application of an offline patient setup verification procedure using portal imaging, *Int J Radiat Oncol Biol Phys* **35**: 321-332 (1996a)

Bel A, van Herk M and Lebesque J V, Target margins for random geometrical treatment uncertainties in conformal radiotherapy, *Med. Phys.* **23:** 1537–1545 (1996b)

Benk V.A., Adams J.A., Shipley W.U., et al., Late rectal bleeding following combined X-ray and proton high dose irradiation for patients with stages T3-T4 prostate carcinoma, *Int J Radiat Oncol Biol Phys* **26**: 551-557 (1993)

Boersma L.J., van den Brink M., Bruce A.M., et al., Estimation of the incidence of late bladder and rectum complications after high-dose (70–78 GY) conformal radiotherapy for prostate cancer using dose-volume histograms, *Int J Radiat Oncol Biol Phys* **41**: 83-92 (1998)

Booth J T and Zavgorodni S F, Modelling the dosimetric consequences of organ motion at CT imaging on radiotherapy treatment planning, *Phys. Med. Biol.* **46:** 1369–1377 (2001)

Bortfeld T, Jiang S B and Rietzel E, Effects of motion on the total dose distribution, *Semin. Radiat. Oncol.* **14:** 41–51 (2004)

Burman C, Kutcher G J, Emami B and Goitein M, Fitting of normal tissue tolerance data to an analytic function, *Int. J. Radiat. Oncol. Bio.l Phys.* **21:** 123–135 (1991)

Cazzaniga LF, Marinoni MA, Bossi A, et al. Interphysician variability in defining the planning target volume in the irradiation of prostate and seminal vesicles. *Radiother Oncol* **47**:293–6 (1998)

Chen J; Lee R J, Handrahan D, Sause W T, Intensity-Modulated Radiotherapy Using Implanted Fiducial Markers With Daily Portal Imaging: Assessment of Prostate Organ Motion, *Int J Radiat Oncol Biol Phys* **68**: 912-919 (2007)

Cheng C.W., Das I.J., Treatment plan evaluation using dose–volume histogram (DVH) and spatial dose–volume histogram (zDVH), *Int J Radiat Oncol Biol Phys* **43**: 1143-1150 (1999)

Chism D.B., Horwitz E.M., Hanlon A.L., Pinover W.H., Mitra R.K., Hanks G.E., Late morbidity profiles in prostate cancer patients treated to 79–84 Gy by a simple four-field coplanar beam arrangement, *Int J Radiat Oncol Biol Phys* **55**: 71-77 (2003)

Cotran R.S., Kumar V., Collins T., The male genital tract, *Robbins pathologic basis of disease*, 6th ed., WB Saunders, Philadelphia, 1011–35 (1999)

Court L., Rosen I., Mohan R., et al. Evaluation of mechanical precision and alignment uncertainties for an integrated CT/LINAC system, *Med Phys,* **30**: 1198-1210 (2003)

Cox J.D., Stetz J., Pajak T.F., Toxicity criteria of the Radiation Therapy Oncology Group (RTOG) and the European Organization for Research and Treatment of Cancer, *Int J Radiat Oncol Biol Phys* **31**: 1341-1346 (1995)

Craig T, Battista J and Van Dyk J, Limitations of a convolution method for modeling geometric uncertainties in radiation therapy II. The effect of a finite number of fractions, *Med. Phys.* **30:** 2012-20 (2003a)

Craig T, Battista J and Van Dyk J, Limitations of a convolution method for modeling geometric uncertainties in radiation therapy I. The effect of shift invariance, *Med. Phys.* **30:** 2001-11 (2003b)

Craig T, Moiseenko V, Battista J and Van Dyk J, The impact of geometric uncertainty on hypofractionated external beam radiation therapy of prostate cancer, *Int. J. Radiat. Oncol. Bio.l Phys.* **57:** 833-42 (2003c)

Craig T, Wong E, Bauman G, Battista J and Van Dyk J, Impact of geometric uncertainties on evaluation of treatment techniques for prostate cancer, *Int. J. Radiat. Oncol. Bio.l Phys.* **62:** 426-36 (2005)

Crook J M, Raymond Y, Salhani D, Yang H and Esche B, Prostate motion during standard radiotherapy as assessed by fiducial markers, *Radiother. Oncol.* **37:** 35–42 (1995)

Dawson L A, Mah K, Franssen E and Morton G, Target position variability throughout prostate radiotherapy, *Int. J. Radiat. Oncol. Biol. Phys.* **42:** 1155–1161 (1998)

de Boer H.C., Heijmen B.J., A protocol for the reduction of systematic patient setup errors with minimal portal imaging workload, *Int J Radiat Oncol Biol Phys*, **50**: 1350-1365 (2001)

Denham J.W., Hauer-Jensen M., The radiotherapeutic injury—a complex wound, *Radiother Oncol* **63:** 129-145 (2002)

Deurloo K., Steenbakkers R., Zijp L., et al., Quantification of shape variation of prostate and seminal vesicles during external beam radiotherapy, *Int. J. Radiat. Oncol. Biol. Phys.* **61:** 228-238 (2005)

Dong L, Development of automated image analysis tools for verification of radiotherapy field accuracy with and electronic portal imaging device (Ph.D. thesis), Houston, TX: The University of Texas Health Science Center at Houston (1995)

Dunscombe P, Loose S, Leszczynski K., Sizes and scources of field placement error in routine irradiation for prostate cancer, *Radiother Oncol* **26**: 174-176 (1993)

Emami B, Lyman J, Brown A, Tolerance of normal tissue to therapeutic irradiation, *Int. J. Radiat. Oncol. Biol. Phys.* **21:** 109-122 (1991)

Fenwick J. D. and Nahum A. E., 'Impact of dose-distribution uncertain uncertainties on rectal *ntcp* modeling I: uncertainty estimates, *Med. Phys.* **28:** 560–569 (2001a).

Fenwick J. D., 'Impact of dose-distribution uncertain uncertainties on rectal *ntcp* modeling I: uncertainty estimates, *Med. Phys.* **28**, 570–581 (2001b).

Fenwick J.D., Khoo V.S., Nahum A.E., Sanchez-Nieto B., Dearnaley D.P., Correlations between dose–surface histograms and the incidence of long-term rectal bleeding following conformal or conventional radiotherapy treatment of prostate cancer, *Int J Radiat Oncol Biol Phy*, **49**: 473-480 (2001c)

Fiorino C., Vavassori V., Sanguineti G., et al., Rectum contouring variability in patients treated for prostate cancer: impact on rectum DVHs and NTCP, *Radiother Oncol*, **63**: 249-255 (2002a)

Fiorino C., Cozzarini C., Vavassori V., et al., Relationships between DVHs and late rectal bleeding after radiotherapy for prostate cancer: analysis of a large group of patients pooled from three institutions, *Radiother Oncol*, **64**: 1-12 (2002b)

Fiorino C, Sanguinett G, Cozzarini C, Fellin G, Foppiano F, Menegotti L, Piazzolia A, Vavassori V and Valdagni R, Rectal Dose-volume considerations in high-dose radiotherapy of localized prostate cancer, *Int J Radiat Oncol Biol Phys* **57**: 953–962 (2003)

Fontenla E, Pelizzari C A, Roeske J C and Chen G T Y, Numerical analysis of a model of organ motion using serial imaging measurements from prostate radiotherapy, *Phys. Med. Biol.* **46:** 2337–58 (2001)

Fontenla E, Pelizzari C A, Roeske J C and Chen G T Y, Using serial imaging data to model variabilities in organ position and shape during radiotherapy, *Phys. Med. Biol.* **46:** 2317–36 (2001)

Foppiano F., Fiorino C., Frezza G., et al., The impact of contouring uncertainty on rectal 3D dose–volume data: results of a dummy run in a multi-centric trial (AIROPROS01-02), *Int J Radiat Oncol Biol Phys*, **57**: 573-579 (2003)

Fowler J F, The linear-quadratic formula and progress in fractionated radiotherapy, *Br. J. Radiol.* **62:** 679-694 (1989)

Fraass, BA, McShan, DL, Kessler, ML, Matrone, GM, Lewis, JD, and Weaver, TA., A computer-controlled conformal radiotherapy system I: Overview, *Int J Radiat Oncol Biol Phys* **33:** 1139–1157 (1995)

Fuss M., Cavanaugh S.X., Fuss C., et al., Daily stereotactic ultrasound prostate targeting: Inter-user variability, *Technol Cancer Res Treat* **2**: 161-170 (2003)

Gall KP and Verhey LJ, Computer-assisted positioning of radiotherapy patients using implanted radiopaque fiducial, *Med Phy* **20:** 1153-1159 (1993)

Ghilezan M.J., Jaffray D.A., Siewerdsen J.H., et al., Prostate gland motion assessed with cine-magnetic resonance imaging (cine-MRI), *Int J Radiat Oncol Biol Phys* **62**: 406-417 (2005)

Goitein M., Non-standard deviations, *Med Phys* **10:** 709-711 (1983)

Hanks G.E., Hanlon A.L., Schultheiss T.E., et al., Dose escalation with 3D conformal treatment: five year outcomes, treatment optimization, and future directions, *Int J Radiat Oncol Biol Phys* **41**: 501-510 (1998)

Hanks G.E., Hanlon A.L., Pinover W.H., Horwitz E.M., Schultheiss T.E., Survival advantage for prostate cancer patients treated with high-dose three-dimensional conformal radiotherapy, *Cancer J Sci Am* **5:** 152-158 (1999)

Hanks G.E., Hanlon A.L., Pinover W.H., Horwitz E.M., Price R.A., Schultheiss T., Dose selection for prostate cancer patients based on dose comparison and dose response studies, *Int J Radiat Oncol Biol Phys* **46**: 823-832 (2000)

Hanley J, Lumley MA, Mageras GS, et al., Measurement of patient positioning errors in three-dimensional conformal radiotherapy of the prostate, *Int J Radiat Oncol Biol Phys* **37**:435-444 (1997)

Hanley J, Debois MM, Mah D, et al, Deep inspiration breath-hold technique for lung tumors: The potential value of target immobilization and reduced lung density in dose escalation, *Int J Radiat Oncol Biol Phys* **45**:603-611, (1999)

Hartford A.C., Niemierko A., Adams J.A., Urie M.M., Shipley W.U., Conformal irradiation of the prostate: estimating long-term rectal bleeding risk using dose–volume histograms, *Int J Radiat Oncol Biol Phys* **36**: 721-730 (1996)

Herman M.G., Balter J.M., Jaffray D.A., et al., Clinical use of electronic portal imaging: Report of AAPM Radiation Therapy Committee Task Group 58, *Med Phys* **28:** 712-737 (2001)

Herman M.G., Pisansky T.M., Kruse J.J., et al., Technical aspects of daily online positioning of the prostate for three-dimensional conformal radiotherapy using an electronic portal imaging device, *Int J Radiat Oncol Biol Phys* **57**: 1131-1140 (2003)

Herring DF, Compton DMJ, The degree of precision required in the radiation dose delivered in cancer radiotherapy, *Br J Radiol* **5**:1112-1 118 (1970)

Horwitz E.M., Hanlon A.L., Pinover W.H., Anderson P.R., Hanks G.E., Defining the optimal radiation dose with three-dimensional conformal radiation therapy for patients with nonmetastatic prostate carcinoma by using recursive partitioning techniques, *Cancer* **92**: 1281-1287 (2001)

Huang E., Dong L., Chandra A., et al., Intrafraction prostate motion during IMRT for prostate cancer, *Int. J. Radiat. Oncol. Biol. Phys.* **53**: 261-268 (2002a)

Huang E.H., Pollack A., Levy L., et al., Late rectal toxicity: dose–volume effects of conformal radiotherapy for prostate cancer, *Int J Radiat Oncol Biol Phys* **54:** 1314-1321 (2002b)

Hunt MA, Schultheiss TE, Desobry GE, Hakki M, Hanks GE, An evaluation of setup uncertainties for patients treated to pelvic sites, *Int J Radiat Oncol Biol Phys.* **32**:227-233 (1995)

Hurkmans CW, Remeijer P, Lebesque JV, Mijnheer B J, Set-up verification using portal imaging: review of current clinical practice, *Radiotherapy and Oncology* **58**: 105-120 (2001)

ICRU Report 24, Determination of absorbed dose in a patient irradiated by beams of x or Gamma rays in radiotherapy procedures, *International Commission on Radiation Units and Measurements,* Washington, DC (1976)

ICRU Report 50, Prescribing, Recording, and Reporting Photon Beam Therapy, *International Commission on Radiation Units and Measurements,* Bethesda, MD (1993)

ICRU Report 62, Prescribing, Recording, and Reporting Photon Beam Therapy (Supplement to ICRU report 50) *International Commission on Radiation Units and Measurements,* Bethesda, MD (1999)

Intensity Modulated Radiation Therapy Collaborative Working Group, Intensity-modulated radiotherapy: Current status and issues of interest, *Int. .J Radiat. Oncol. Biol. Phys.* **51:** 880–914 (2001)

Jackson A, Partial irradiation of the rectum, *Semin Radiat Oncol* **11:** 215-223 (2001a)

Jackson A, Skwarchuk M, Zelefsky M, Late rectal bleeding after 3D-conformal radiation therapy of prostate cancer (II): Volume effects and dose volume histograms, *Int. J. Radiat. Oncol. Biol. Phys.* **49:** 685—698 (2001b)

Jaffray DA, Yan D, and Wong JW, Managing Geometric Uncertainty in Conformal Intensity-Modulated Radiation Therapy, *Seminars in Radiation Oncology*, **9:** 4-19 (1999)

Jaffray D.A., Siewerdsen J.H., Wong J.W., et al., Flat-panel cone-beam computed tomography for image-guided radiation therapy, *Int J Radiat Oncol Biol Phys* **53:** 1337-1349 (2002)

Jiang R, Barnett R, Chow J, Grigorov G, and Chen J, Improved absorbed dose calculations incorporating internal organ motion, Med. Phys. **32**: 2423 (2005)

Jiang R, Barnett R, Chow J, Grigorov G, and Chen J, Dose gradient analyses in the prostate organ motion: treatment plan evaluation independent of DVH, *Med. Phys.* **33:** 2661 (2006a)

Jiang R, Barnett R, Chow J, Grigorov G, and Chen J, Dynamic evaluation for the treatment outcome incorporating prostate organ motion, *Med. Phys.* **33:** 2661 (2006b)

Jiang R, Barnett R, Chow J and Chen J, The use of spatial dose gradients and probability density function to evaluate the effect of internal organ motion for prostate IMRT treatment planning, *Phys. Med. Biol.* **52:** 1469-1484 (2007a)

Jiang R, Barnett R, Chow J and Chen J, Evaluation of prostate IMRT treatment planning incorporating internal organ motion using a dose gradient analysis, *Radiotherapy & Oncology,* **84**: S68-S69 (2007b)

Jiang R, Osei E, Barnett R, Fleming K, and Panjwani D, Simultaneous evaluation of daily on-line set-up errors and organ motion uncertainty during conformal radiation treatment of the prostate, *Radiotherapy & Oncology* **84**: S68 (2007c)

Jiang R, Barnett R, Chow J and Chen J, Estimating Rectal Complication in Prostate IMRT Treatment Planning Using Maximum Dose Gradient, *Med. Phys.* **34**: 2447 (2007d)

Johns H E, Cunningham J R, The Physics of Radiology, Thomas, Springfield, Maryland, USA, (1994).

Jones D, Hafermann MD, Rieke JW, Vermeulen SS, An estimate of the margin required when defining blocksd around the prostate, *Br J Radiol* **68**: 740-746 (1995)

Keall P J, Beckham W A, Booth J T, Zavgorodni S F and Oppelaar M, A method to predict the effect of organ motion and set-up variations on treatment plans, *Australas. Phys. Eng. Sci. Med.* **22:** 48–52 (1999)

Kitamura K., Shirato H., Seppenwoolde Y., et al., Three-dimensional intrafractional movement of prostate measured during real-time tumor-tracking radiotherapy in supine and prone treatment positions, *Int J Radiat Oncol Biol Phys* **53**: 1117-1123 (2002)

Kuban D, Pollack A, Huang E, *et al.,* Hazards of dose escalation in prostate cancer radiotherapy, *Int J Radiat Oncol Biol Phys* **57**:1260–1268 (2003)

Kupelian P.A., Reddy C.A., Carlson T.P., Willoughby T.R., Dose/volume relationship of late rectal bleeding after external beam radiotherapy for localized prostate cancer: Absolute or relative rectal volume?, *Cancer J* **8**: 62-66 (2002a)

Kupelian A.P., Reddy C.A., Carlson T.P., et al., Preliminary observations on biochemical relapse-free survival rates after short-course intensity-modulated radiotherapy (70 Gy at 2.5 Gy/fraction) for localized prostate cancer, *Int J Radiat Oncol Biol Phys* **53:** 904-912: (2002b)

Kutcher G J, Burman C, Brewster L, Histogram reduction method for calculating complication probabilities for three-dimensional treatment planning evaluations, *Int. J. Radiat. Oncol. Biol. Phys.* **21:** 137-146 (1991)

Kutcher, GJ; Mageras, GS; Leibel, SA, Control, correction, and modeling of setup errors and organ motion, *Semin Radiat Oncol* **5**: 134-145 (1995)

Kutcher G.J., Leibel S.A., Ling C.C., Zelefsky M., Fuks Z., New wine in an old bottle? Dose escalation under dose–volume constraints: a model of conformal therapy of the prostate, *Int J Radiat Oncol Biol Phys* **35:** 415-416 (1996)

Lam, KL and Ten Haken, RK, Improvement of precision in spatial localization of radio-opaque markers using the two-film technique, *Med Phys* **18**: 1126–1131 (1991)

Langen KM, Jones DTL, Organ motion and its management, *Int J Radiat Oncol Biol Phys* **50**: 265-278 (2001)

Lattanzi, J, McNeeley, S, Pinover, W, Horwitz, E, Das, I, Schultheiss, TE and Hanks, GE, A comparison of daily CT localization to a daily ultrasound-based system in prostate cance, *Int J Radiat Oncol Biol Phys* **43**: 719–725 (1999)

Lebesque J V, Bruce A M, Guus Kroes A P, Touw A, Shouman T and van Herk M, Variation in volumes, dose-volume histograms, and estimated normal tissue complication probabilities of rectum and bladder during conformal radiotherapy of T3 prostate cancer, *Int. J. Radiat. Oncol. Biol. Phys.* **33:** 1109–19 (1995)

Leong J, Implementation of random positioning error in computerised radiation treatment planning systems as a result of fractionation, *Phys. Med. Biol.* **32:** 327–34 (1987)

Li J G and Xing L, Inverse planning incorporating organ motion, *Med. Phys.* **27**: 1573–1578 (2000)

Lind B K, Kallman P, Sundelin B, and Brahme A, Optimal radiation beam profiles considering uncertainties in beam patient alignment, *Acta Oncol.* **32:** 331–342 (1993)

Little D, Dong L, Levy L B, Chandra A and Kuban D A, use of portal images and bat ultrasonography to measure setup error and organ motion for prostate IMRT:

Implication for the treatment margins cancer, *Int. J. Radiat. Oncol. Biol. Phys.* **56:** 1218-1224 (2003)

Litzenberg, D, Dawson, L, Sandler, H, Sanda, MG, McShan, DL, Ten Haken, RK, Lam, KL, Brock KK and Balter, JM, Daily prostate targeting using implanted radiopaque markers, *Int. J Radiat Oncol Biol Phys* **52**: 699-703 (2002)

Litzenberg, Dale W.; Balter, James M.; Lam, Kwok L., Sandler, Howard M.; Ten Haken, Randall K., Retrospective analysis of prostate cancer patients with implanted gold markers using off-line and adaptive therapy protocols, *International Journal of Radiation Oncology Biology Physics* **63**: 123-133 (2005)

Lu Y., Li S., Spelbring D., et al, Dose–surface histograms as treatment planning tool for prostate conformal therapy, *Med Phys* 22 (1995)

Luchka K, Shalev S, Pelvic irradiation of the obese patient: a treatment strategy involving megavoltage simulation and intratreatment setup corrections, *Med Phys* **23**:1897-1902 (1996)

Lujan A E, Larsen E W, Balter J M, and Ten Haken R K, A method for incorporating organ motion due to breathing into 3D dose calculations, *Med. Phys.* **26:** 715–720 (1999a)

Lujan A E, Ten Haken R K, Larsen E W, and Balter J M, Quantization of setup uncertainties in 3-D dose calculations, *Med. Phys.* **26:** 2397–2402 (1999b)

Lyman J T, Complication probability as assessed from dose-volume histograms, *Radiat. Res.* **104:** S13–S19 (1985)

Lyman J.T., Wolbarst A.B., Optimization of radiation therapy. III. A method of assessing complication probabilities from dose–volume histograms, *Int J Radiat Oncol Biol Phys* **13**: 103-109 (1987)

MacKay R. I., Hendry J. H., Moore C. J., Williams P. C., and Read G., Predicting late rectal complications following prostate conformal radiotherapy using biologically effective doses and normalised dose-surfacehistograms, *Br. J. Radiol.* **70:** 517–526 (1997)

Mageras G S, Kutcher G J, Leibel S A, Zelefsky M J, Melian E, Mohan R, and Fuks Z, A method of incorporating organ motion uncertainties into three-dimensional conformal treatment plans, *Int. J. Radiat. Oncol. Biol. Phys.* **35:** 333–342 (1996)

Mah D., Freedman G., Milestone B., et al., Measurement of intrafractional prostate motion using magnetic resonance imaging, *Int J Radiat Oncol Biol Phys* **54** 568-575 (2002)

Martinez A.A., Yan D., Lockman D., et al., Improvement in dose escalation using the process of adaptive radiotherapy combined with three-dimensional conformal or

intensity-modulated beams for prostate cancer, *Int J Radiat Oncol Biol Phys* **50**: 1226-1234 (2001)

Mechalakos J.G., Mageras G.S., Zelefsky M.J., et al., Time trends in organ position and volume in patients receiving prostate three-dimensional conformal radiotherapy, *Radiother Oncol* **62:** 261-265 (2002)

McCarter S D and Beckham W A, Evaluation of the validity of a convolution method for incorporating tumour movement and set-up variations into the radiotherapy treatment planning system, *Phys. Med. Biol*. **45:** 923–931 (2000)

McKenzie A L, van Herk M and Mijnheer B, The width of margins in radiotherapy treatment plans, *Phys. Med. Biol.* **45:** 3331–3342 (2000a)

McKenzie A L, How should breathing motion be combined with other errors when drawing margins around clinical target volumes, *Br. J. Radiol.* **73:** 973–977 (2000b)

McKenzie A., van Herk M., Mijnheer B., Margins for geometric uncertainty around organs at risk in radiotherapy, *Radiother Oncol* **62**: 299-307 (2002)

Melian E, Mageras G S, Fuks Z, Leibel S A, Niehaus A, Lorant H, Zelefsky M, Baldwin B and Kutcher G J, Variation in prostate position: quantitation and implications for three-dimensional conforal treatment planning, *Int. J. Radiat. Oncol. Biol. Phys.* **38:** 73–81 (1997)

Michalski J.M., Purdy J.A., Winter K., et al., Preliminary report of toxicity following 3D radiation therapy for prostate cancer on 3DOG/RTOG 9406, *Int J Radiat Oncol Biol Phys* **46**: 391-402 (2000)

Michalski J, Purdy J, Bruner D W and Amin M, A phase III randomized study of high dose 3D-CRT/IMRT versus standard dose 3D-CRT/ IMRT in patients treated for localized prostate cancer, *RTOG 0126* (2004)

Millender LE, Aubin M, Pouliot J, et al., Daily electronic portal imaging for morbidly obese men undergoing radiotherapy for localized prostate cancer, *Int J Radiat Oncol Biol Phys* **59**: 6–10 (2004)

Mirabell R., Taussky D., Rinaldi D., et al., Influence of rectal volume changes during radiotherapy for prostate cancer: a predictive model for mild-to-moderate late rectal toxicity, *Int J Radiat Oncol Biol Phys* Volume: **57**: 1280-1284, (2003)

Morr J., DiPetrillo T., Tsai J.S., et al., Implementation and utility of a daily ultrasound-based localization system with intensity-modulated radiotherapy for prostate cancer, *Int J Radiat Oncol Biol Phys* **53**: 1124-1129 (2002)

Nederveen A.J., van der Heide U.A., Dehnad, H., Measurements and clinical consequences of prostate motion during a radiotherapy fraction, *Int J Radiat Oncol Biol Phys* **53**: 206-214 (2002)

Nederveen AJ, Dehnad H, van der Heide UA, van Moorselaar RJA, Hofman P and Lagendijk JJW, Comparison of megavoltage position verification for prostate irradiation based on bony anatomy and implanted fiducials, *Radiotherapy and Oncol* **68**: 81-88 (2003)

Niemierko A, Reporting and analyzing dose distributions: A concept of equivalent uniform dose, *Med. Phys*. **24:** 103–110 (1997)

Nuyttens J.J., Milito S., Rust P.F., Turrisi A.T. III, Dose-volume relationship for acute side effects during high dose conformal radiotherapy for prostate cancer, *Radiother Oncol* **64**: 209-214 (2002)

O'Brien P.C., Radiation injury of the rectum, *Radiother Oncol* **60**: 1-14 (2001)

O'Brien P.C., Franklin C.I., Poulsen M.G., et al., Acute symptoms, not rectally administered sucralfate, predict for late radiation proctitis - Longer term follow-up of a phase III trial—Trans-Tasman Radiation Oncology Group, *Int J Radiat Oncol Biol Phys* **54:** 442-449 (2002)

O'Dell W G, Schell M C, Reynolds D, and Okunieff P, Dose broadening due to target position variability during fractionated breath-held radiation therapy, *Med. Phys.* **29:** 1430–1437 (2002)

Okunieff P, Morgan D, Niemierko A and Suit H D, Radiation doseresponse of human tumors, *Int. J. Radiat. Oncol. Biol. Phys.* **32**: 1227–1237 (1995)

Padhani A.R., Khoo V.S., Suckling J., et al., Evaluating the effect of rectal distension and rectal movement on prostate gland position using cine MRI, *Int. J. Radiat. Oncol. Biol. Phys.* **44**: 525-533 (1999)

Palta J R and Mackie T R, Intensity Modulated Radiation Therapy—the State of the Art, Madison, WI, *Medical Physics Publishing* (2003)

Pinnacle[3] SmartSim[TM] User guide version 6.0, Plan evaluation tools, Philips Medical Systems Company, **12:** 21–24 (2001)

Pinnacle User guide Inverse Planning and IMRT for PINNACLE[3], Objectives and constraints, Philips Medical Systems Company, 2-2/2-12 (2002)

Pollack A., Zagars G.K., Starkschall G., et al., Conventional vs. conformal radiotherapy for prostate cancer - Preliminary results of dosimetry and acute toxicity, *Int J Radiat Oncol Biol Phys* **34:** 555-564 (1996)

Pollack A., Zagars G.K., Starkschall G., et al., Prostate cancer radiation dose response - Results of the M.D. Anderson Phase III randomised trial, *Int J Radiat Oncol Biol Phys* **53**: 1097-1105 (2002)

Pouliot J, Aubin M, Langen K M, Liu YM, Pickett B, Shinohara K, et. al. (Non)-migration of radiopaque markers used for on-line localization of the prostate with an electronic portal imaging device, *Int J Radiat Oncol Biol Phys* **56**: 862-866 (2003)

Purdy JA, Dose-volume specification: New challenges with intensity-modulated radiation therapy, *Semin Radiat Oncol* **12**:199-209 (2002)

Purdy JA, Current ICRU Definitions of Volumes: Limitations and Future Directions, *Semin Radiat Oncol* **14**: 27-40 (2004)

Qian J., Wollan P., Bostwick D.G., The extent and multicentricity of high-grade prostatic intraepithelial neoplasia in clinically localized prostatic adenocarcinoma, *Hum Pathol* **28**: 143--148 (1997)

Rasch C, Keus R, Pameijer FA, et al, The potential impact of CT-MRI matching on tumor volume delineation in advanced head and neck cancer, *Int J Radiat Oncol Biol Phys* **39**:841-848 (1997)

Rasch C, Barillot I, Remeijer P, et al, Definition of the prostate in CT and MRI: A multi-observer study, *Int J Radiat Oncol Biol Phys* **43**:57-66 (1999)

Roach M, Faillace-Akazawa P, Malfatti C, et al, Prostate volumes defined by magnetic resonance imaging and computerized tomographic scans for three-dimensional conformal radiotherapy, *Int J Radiat Oncol Biol Phys* **35**:1011-1018 (1996)

Roach M, Faillace-Akazawa P, Malfatti C, Prostate volumes and organ movements defined by serial computerized tomographic scans during three-dimensional conformal radiotherapy, *Radiat Oncol Invest* **5**:187-194 (1997)

Roeske J C, Forman J D, Mesina C F, He T, Pelizzari C A, Fontenla E, Vijayakumar S and Chen G T, Evaluation of changes in the size and location of the prostate, seminal vesicles, bladder, and rectum during a course of external beam radiation therapy, *Int. J. Radiat. Oncol. Biol. Phys*. **33:** 1321–1329 (1995)

Rudat V, Flentje M, Oetzel D, Menke M, Schlegel W and Wannenmacher M, Influence of the positioning error on 3D conformal dose distributions during fractionated radiotherapy *Radiother. Oncol*. **33:** 56–63 (1994)

Rudat V, Schraube P, Oetzel D, Zierhut D and Flentje M, Combined error of patient positioning variability and prostate motion uncertainty in 3D conformal radiotherapy of localized prostate cancer, *Int. J. Radiat. Oncol. Biol. Phys*. **35:** 1027–1034 (1996)

Ruy J.K., Winter K., Michalski J.M., et al., Interim report of toxicity from 3D conformal radiation therapy (3D-CRT) for prostate cancer on 3DOG/RTOG 9406, level III (79.2 Gy), *Int J Radiat Oncol Biol Phys* **54**: 1036-1046 (2002)

Sandler HM, Bree RL, McLaughlin PW, Grossman HB and Lichter AS, Localization of the prostatic apex for radiation therapy using implanted markers, *Int J Radiat Oncol Biol Phys* **27**: 915–919 (1993)

Scarbrough, Todd J.; Golden, Nanialei M.; Ting, Joseph Y.; Fuller, Clifton D.; Wong, Adrian; Kupelian, Patrick A.; Thomas, Charles R., Comparison of ultrasound and implanted seed marker prostate localization methods: Implications for image-guided radiotherapy, *Int J Radiat Oncol Biol Phys* **65:** 378-387 (2006)

Schaly B, Kempe J A, Bauman G S, Battista J J, Van Dyk J, Tracking the dose distribution in radiation therapy by accounting for variable anatomy, *Phys. Med. Biol.* **49:** 791-805 (2004)

Schaly B, Bauman G S, Song W, Battista J J, Van Dyk J, Dosimetric impact of image-guided 3D conformal radiation therapy of prostate cancer *Phys. Med. Biol.* **50:** 3083-101 (2005a)

Schaly B, Bauman G S, Battista J J, Van Dyk J, Validation of contour-driven thin-plate splines for tracking fraction-to-fraction changes in anatomy and radiation therapy dose mapping, *Phys. Med. Biol.* **50:** 459-75 (2005b)

Schiffner DC.; Gottschalk AR.; Lometti M; Aubin M; Pouliot J; Speight J; Hsu IC; Shinohara K; Roach M, Daily electronic portal imaging of implanted gold seed fiducials in patients undergoing radiotherapy after radical prostatectomy, *International Journal of Radiation Oncology Biology Physics* **67**: 610-619 (2007)

Schild S E, Casale H E and Bellefontaine L P, Movements of the prostate due to rectal and bladder distension: Implications for radiotherapy, *Med. Dosim.* **18:** 13–15 (1993)

Schultheiss TE, Lee WR, Hunt MA, *et al.,* Late GI and GU complications in the treatment of prostate cancer, *Int J RadiatOncol Biol Phys* **37**: 3–11 (1997)

Schwarz M., Lebesque J.V., Mijnheer B.J., et al., Sensitivity of treatment plan optimisation for prostate cancer using the equivalent uniform dose (EUD) with respect to the rectal wall volume parameter, *Radiother Oncol* **73:** 209--218 (2004)

Shu H.K., Lee T.T., Vigneauly E., et al., Toxicity following high-dose three-dimensional conformal and intensity-modulated radiation therapy for clinically localized prostate cancer, *Urology* **57**: 102-107 (2001)

Skwarchuk MW, Jackson A, Zelefsky MJ, *et al.,* Late rectal toxicity after conformal radiotherapy of prostate cancer (I): Multivariate analysis and dose-response, *Int J Radiat Oncol Biol Phys* **47**:103–113 (2000)

Slater, JD, Yonemoto, L, Rossi, C, Reyes-Molyneux, N, Bush, DA. Antoine, JE, Loredo, LN, Schulte, RW, Teichman SL and Slater, LM., Conformal proton therapy for prostate carcinoma*, Int J Radiat Oncol Biol Phys* **42**: 299–304 (1998)

Song W, Schaly B, Bauman G, Battista J, Van Dyk J, Image-guided adaptive radiation therapy (IGART): Radiobiological and dose escalation considerations for localized carcinoma of the prostate, *Med. Phys*. **32:** 2193-203 (2005)

Song W Y, Schaly B, Bauman G, Battista J J, Van Dyk J, Evaluation of image-guided radiation therapy (IGRT) technologies and their impact on the outcomes of hypofractionated prostate cancer treatments: a radiobiologic analysis, *Int. J. Radiat. Oncol. Biol. Phys*. **64:** 289-300 (2006)

Stasi, Michele; Munoz, Fernando; Fiorino, Claudio; Pasquino, Massimo; Baiotto, Barbara; Marini, Piergiorgio; Malinverni, Giuseppe; Valdagni, Riccardo; Gabriele, Pietro, Emptying the rectum before treatment delivery limits the variations of rectal dose-volume parameters during 3DCRT of prostate cancer, *Radiotherapy and Oncology* **80:** 363-370 (2006)

Storey M, Pollack A, Zagars G, Smith L, Antolak J and Rosen I, Complications from Radiotherapy Dose Escalation in Prostate Cancer: Preliminary Results of a Randomized Trial, *Int J Radiat Oncol Biol Phys* **48**: 635-642 (2000)

Stroom J C, de Boer H C J, Huizenga H and Visser A G, Inclusion of geometrical uncertainties in radiotherapy treatment planning by means of coverage probability, *Int. J. Radiat. Oncol. Biol. Phys.* **43:** 905–919 (1999)

Stroom J.C., Kroonwijk M., Pasma K.L., et al., Detection of internal organ movement in prostate cancer patients using portal images, *Med Phys* **27:** 452-461 (2000)

Stroom JC.; Heijmen BJM, Geometrical uncertainties, radiotherapy planning margins, and the ICRU-62 report, *Radiotherapy and Oncology* **64:** 75-83 (2002)

Tai P, Van Dyk J, Battista J, Yu E, Stitt L, Tonita J, Agboola O, Brierley J, Dar R, Leighton C, Malone S, Strang B, Truong P, Videtic G, Wong CS, Wong R, Youssef Y, Improving the consistency in cervical esophageal target volume definition by special training, *Int J Radiat Oncol Biol Phys* **53**: 766-74 (2002)

Ten Haken R K, Forman J D, Heimburger D K, Gerhardsson A, McShan D L, Perez-Tamayo C, Schoeppel S L, and Lichter A S, Treatment planning issues related to prostate movement in response to differential filling of the rectum and bladder, *Int. J. Radiat. Oncol. Biol. Phys*. **20:** 1317–1324 (1991)

Teh B.S., Mai W.-Y., Uhl B.M., et al., Intensity-modulated radiation therapy (IMRT) for prostate cancer with the use of a rectal balloon for prostate immobilization - Acute toxicity and dose–volume analysis, *Int J Radiat Oncol Biol Phys* **49:** 705-712 (2001)

Tinger A; Michalski JM.; Cheng A; Low DA.; Zhu R; Bosch WR.; Purdy JA.; Perez CA., A critical evaluation of the planning target volume for 3-D conformal radiotherapy of prostate cancer, *Int. J. Radiat. Oncol. Biol. Phys.* **42:** 213–221 (1998)

Tucker S L, Cheung R, Dong L, Liu H, Thames H D, Huang E H, Kuban D, and Mohan R, Dose-volume response analyses of late rectal bleeding after radiotherapy for prostate cancer*, Int J Radiat Oncol Biol Phys* **59**: 353-365 (2004)

Urie M. M.,Goitein M., Doppke K., Kutcher J. G., LoSasso T., Mohan R., Munzenrider J. E., Sontag M, and Wong J. W., The role of uncertainty analysis in treatment planning, *Int. J. Radiat. Oncol., Biol., Phys.* **21:** 91–107 (1991)

Van den Heuvel F; Fugazzi J; Seppi E; Forman JD., Clinical application of a repositioning scheme, using gold markers and electronic portal imaging *Radiotherapy and Oncology* **79:** 94-100 (2006)

Van Dyk J, The modern technology of radiation oncology, *Medical physics publishing,* Madison, Wisconsin (1999)

van Herk M, Bruce A, Guus Kroes A P, Shouman T, Touw A and Lebesque J V, Quantification of organ motion during conformal radiotherapy of the prostate by three dimensional image registration, *Int. J. Radiat. Oncol.Biol. Phys.* **33:** 1311–20 (1995)

van Herk M, Remeijer P, Rasch C, and Lebesque J V, The probability of correct target dosage: Dose-population histograms for deriving treatment margins in radiotherapy, *Int. J. Radiat. Oncol. Biol. Phys.* **47:** 1121–1135 (2000)

van Herk M, Remeijer P, and Lebesque J V, Inclusion of geometric uncertainties in treatment plan evaluation, *Int. J. Radiat. Oncol. Biol. Phys*. **52:** 1407–1422 (2002)

van Herk M, Errors and margins in radiotherapy, *Seminars in Radiation Oncology* **14**: 52-64 (2004)

Vicini F.A., Abner A., Baglan K.L., Kestin L.L., Martinez A.A., Defining a dose–response relationship with radiotherapy for prostate cancer: is more really better?, *Int J Radiat Oncol Biol Phys* **51**: 1200-1208 (2001)

Vigneault E, Pouliot J, Laverdiere J Roy J and Dorion M, Electronic portal imaging device detection of radioopaque markers for the evaluation of prostate position during megavoltage irradiation: A clinical study, *Int. J. Radiat. Oncol. Biol. Phys*. **37:** 205-212 (1997)

Wachter S., Gerstner N., Goldner G., Potzi R., Wambersie A., Potter R., Rectal sequelae after conformal radiotherapy of prostate cancer: Dose-volume histograms as predictive factors, *Radiother Oncol*, **59:** 65-70 (2001)

Webb S, The Physics of Three-dimensional Radiation Therapy—Conformal Radiotherapy, Radiosurgery and Treatment Planning (Bristol: *Institute of Physics Publishing*) (1993)

Webb S, The Physics of Conformal Radiotherapy—Advances in Technology (Bristol: *Institute of Physics Publishing*) (1997)

Webb S, Intensity Modulated Radiation Therapy (Bristol: *Institute of Physics Publishing*) (2000)

Webb S, Contemporary IMRT—Developing Physics and Clinical Implementation (Bristol: *Institute of Physics Publishing*) (2004)

Webb S, Motion effects in (intensity modulated) radiation therapy: a review *Phys. Med. Biol.* **51:** R403–R425 (2006)

Wong J., Yan D., Michalski J., et al., The cumulative verification image analysis tool for offline evaluation of portal images, *Int J Radiat Oncol Biol Phys* **33**: 1301-1310 (1995)

Wong J.R., Grimm L., Uematsu M., et al., Image-guided radiotherapy for prostate cancer by CT-linear accelerator combination: Prostate movement and dosimetric considerations, *Int. J. Radiat. Oncol. Biol. Phys.* **61**: 561-569 (2005)

Wu J., Haycocks T., Alasti H., et al., Positioning errors and prostate motion during conformal prostate radiotherapy using on-line isocenter set-up verification and implanted prostate markers, *Radiother. Oncol.* **61:** 127—133 (2001)

Wu Q., Mohan R., Niemierko A., et al., Optimization of intensity-modulated radiotherapy plans based on the equivalent uniform dose, *Int J Radiat Oncol Biol Phys* **52**: 224-235 (2002)

Yan D, Vicini F, Wong J and Martinez A, Adaptive radiation therapy, *Phys. Med. Biol.* **42**: 123–132 (1997)

Yan D, Jaffray D A and Wong J W, A model to accumulate fractionated dose in a deforming organ, *Int. J. Radiat.Oncol. Biol. Phys.* **44:** 665 (1999)

Yan D., Lockman D., Brabbins D., Tyburski L., Martinez A., An off-line strategy for constructing a patient-specific planning target volume in adaptive treatment process for prostate cancer, *Int J Radiat Oncol Biol Phys* **48**: 289—302 (2000)

Zelefsky M.J., Leibel S.A., Kutcher G.J., et al., The feasibility of dose escalation with three-dimensional conformal radiotherapy in patients with prostatic carcinoma, *Sci Am* **1:** 142-149 (1995)

Zelefsky MJ, IIappersett L, Leibel SA, et al, The effect of treatment positioning on normal tissue dose in patients with prostate cancer treated with three-dimensional conformal radiotherapy, *Int J Radiat Oncol BioI Phys* **37**:I3-19 (1997)

Zelefsky M, Leibel S, Gaudin PB, Kutcher GJ, Fleshner NE, Venkatramen ES, Reuter ES, Reuter VE, Fair WR, Ling CC and Fuks Z, Dose Escalation with Three-Dimensional Conformal Radiation Therapy Affects the Outcome in Prostate Cancer, *Int J Radiat Oncol Biol Phys*. **41:** 491-500 (1998)

Zelefsky M J, Crean D, Mageras G S, Lyass O, Happersett L, Ling C C, Leibel S A, Fuks Z, Bull S, Kooy H M, van Herk M, and Kutcher G J, Quantification and predictors of prostate position variability in 50 patients evaluated with multiple CT scans during conformal radiotherapy, *Radiother. Oncol*. **50:** 225–234 (1999)

Zelefsky M.J., Fuks Z., Hunt M., et al., High-dose intensity modulated radiation therapy forv prostate cancer: early toxicity and biochemical outcome in 772 patients, *Int J Radiat Oncol Biol Phys* **53**: 1111-1116 (2002a)

Zelefsky M.J., Fuks Z., Leibel S.A., Intensity-modulated radiation therapy for prostate cancer, *Semin Radiat Oncol* **12**: 229-237 (2002b)

Zellars RC, Roberson PL, Strawderman M, Zhang D, Sandler HM, Ten Haken RK, Osher D and McLaughlin PW, Prostate position late in the course of external beam therapy: patterns and predictors, *Int J Radiat Oncol. Biol Phys* **47**: 655-660 (2000)

Zhou S.M., Marks L.B., Tracton G.S., et al., A new three-dimensional dose distribution reduction scheme for tubular organs, *Med Phys* **27**: 1727--1731 (2000)

List of Publications

Publications in Referred Journals

R. Jiang, R. Barnett, J. Chow and J. Chen, The use of spatial dose gradients and probability density function to evaluate the effect of internal organ motion for prostate IMRT treatment planning, *Phys. Med. Biol.* **52,** 1469-1484 (2007)

R. Jiang, R. Barnett, J. Chow and J. Chen, Evaluation of prostate IMRT treatment planning incorporating internal organ motion using a dose gradient analysis, *Radiotherapy & Oncology*, **84**, S68-S69 (abstract) (2007)

R. Jiang, E. Osei, R. Barnett, K. Fleming, and D. Panjwani, Simultaneous evaluation of daily on-line set-up errors and organ motion uncertainty during conformal radiation treatment of the prostate, *Radiother. Oncol*, **84**, S68 (abstract) (2007)

R. Jiang, R. Barnett, J. Chow and J. Chen, Estimating Rectal Complication in Prostate IMRT Treatment Planning Using Maximum Dose Gradient, *Med. Phys.* **34**, 2447 (abstract) (2007)

J. Chow, G. Grigorov and **R. Jiang**, Dosimetry Along Edges of An Irregular MLC Field with Different Stepping Angles, *Med. Phys.* **34**, 2443 (abstract) (2007)

R. Jiang, R Barnett, J Chow, G Grigorov, and J Chen, Dose gradient analyses in the prostate organ motion: treatment plan evaluation independent of DVH, *Med. Phys.* **33**, 2661 (abstract) (2006)

R. Jiang, R Barnett, J Chow, G Grigorov, and J Chen, Dynamic evaluation for the treatment outcome incorporating prostate organ motion, *Med. Phys.* **33**, 2661 (abstract) (2006)

J. Chow, G. Grigorov and **R. Jiang**, Intensity modulated radiation therapy with irregular multileaf collimated field: A dosimetric study on the penumbra region with different leaf stepping patterns, *Med. Phys.* **33**, 4606-4613 (2006)

J. Chow, G. Grigorov and **R. Jiang**, Improved peripheral dose calculation accuracy for a small MLC field brought by the latest commercial treatment planning system, *Journal of Radiotherapy in Practice*, **5**, 121-128 (2006)

G. Grigorov, J. Chow, L. Grigorov, **R. Jiang**, and R. Barnett, IMRT: Improvement in treatment planning efficiency using NTCP calculation independent of the dose-volume-histogram, *Med. Phys*. **33**, 1250-1258 (2006)

J. Chow, B. Wattlaufer and **R. Jiang**, Dosimetric effects on the penumbra region of irregular multi-leaf collimated fields, *Phys. Med. Biol*. **51**, N31–N38(2006)

G. Grigorov, J. Chow, L. Grigorov, **R. Jiang**, and R. Barnett, IMRT prostate planning: a graphical rectal NTCP determination, *Med. Phys*. **33**, 2673 (abstract) (2006)

J. Chow, G. Grigorov, and **R. Jiang**, Improvements of a Commercial Treatment Planning System On the MLC Field, *Med. Phys*. **33**, 2110 (abstract) (2006)

R. Jiang, R. Barnett, J. Chow, G. Grigorov, and J. Chen, Improved absorbed dose calculations incorporating internal organ motion, *Med. Phys*. **32**, 2423 (abstract), (2005)

Conference Presentations

R. Jiang, R. Barnett, J. Chow and J. Chen, Estimating rectal complication in prostate IMRT treatment planning using maximum dose gradient, The American Association of Physicists in Medicine (AAPM), Minneapolis, USA (2007)

R. Jiang, R. Barnett, J. Chow, and J. Chen, Evaluation of prostate IMRT treatment planning incorporating internal organ motion using a dose gradient analysis, COMP, Toronto, Canada (2007)

R. Jiang, E. Osei, R. Barnett, K. Fleming, and D. Panjwani, Simultaneous evaluation of daily on-line set-up errors and organ motion uncertainty during conformal radiation treatment of the prostate, Canadian Organization of Medical Physics (COMP), Toronto, Canada (2007)

J. Chow, G. Grigorov and **R. Jiang**, Dosimetry Along Edges of An Irregular MLC Field with Different Stepping Angles, The American Association of Physicists in Medicine (AAPM), Minneapolis, USA (2007)

P. Charland, E. Osei, **R. Jiang**, B. Schaly, A. fleck, D. Panjwani, D. Gopaul, and R. Barnett, Multi-criteria Treatment Planning Assessment: Emulating the Radiation Oncologist's Thought Process, Canadian Organization of Medical Physics (COMP), Toronto, Canada (2007)

R. Jiang, R Barnett, J Chow, G Grigorov, and J Chen, Dynamic evaluation for the treatment outcome incorporating prostate organ motion, Canadian Organization of Medical Physics (COMP), Saskatoon, Canada (2006)

R. Jiang, R Barnett, J Chow, G Grigorov, and J Chen, Dose gradient analyses in the prostate organ motion: treatment plan evaluation independent of DVH, Canadian Organization of Medical Physics (COMP), Saskatoon, Canada (2006)

G Grigorov, J Chow, L Grigorov, **R. Jiang**, and R Barnett, IMRT prostate planning: a graphical rectal NTCP determination, Canadian Organization of Medical Physics (COMP), Saskatoon, Canada (2006)

J Chow, G Grigorov, and **R. Jiang**, Improvements of a Commercial Treatment Planning System On the MLC Field, The American Association of Physicists in Medicine (AAPM), Orlando, USA (2006)

R. Jiang, R Barnett, J Chow, G Grigorov, and J Chen, Improved absorbed dose calculations incorporating internal organ motion, Canadian Organization of Medical Physics (COMP), Hamilton, Canada (2005)